SPACE TETHER DEPLOYMENT CONTROL FOR NANOSATELLITES

LATHEEPAN MURUGATHASAN

A DISSERTATION SUBMITTED TO THE FACULTY OF GRADUATE STUDIES IN PARTIAL FULFILLMENT OF THE REQUIREMENTS FOR THE DEGREE OF

DOCTOR OF PHILOSOPHY

GRADUATE PROGRAM IN EARTH AND SPACE SCIENCE
YORK UNIVERSITY
TORONTO, ONTARIO

NOVEMBER 2020

ABSTRACT

This thesis investigates the deployment control of space tethers for nanosatellites. More specifically, the problem space is reduced to the deployment of a tether that is housed and autonomously operated on a nanosatellite, connected to a relatively massive satellite. Novel control schemes for this objective has been derived and analyzed in detail, along with the development of linear and nonlinear observers to reduce the resources required to support the deployment process. Furthermore, pulse width pulse frequency modulation technique is leveraged to simplify the actuator required for this mechanism. Finally, advanced simulations that include a multitude of disturbances in the low Earth space environment is introduced to analyze the performance of deployment controllers. The main contributions of this work are the development of controllers under state constraints, the application of a unique nonlinear observer to the TSS state measurement problem and, the application of advanced simulations to validate the performance of TSS deployment controllers under a variety of disturbances. Experimental validation, model uncertainties as well as attitude dynamics has been omitted from the scope of this thesis and is left for future work.

PERMISSION TO LEND OR SELL

SPACE TETHER DEPLOYMENT CONTROL FOR NANOSATELLITES

By Latheepan Murugathasan

a thesis submitted to the Faculty of Graduate Studies of York University in partial fulfillment of the requirements for the degree of

DOCTOR OF PHILOSOPHY

Permission has been granted to the LIBRARY OF YORK UNIVERSITY to lend or sell copies of this thesis, to the NATIONAL LIBRARY OF CANADA to microfilm this thesis and to lend or sell copies of the film, and to **UNIVERSITY MICROFILMS** to publish an abstract of this thesis.

The author reserves other publication rights, and neither the thesis nor extensive extracts from it may be printed or otherwise reproduced without the author's written permission.

AUTHOR CERTIFICATE

SPACE TETHER DEPLOYMENT CONTROL FOR NANOSATELLITES

by Latheepan Murugathasan

By virtue of submitting this document electronically, the author certifies that this is a true electronic equivalent of the copy of the dissertation approved by York University for the award of the degree. No alteration of the content has occurred and if there are any minor variations in formatting, they are as a result of the conversion to Adobe Acrobat format (or similar software application).

Examination Committee members:

1. Dr. Regina Lee
2. Dr. Aleksander Czekanski
3. Dr. Roger Kempers
4. Dr. Guangjun Liu
5. Dr. Franz Newland

Thesis Title:	Space Tether Deployment Control for Nanosatellites
Degree and Year:	Doctor of Philosophy 2020
Name:	Latheepan Murugathasan
Department:	Graduate Program in Earth and Space Science
University:	York University

ACKNOWLEDGEMENTS

A sincere thank you to my supervisor Dr. George Zhu for his guidance and support throughout my dissertation. His insights, wisdom and academic rigor has been invaluable to my growth and I am forever grateful. I would also like to thank my committee members Dr. Regina Lee, Dr. Alex Czekanski and Dr. George Vukovich for their constructive criticism and positive feedback over the years. I am very fortunate to learn from their expertise and extremely appreciative of all their efforts.

I would also like to acknowledge Dr. Franz Newland who although was not a member of my committee, provided outstanding mentorship. It was truly a blessing to absorb some of his knowledge and work with such a great professional. My colleagues Udai Bindra, Junjie Kang, Peng Li, Chonggang Du, Jude Furtal and Gangqiang Li deserve recognition for their support and constructive feedback throughout my thesis. I really enjoyed our academic exchanges and intriguing conversations.

To my parents, this thesis is dedicated to you. This thesis is a result of your years of hard work, perseverance and dedication. I would also like to thank my siblings, family and my in-laws for their moral support. Finally, my deepest gratitude and dedication goes to my wife Babitha for her unbounded support and love. I do not know if I would have made it this far without you. Your strength and wisdom have willed me thus far.

TABLE OF CONTENTS

LIST OF TABLES

LIST OF FIGURES

SYMBOLS AND CONVENTION

All units are given in SI units, time in seconds (s), distance in meters (m), frequency in Hertz (Hz), velocity in meters per second (m/s), and stress in Pascals (Pa) except where otherwise noted.

All the vectors, matrices and unit vectors of axes are shown in bold face. Derivatives with respect to time and true anomaly are denoted as $\dot{x}$ and x' respectively.

LIST OF SYMBOLS

l	Tether Length
$l_{\max}$	Maximum/Desired Tether Length
m_i	Mass of *i*th Object
m_e	Effective Mass of Tethered System
m_t	Tether Mass
x_i	*i*th State Variable
x_{i0}	Initial Condition of *i*th State Variable
$L_f h(\mathbf{x})$	Lie derivative of h with respect to f
M_M	Mass of the Earth
M	Center of Mass
Q_i	Generalized Force acting on the *i*th generalized coordinate
R_i	Distance from Center of the Earth to the *i*th Object

T	Tether Tension
$V(\mathbf{x})$	Lyapunov Function
α	True Anomaly
ϕ	Out-of-plane Libration Angle
θ	In-plane Libration Angle
ξ	Normalized Tether Length
Ω	Orbital Angular Velocity

LIST OF ABBREVIATIONS

AIT	Assembly, Integration and Testing
CM	Center of Mass
EDT	Electrodynamic Tether
EOL	End-of-Life
LEO	Low Earth Orbit
LVLH	Local Vertical Local Horizontal
PBF	Passivity-Based Feedback
PD	Proportional and Derivative
PWPF	Pulse Width Pulse Frequency Modulation
SIL	Software In the Loop
SIMO	Single Input Multi Output
STK	Systems Tool Kit
TSS	Tethered Satellite System

Chapter 1 INTRODUCTION AND JUSTIFICATION

Summary: In this chapter, the problem is defined and justified. Then, the method of approach adopted in achieving the set objectives is outlined. Furthermore, a summary of the layout of the thesis is provided.

1.1 BACKGROUND

Tethered Space System (TSS) have numerous applications in the space. These include, earth observation, generation of electricity, plasma physics, transfer of momentum, orbital transfer, radio-wave reflection, formation flying, debris capture, and the most popular, propellant-less propulsion such as de-orbiting spacecrafts at their end-of-life (EOL). The TSS consists of a long tether that connects two or more spacecrafts and generally, the tether comes in two variety's, either rope or tape. In either case, the tether may also be conductive, depending on the application, and extend from ranges of a few meters to tens of kilometers. As such, it is not feasible to send the TSS in a deployed state. The tether needs to be stowed and a mechanism is needed to deploy the tether into a desired configuration. Therefore, successful deployment of the tether is mission critical for TSS. For many of the tether applications, and especially for the de-orbiting case, it is essential that the tether is deployed and stabilized around the local vertical (nadir/zenith). Furthermore, it is imperative that the desired orientation of the satellites is achieved as the tether may not be able to operate in other orientations.

In 1960, NASA demonstrated the first tether mission with Gemini 11. Since then there have been more than twenty TSS missions in suborbital and low earth orbit (LEO) altitudes. Table 1-1 outlines the history of tether missions to date [1-12]. For many of these missions, the tether was deployed passively and stabilized by the gravity-gradient. However, there were two missions, SEDS-II and YES2 that were able to achieve closed-loop tether deployment. The flight data retrieved from these missions indicate superior performance of closed-loop controllers. Furthermore, it is interesting to note that many of the missions relied on a spring to provide an initial impulse, and then a braking mechanism is used to reduce the tether velocity. This appears to be the simplest tether deployment mechanism.

Table 1-1 History of Tethered Satellite Missions

Mission	**Date**	**Agency**	**Orbit**	**Length**	**Deployment method & control law**
Gemini 11	1967	NASA	LEO	30m	Deployed. Thrusters on both spacecraft with one controlled by human.
Gemini 12	1967	NASA	LEO	30m	Deployed. Control was the same as Gemini 11.
H-9M-69	1980	NASA	Sub-orbital	500m	Partially deployed (38m). Spring ejection.
S-520-2	1981	NASA/ISAS	Sub-orbital	500m	Partially deployed (65m). Spring ejection.
Charge-1	1983	NASA/ISAS	Sub-orbital	500m	Deployed. Spring ejection with thruster on sub-satellite.
Charge-2	1984	NASA/ISAS	Sub-orbital	500m	Deployed. Control was the same as Charge-1.
Oedipus-A	1989	CSA/ NASA	Sub-orbital	958m	Deployed. Spring ejection with thruster on two-satellites.
Charge-2B	1992	NASA	Sub-orbital	500m	Deployed.
TSS-1	1992	NASA/ISA	LEO	260m	Partially deployed and retrieved. Velocity Control & active reel out. Thruster on sub-

					satellite for initial push for deployment.
SEDS-1	1993	NASA	LEO	20km	Downward deployed. Spring ejection and open loop brake control. Tether cut due to large swing.
PMG	1993	NASA	LEO	500m	Upward deployed.
SED-2	1994	NASA	LEO	20km	Deployed in local vertical by closed-loop robust control law. Spring ejection.
Oedipus-C	1995	CSA/ NASA	Sub-orbital	1170m	Deployed. Spring ejection. Stable by spinning with spin axis aligned with magnetic field.
TSS-1R	1996	NASA/ISA	LEO	19.6km	Deployed & severed by arcing.
TiPS	1996	NRO/ NRL	LEO	4km	Deployed. Spring ejection. Survived 12 years on-orbit.
YES	1997	T. U. Delft	GTO	35km	Not deployed to avoid a collision with other spacecraft
ATEx	1999	NRL	LEO	6km	Partially deployed (22m). Spring ejection.
PicoSAT1.0	2000	Aerospace Corp.	LEO	30m	Deployed & operated for 3 days.
ProSEDS	2003	NASA	LEO	15km	Hardware built, mission cancelled
DTUsat-1	2003	TUD	LEO	450m	Satellite failed in space.
MAST	2007	NASA	LEO	1km	Tether failed to deploy.
YES-2	2007	ESA	LEO	30km	Deployed. Spring ejection & closed-loop brake control.
Cute-1.7 +APDII	2008	Tokyo Tech	LEO	10m	Tether failed to deploy
STARS	2009	Kagawa U	LEO	10m	Deployed
T-Rex	2010	JAXA	Suborbital	300m	Deployed. Spring ejection & passive braking.
STARS-C	2016		LEO	30m	Partial Deployment
KITE	2017		Suborbital	720m	Tether failed to deploy.

It is also interesting to note that many of these missions have failed because of the deployment mechanism, for instance, the tether jams and the mission cannot achieve any tether deployment or only partial deployment. In addition to these missions, there have been numerous control strategies that have been explored for tether deployment control. In these controller developments, a simplified model of the tether system is used and can be classified as a single-input, multiple-output (SIMO) system where the input to the system is the tether tension. In fact, existing works have shown that the system could be stabilized through the tension alone. However, this simplified model makes many assumptions including a massless rigid tether and only considers in-plane (orbital plane) motion. Extensions of the model have been studied but controller development becomes intractable. However, in the SEDS-II and YES2 missions, the simplified planar model described above was used and a simple linear controller achieved impressive results [13] [14].

1.2 Justification for the Proposed Research

Clearly there is a need for a much simpler yet reliable deployment mechanism as this has been labelled the root cause of failures of many previous tethered missions. These numerous failures have restricted tether technology to purely research and development in academia world. In order to regain the confidence of the space community in space tethers, this technology would benefit from some form of nanosatellite demonstration. However, existing research and missions have focused on much larger scale satellites and it is important to acknowledge the limitations presented by the nanosatellite platform in controller development. Furthermore, future tethered missions would benefit from a self-sufficient, independently operated nanosatellite that can be attached to any spacecraft. This modular approach allows the tether to act as a payload and mission designers need only be concerned with the appropriate mechanical interfaces. Thus, this thesis will propose controllers for the deployment of space tethers of such independently operated nanosatellites, which can be attached to most large spacecraft.

There have also been extensive researches conducted on deployment control of space tethers. However, many of the control approaches fail to acknowledge key and fundamental aspects of the deployment mechanism. For example, many of the existing mechanisms employ some type of braking strategy together with the passive deployment mechanisms using springs. This places a constraint on the system such that given an initial impulse, the tether velocity can only be reduced (i.e., tether cannot be accelerate; monotonic deployment). Only a few researchers have examined this property but, they tackled this problem from purely a numerical approach [15]. It is advantageous to incorporate this property directly into the system model, or controller development in order to guarantee applicability and feasibility with the appropriate deployment mechanism. This thesis will develop analytic controllers that can be proved to satisfy this constraint and simulation results will be used to validate the approach.

The TSS, in the most basic form, consists of four states, the length, length rate, libration angle, and libration angle rate in the tether deployment process. The libration angle represents the angle that the tether makes with respect to the local vertical. Many existing approaches and controller development assume that this state is readily available for feedback via measurements. However, it is quite difficult and/or expensive to obtain these measurements especially on a nanosatellite. This thesis will examine approaches that will alleviate the need for libration angle measurements.

1.3 RESEARCH OBJECTIVES

The main objective of this thesis is to develop controllers that stabilize the deployment dynamics of the tether system to satisfy the following requirements

- Feasibility of the controllers for nanosatellites
- Monotonic deployment velocity for brake mechanism
- Minimize the number of feedback states

First, feasibility of the controllers for nanosatellites will be discussed in the context of the following criteria,

1. Simplicity (Computational Complexity)
2. Control Effort

Simplicity of the controller is essential because of the limited computational resources available on nanosatellites. Control laws in analytical forms are preferred because they can be computed in essentially constant time at each time step. Whereas numerical control requires iterative updates at each time step that can place unnecessary burden on the on-board computer, especially since these controllers have strict timing requirements for real-time response. Control effort also needs to be minimized because there are practical limits to the amount of control force that can be produced. Ultimately, there will be trade-offs between performance and resource consumption but, the objective of this thesis is to produce controllers with reasonable control inputs.

Second, the use of a braking mechanism imposes a constraint on the length rate of the tether system as it cannot be "reeled back in". The following goals have been defined for the braking controller:

1. Monotonic deployment
2. Positive control input

The monotonic deployment of the space tether will be incorporated directly into the controller development and will be proved analytically and validated through simulations. Positive control input is implied for braking mechanisms and although it will not be proved directly, it will be validated through simulations. In theory, saturation limits can be applied to ensure this property, however, this approach will be limited whenever possible.

Third, extra goals for the controllers are:

1. Restrict feedback states to length and length rate
2. Analyze behavior of system under disturbances

The length and length rate are relatively simple measurements compared to the other states of the tether system. As such, feedback will be restricted to these states while the remainder is estimated if needed. Atmospheric drag has been identified as the most significant disturbance on the system. The controller will not be designed to compensate for this disturbance but, the effects will be analyzed with simulations to characterize the performance and validate the objectives. It is important to note that to fully analyze the behavior of the system under atmospheric drag, a more advanced model than the one presented in this thesis is required. Nonetheless, preliminary results with this disturbance will be discussed.

1.3.1 Expected Outcomes of Research

This research aims to produce closed-loop feedback controllers for computationally constrained platforms such as nanosatellites, state observers to estimate unknown states and, validation of control laws under advanced simulation. Linear and nonlinear analytical control laws that are mathematically proved to be stable for the TSS will be developed and, the nonlinear controllers will be shown to be applicable to a specific class of TSS deployment mechanisms in which the tether cannot be reeled back in. Full state observers that address a unique constraint imposed by a simple length measurement system will be applied to the TSS and finally, simulations which incorporate advanced dynamics models will be utilized to determine the effectiveness of the proposed controllers and dynamic models.

1.4 Outline of Approach Methodology

The dynamics of the tether system will be derived from first principles to gain some insight into the system as well as understand the assumptions and limitations of the model. Linear controllers will then be developed to form a baseline and provide a benchmark for the more advanced controllers. The development of linear controllers will also yield greater insight into the system and highlight the effects/impacts of the nonlinear terms.

Nonlinear controllers will be developed using a variety of tools from control theory, and stability of these controllers will be analyzed from a Lyapunov view. Some of the developments will rely on the choice of a manifold (i.e., desired trajectory of the system). The intuition gained from the dynamics analysis and physical properties of the system will aid in the choice of these manifolds and the results will be discussed from this vantage point as well.

The constraint imposed by the braking mechanism, specifically the monotonicity of the tether deployment, is incorporated into the controller development through the invariance principle. Essentially, we chose a mathematical set to meet the constraint/requirements of the system, and then show that the closed-loop system is invariant to (bounded by), this desired set. This approach allows the controller development to be abstracted away from the constraint. Then, once the controller has been developed, this approach is applied to determine the control gains and conditions necessary to satisfy such constraint.

After development of the continuous control laws, discretization will be performed via pulse-width, pulse-frequency (PWPF) modulation. This converts the continuous controller into a series of pulses that approximate the continuous signal. The controllers with augmented PWPF will be simulated under identical conditions to determine the effects and performance.

Observers for the TSS will then be designed. Both linear and nonlinear observers will be derived and compared. Followed by case studies that integrate these observers with PWPF modulated linear and nonlinear controllers.

Finally, more advanced simulations will be conducted in lieu of ground based experiments. The fidelity and advanced models of commercial software will be leveraged to study the controller performance and tether dynamics under a myriad of disturbances found in the low-earth orbit space environment.

1.5 LAYOUT OF THESIS DOCUMENT

This document contains seven chapters. Following the Introductory Chapter 1, Chapter 2 provides a critical review of relevant work in three main areas: (1) existing dynamic models and their limitations, (2) controller development mainly in literature as well as a few in practice, (3) existing ground-based testing platforms. Chapter 3 gives a detailed description of the dynamics of TSS. Chapter 4 outlines the Controller development. In Chapter 5, observers are applied to the TSS. In Chapter 6, a Software-In-The-Loop Simulation is presented. Finally, in Chapter 7, the work is concluded by identifying the original contributions of the thesis and outlining the directions for future work.

1.6 PUBLICATIONS GENERATED FROM THESIS STUDY

Apart from this thesis, significant contribution was made towards a nanosatellite demonstration of a tethered satellite mission named DESCENT. Many of the insights and limitations of the nanosatellite platform was gained from this project and incorporated into this thesis.

The contributions of this thesis to the academic community can be found in these peer-review journal publications and conference proceedings.

1. Zhu, Z.H. and **Murugathasan, L.**, "Dynamic Control of Space Tether Deployment", *International Journal of Space Science and Engineering*, vol. 3, no. 2, pp.

113-128, 2015

2. **Murugathasan, L.** and Zhu, Z.H., "Deployment Control of Tethered Space Systems With Explicit Velocity Constraint and Invariance Principle", *Acta Astronautica*, vol. 157, pp. 390-396, 2019

3. **Murugathasan, L.,** Bindra, U., Du, C., Zhu, Z.H. and Newland F.T., "A Software and Hardware Redundancy Architecture for Using Raspberry Pi Modules as Command & Data Handling Systems for the DESCENT Mission", *ASTRO CASI*, Quebec City, Canada, 2018

4. Kang, J., Zhu, Z.H., Bindra, U., **Murugathasan, L.,** Furtal, J., and Li, G., "Deployment Mechanism for DESCENT Mission", *ASTRO CASI*, Quebec City, Canada, 2018

5. Jain, V., **Murugathasan, L.,** Bindra, U., Li, G., Kang, J., Furtal, J., Newland, F.T., Zhu, Z.H., Alger, M., Gleeson, E., and de Ruiter, A., "CubeSats can serve multiple stakeholders too: use of the DESCENT mission to develop national and international collaboration" *ASTRO CASI*, Quebec City, Canada, 2018

6. Jain, V., Bindra, U., **Murugathasan, L.,** Newland, F.T. and Zhu, Z.H., "Practical Implementation of test-as-you-fly for the DESCENT CubeSat Mission", *AIAA SpaceOps*, Marseille, France, 2018

7. Bindra, U., **Murugathasan, L.,** Jain, V., Li, G., Kang, J., Du, C., Zhu, Z.H., Newland, F.T. , Alger, M., Shonibare, O., de Ruiter, A., "DESCENT: Mission Architecture and Design Overview", *AIAA Space and Astronautics Forum and Exposition*, Orlanda, USA, 2017

Chapter 2 LITERATURE REVIEW

Summary: In this chapter, the common dynamics models, as well as existing controller development and ground-based test experiments of the TSS found in the literature is reviewed. To conclude, the limitations of the existing work is highlighted and the motivation for the work of this thesis is presented.

2.1 SPACE TETHER MODELS

The dynamics of tether deployment is quite complicated due to its nonlinear behavior and coupling between states even in the most simplified model of the system. The “Dumbbell” model which considers two point masses (the main satellite and sub satellite/payload) and a massless tether is the most popular choice in literature because of its feasibility in controller design [12]. Assume the TSS is in a circular orbit of Earth. The “Dumbbell” model in non-dimensional form is shown below [16]:

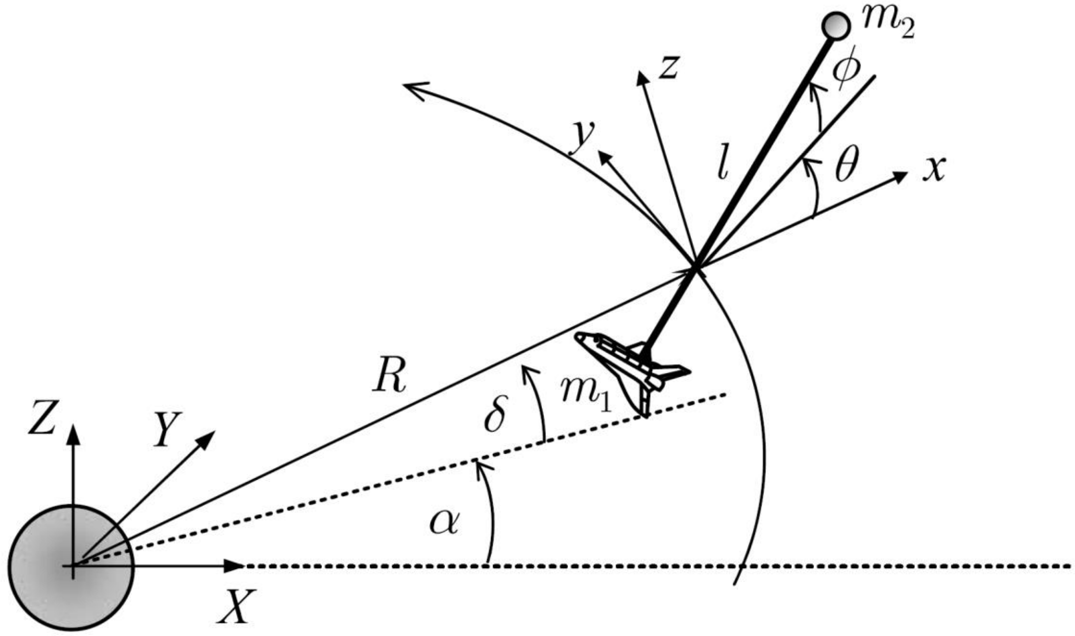

Figure 2.1   Three-Dimensional Tether Dumbbell Model [17]

$$\begin{aligned}
&\ddot{\theta}+2\left(\dot{\theta}-1\right)\left(\frac{\dot{\xi}}{\xi}-\dot{\phi}\tan\phi\right)+3\sin\theta\cos\theta=\frac{Q_\theta}{m_e\Omega^2 l_c^2\xi^2\cos^2\phi}\\
&\ddot{\phi}+2\dot{\phi}\left(\frac{\dot{\xi}}{\xi}\right)+\left(\left(\dot{\theta}-1\right)^2+3\cos^2\theta\right)\sin\phi\cos\phi=\frac{Q_\phi}{m_e\Omega^2 l_c^2\xi^2}\\
&\ddot{\xi}-\xi\left(\dot{\phi}^2+\left(\dot{\theta}-1\right)^2\cos^2\phi+3\cos^2\phi\cos^2\theta-1\right)=\frac{-T}{m_e\Omega^2 l_c}
\end{aligned}\tag{2.1}$$

where $\xi = {}^{l}\!/_{l_{\max}}$ is the dimensionless tether length, $l_{\max}$ is the desired tether length, θ and ϕ are the in-plane and out-of-plane angles respectively, $m_e = m_1 m_2/\left(m_1+m_2\right)$ with m_1 being the mass of the main satellite and m_2 the mass of the sub-satellite/payload, Ω is the orbital angular velocity, Q_θ and Q_ϕ are the generalized forces in the in-plane (pitch) and out-of-plane (roll) coordinates respectively, and T is the tension force in the tether. It is clear that this model neglects the attitude dynamics of the two spacecraft at the ends of tether and tether flexibility. Also this model is valid only for circular orbits, for eccentric orbits, the model is more complicated and includes other orbital parameters such as orbit eccentricity, semi-major axis, eccentricity, true anomaly [18].

This model can be extended however to include longitudinal flexibility of the tether by incorporating the strain into the length and the stiffness EA (Young's Modulus and Area) into the Tension [16]. If a fully flexible model is desired, two common approaches are found in the literature. First, a continuum model and a modal approximation of tether displacements is incorporated where the modal functions are functions of time because of the deployment stage [19]. Second, a discrete model is used based on finite element method [20], or a series of beads connected by massless rigid rods [17], springs [21] [22], or combination of springs and dashpots [23] [24].

Furthermore, the basic "Dumbbell" model can also be extended to include flexible modes of the tether, attitude dynamics of the two satellites, effects of external forces, such as gravitational perturbation, aerodynamic drag, solar radiation pressure, and electro-dynamic force as well [12]. Including these extensions would result in an extremely complicated model that is not feasible for analytical analysis but instead is used to simulate the dynamic behavior of the TSS and evaluate the tether deployment performance of the controller [25].

In addition to the dynamic modelling, the disturbance from space environment also affect the dynamic behavior of TSS. Yu and Jin studied the effects of J2 perturbation and heating effects from solar radiation, Earth's infrared radiation and satellite's infrared radiation [26]. Their study showed that J2 perturbation not only depends on the orbital parameters but also on system parameters such as sliding friction force between tether and deployment device. Also, the heating effect causes differential motions of the sub satellite in the clockwise (backward; away from CM motion) and anti-clockwise (forward; towards CM motion) direction during retrieval and affects the tension of the tether.

There have also been studies that analyze the effects of the tether on attitude dynamics through coupling of rotational and translational dynamics [27] [28]. Darabi and Assadian were able to leverage this model and develop novel attitude controllers that utilized not only reaction wheels onboard the spacecraft but also the tether tension [27]. The inclusion of the tether tension allowed the control effort required by the reaction wheels to be reduced significantly.

2.2 SPACE TETHER DEPLOYMENT/RETRIEVAL CONTROL STRATEGIES

There have been numerous control strategies that have been explored for tether deployment [5] [12] [25] [29] [30]. Majority if not all of the systems that are studied are SIMO systems. The control variable is often the tension in the tether and analysis results show that it is more than sufficient to stabilize the system in the in-plane libration via due to the coupling between the tension and the in-plane libration. A few cases were studied in which the length/length rate or the number of brake actions was used as the control variable [13] [14] [25] [31]. There have also been studies which include thrusters on the sub-satellite that allow control of the out-of-plane libration [32] [33]. The addition of an extra control variable is necessary because the tension or length rate alone cannot control the out-of-plane libration due to the high-order, or weak, coupling between the tension and the out-of-plane libration. Many control strategies only assume length and/or length rate available for feedback which is a reasonable assumption; however, there are cases which assume all states are available for feedback which is less realistic due to the difficulty in measuring the libration angle and angular rate. State observers can be introduced but they would complicate the controller and the performance and/or stability of the system may be affected. In many cases, constraints are imposed on the system and as a result, an optimal control strategy is the most popular solution found in the literature. Other strategies include basic state feedback methods, adaptive neural control and a few nonlinear approaches using Lyapunov functions. Another major concern is that the simulation results found in majority of the literature, did not include external disturbances such as atmospheric drag, J2 and others.

2.2.1 Tension Control Law

The most basic strategy is a simple tension control law that was derived by the linearized "Dumbbell" model and neglect of the out-of-plane dynamics [34]. Stability regions for the feedback gains were derived from the linearized model and simulated with the nonlinear model. The controller was able to achieve stability with the nonlinear dumbbell model. However, it is uncertain how it would respond to external disturbances and uncertainties within the model.

Wen et al. extended the simple tension control law to incorporate a tension constraint [35]. The constraint was introduced via a saturation function. The controller was proved stable by Lyapunov method and able to achieve very fast deployment.

2.2.2 Optimal Control Law

Williams et al. determined open-loop optimal trajectories by comparing various cost functions on the deployment dynamics and developed a closed-loop linear state feedback control law by linearizing about the optimal trajectories and numerically solving a receding horizon control problem [6]. The open-loop optimal trajectory also included atmospheric drag and orbit eccentricity in the computation and had also used the number of brake turns as the control input as opposed to the more common tension control. The controllers were tested with large disturbances to the hardware model and environmental variables and were shown to be effective. However, low ejection velocities coupled with higher than normal tension parameters in the deployment hardware were the most problematic for control and provided little tolerance for correcting errors. Williams then extended the work in [6] to include a flexible tethered model and perform the same optimizations and used a tension control law to stabilize the system [17].

Netzer and Kane generated the open-loop optimal path for deployment with a simple model and then verified the solution with the "full" nonlinear model and then used a regulator to ensure it follows the trajectory [36]. However, they had only shown the results for retrieval and did not mention if the regulator was used for the deployment process as well. They also had additional control variables by including thrusters on the sub satellite.

William and Trivailo made a comparison of various cost functions for the open-loop optimal control of a tethered satellite system in the planar case (neglecting out of plane dynamics) which they later extended to include control for librations in elliptic orbits [37] [38]. Williams then further examined the open-loop optimal control problem and concluded that minimum tension and minimum libration angles are not the most important in the determination of open-loop deployment and retrieval trajectories [39]. Instead he claims the best control objectives should incorporate the minimization of system accelerations. In his analysis he considers inelastic and elastic tethers and proves that the deployment and retrieval reference trajectories are symmetrical under certain conditions.

Steindl and Troger present an open-loop time optimal control strategy using the Maximum Principle that minimizes the deviation from the radial position [40]. The control law was developed with a simple massless model of the tether but they applied their controller to a flexible massive tether system based on finite element discretization and showed that the results were in agreement with the simple model.

Steindl also proposed an optimal deployment controller that is applicable to tethers in elliptic orbits [41]. However, the goal of his controller was to steer the tether that was initially close to the local vertical to a periodic motion farther away in the shortest time. He also extended the model to consider the mass and lateral oscillations of the tether itself [42].

2.2.3 Lyapunov Based Control law

Hironori and Shintaro developed a control law by minimizing a mission control function [43]. The mission control function was generated using a Lyapunov approach to stabilize the final mission state (equilibrium state). They had used the planar dumbbell model in their simulation and it is uncertain how the controller will respond to a more realistic model or uncertainties in the plant. Kokubun and Fujii then extended the work of Hironori and Shintaro by including an elastic tether in the dynamics model (continuum model) and applied the mission function control algorithm [44].

Vadali developed a tension control law using Lyapunov stability and only considered the planar dumbbell model [45]. His work was then later extended with Kim and they presented a feedback control law using Lyapunov stability theory with tension and out-of-plane thrusting as the control variables and used the three dimensional dumbbell models [46]. They had used the thrusters for the retrieval process because the convergence of the states was unacceptably slow without the thrusters. They present two methods to stabilize the system about the equilibrium. In the first method they perform a nonlinear coordinate transformation to partially decouple the in-plane and out-of-plane dynamics and they second method is based on an integral of motion of the coupled system. They also use the integral of motion method to develop a tether rate control law as well. Kim and Vadali also studied the system with the tether mass and aerodynamic drag and showed that the drag has a considerable effect on the dynamics of the system [33].

Luo et al. were able to show that an optimal control law is able to stabilize the system with consideration of a flexible tether and satellite attitude dynamics and control [47]. The controller was developed using the standard dumbbell model, but the simulations were conducted with a flexible bead tether.

2.2.4 Fractional Order and Sliding Mode Control law

Sun and Zhu first applied the concept of fractional order control laws to the tether deployment and retrieval problem [48] [49]. Mohsenipour then extended the concept using the controller of the form,

$$T = D^{\alpha} x_2 - D^{\alpha} x_1 + k_1 x_1 + k_2 x_2 + k_3 x_3 + k_4 x_4 + 3 \tag{2.2}$$

where D and k_i are control gains and α is a fractional exponent. The fractional exponent aids in the robustness of the controller to take into account uncertainties and assumptions in the model such as circular orbit [50]. Xu et al. extended the idea of fractional order system by developing a fractional order sliding mode control [51]. In their work, they defined two sliding surfaces and coupled them together via an adaptive fuzzy law. The system response looks promising however, their control input appears to have significant oscillatory behavior which may not be practical. Kang et al. improved upon this work by removing the oscillations found in the control input and improving the robustness of the system under sinusoidal disturbances [52].

Zhong et al. also developed a fractional order adaptive sliding mode controller [53]. Their control input included in-plane and out-of-plane thrusters but were able to achieve extremely fast deployment, with negligible chattering.

Wang et al. developed a second order sliding mode controller based on the dumbbell model and was able to achieve reasonably fast deployment (within an orbit) and showed robustness to varying amounts of disturbances [54] . However, there exists a significant amount of chattering for some control gains which needs to be addressed. Ma and Sun improved upon their work and developed a full-order sliding mode control for deployment and retrieval [55]. They were able to address the chattering issue however, the deployment times increased significantly.

Ma and Sun also proposed an adaptive sliding mode controller for tether deployment [56]. The controller was able to achieve successful deployment, but the control input has excessive oscillations which may be a result of chattering common to sliding mode controllers. Ma et al. improved on their previous work by introducing the boundary layer technique to avoid the chattering problem [57]. Chen et al. also developed an adaptive sliding mode controller that combines the typical tension control with EDT current control [58]. This additional control authority allows the system to become fully actuated. Furthermore, the adaptive component as well as fully actuated control allows robust performance under parameter variations such as mass uncertainties, initial perturbation and external disturbances.

2.2.5 Other Control laws

Misra and Modi investigated the deployment and retrieval dynamics and control by linearly varying the difference between the undeformed length of the tether and a commanded length with the state vector [59]. Their control input was the length rate which they claim to be easier to implement as opposed to the traditional tension input. The commanded length rate was a piecewise function with exponential and uniform components because it was simple and efficient. They neglect the out of plane motion because the derivation of their control law is based on the linearization of the system and the out of plane angle cannot be controlled by the length rate.

Glabel et al. proposed the adaptive neural control for the deployment process of a tether assisted re-entry mission [60]. They combine two neural networks, a controller network and plant model network with the controller network being initialized by multiple linear quadratic regulators and the plant model is trained to predict deviations from an optimized reference path which is generated from an open-loop optimal control which minimizes the braking force.

Bainum and Kumar developed control laws based on the linear regulator problem with the tension of the tether as the control variable and included the aerodynamic force into the three dimensional dumbbell model but they assume all states are available for feedback [61].

Lorenzini and Bortolami solved a nonlinear, nonautonomous control problem with numerically formulated feedback linearization and an ad hoc feedback law which was derived using a linearized variational model to ensure robustness [13]. The performance of their controller was verified using flight data and proved to be very successful by meeting mission requirements with ample margins. Specifically, the maximum libration amplitude was less than 4 deg and final tether velocity was less than 0.02m/s (design requirements were <10 deg and <1m/s respectively).

Takeichi et al. studied the control of a tethered system in elliptical orbits [62]. They studied an on-off control strategy using a thruster on the sub satellite to stabilize a periodic orbit (phase-plane orbit) and so the final state of the system is not the traditional local vertical found in the literature but a state that is in the neighborhood around the periodic solution. Their numerical simulation neglect elasticity, lateral deflection, damping and out-of-plane motions which can have a significant impact on the dynamics of the system.

Barkow et al. used the two dimensional dumbbell models and developed a pendulum control and targeting and chaos control [63]. Both controllers are activated after full free deployment of the tether and reduce the large amplitude oscillations at the end of free deployment. They compared their two control strategies (pendulum and controlling chaos) with four different control strategies: free deployment due to gravity gradient vector, forced braked deployment, Kissel's law using a linear PD Controller, open-loop time optimal control and showed that their controllers require less energy. They do not show an analytical model of their controller nor do they prove their controller will work.

Yu et al. also leveraged the electrodynamic force to stabilize the deployment process in three dimensions [64]. In their strategy, the deployment process is uniform (open-loop) and the in-plane and out-of-plane libration angles are controlled by the current through the tether. Their results show that the system can be stabilized, albeit for small initial conditions and fairly oscillatory response. However, their deployment times is very long as compared to other controllers in the literature. Wen et al. were able to improve upon this to include a closed-loop deployment control law with EDT control [65]. Their deployment times are much faster, can operate over a larger range of initial conditions and only the out-plane angle has excessive oscillations which damp out over a longer period of time.

Zhang and Huang introduced a virtual signal that they claim to strengthen the coupling between the length and the in-plane libration angle [66]. Then, with this new virtual signal, they developed a controller that with a PD structure to stabilize the system. Although the approach is unique, the response of the system is relatively poor as compared to other controllers in the literature. The deployment times were on the order of 5~10 orbits and they did not plot the control input to the system.

Kang and Zhu developed a novel control law using an artificial potential energy function and dissipative function [67]. Furthermore, constraints on control input and nonnegative deployment velocity were introduced via optimal control.

Wen et al. proposed a model predictive controller for the deployment and retrieval of space tethers [68]. In their controller, they transformed the nonlinear optimal control problem into a series of linear control problems which reduced the computational complexity significantly. Furthermore, through the use of optimal control, they were able to incorporate the positive tension constraint into the problem directly.

Yu et al. developed an analytic controller under a flexible tether model [69]. They assumed the tether to be a massless elastic rod as opposed to the common assumption of massless rigid rod. This introduced the strain of the tether into the dynamic equations. The controller can stabilize the system even under a fully flexible model however, it appears that the out-of-plane angle is also stabilized by the controller. This is a surprising result that may have arose from either the flexible model, eccentric orbit, or a combination of the two.

Although in most applications, it is desirable to stabilize the tether along the local vertical, there may be a need for the tether to maintain a periodic oscillation about the local vertical. Shi et al. developed a sliding mode controller that is able to stabilize periodic motion about the local vertical in elliptic orbits [70].

Zakrzhevskii proposed an interesting approach to the deployment problem by relating the tether length to the angular momentum of the tether [71] [72]. The tether length is controlled to purposefully change the angular momentum under the gravitational moment until the tether is aligned with the local vertical. The controller was simulated with an elastic tether in a circular orbit, but it would be interesting to see the performance under disturbances and model uncertainties as the controller lacked feedback terms and there was no proof of stability.

2.3 Nonnegative Length Rate During Deployment

Liu et al. first tackled the problem of the positive velocity constraints for the tether deployment process [15]. They designed a reference trajectory with the desirable properties and then used a trajectory tracking controller to achieve the objective. Furthermore, they also incorporated a pulse-width pulse-frequency (PWPF) modulated signal on the control input to simply the actuator. Although some responses have oscillatory motion with the use of the PWPF signal, overall, the deployment is fast, and the constraints are satisfied. The authors later used a similar approach to constrain the maximum libration angle [73].

2.4 Ground Based Experiments

There have been a few platforms to test the deployment of space tether technologies. Olivieri et al. demonstrated their test campaign in partnership with ESA's science programs ("Fly your Thesis" and "Drop your Thesis") [74]. The programs allow students to leverage some of ESA's facilities and equipment such as parabolic flights and drop towers to emulate the micro-gravity environment of space. However, their experiments lacked the presence of the Coriolis force which is a vital component of tether dynamics.

Bindra and Zhu developed an inclinable air-bearing turntable [75]. In their testbed, they attempted to recreate the forces seen in orbit including the Coriolis force. Simulation results were compared with experiments and the results were promising.

Yu et al. demonstrated tether deployment with an analytical control law on an air-bearing table [69]. They used thrusters on the satellite simulators to emulate the forces the system would experience in space such as Coriolis and microgravity and then used tension control to control the tether deployment.

2.5 MOTIVATION AND PROPOSED METHODOLOGY

The TSS system has been studied extensively, both from a dynamics and control theory perspective. Beginning with the simplest of models (dumbbell), academics have slowly relaxed assumptions to introduce more degrees of freedom and added various external forces/effects just as J2 perturbation, atmospheric drag, etc. From a controller standpoint, the model has been mostly limited to the simple planar dumbbell. This is a result of its simplicity as well as its effectiveness. As mentioned in Chapter 1, Section 1, two orbital missions relied on this simple model to achieve closed-loop controlled deployment of the TSS with impressive results.

From Table 1, it is evident that the spring and brake type deployment mechanism is the simplest and most popular choice. However, the literature does not address the key constraint of this mechanism within the controller development. In this mechanism, the system is provided an initial impulse via the spring, and then the brake is used to slow the deployment velocity and control the tether deployment profile. As such, the tether deployment velocity throughout this deployment process must be non-negative. Furthermore, all feasible controllers must maintain non-negative tension in the tether as well. This thesis will directly address this constraint in the controller development.

Many of the existing control strategies assume full-state feedback. In practice, this may not be feasible especially in the context of nanosatellites. The concept of observers and their applications to the TSS needs to be explored. This thesis will provide a couple approaches to designing observers for the TSS and analyze their behavior.

The proposed methodology described in Section 1.4 is shown in the block diagram below.

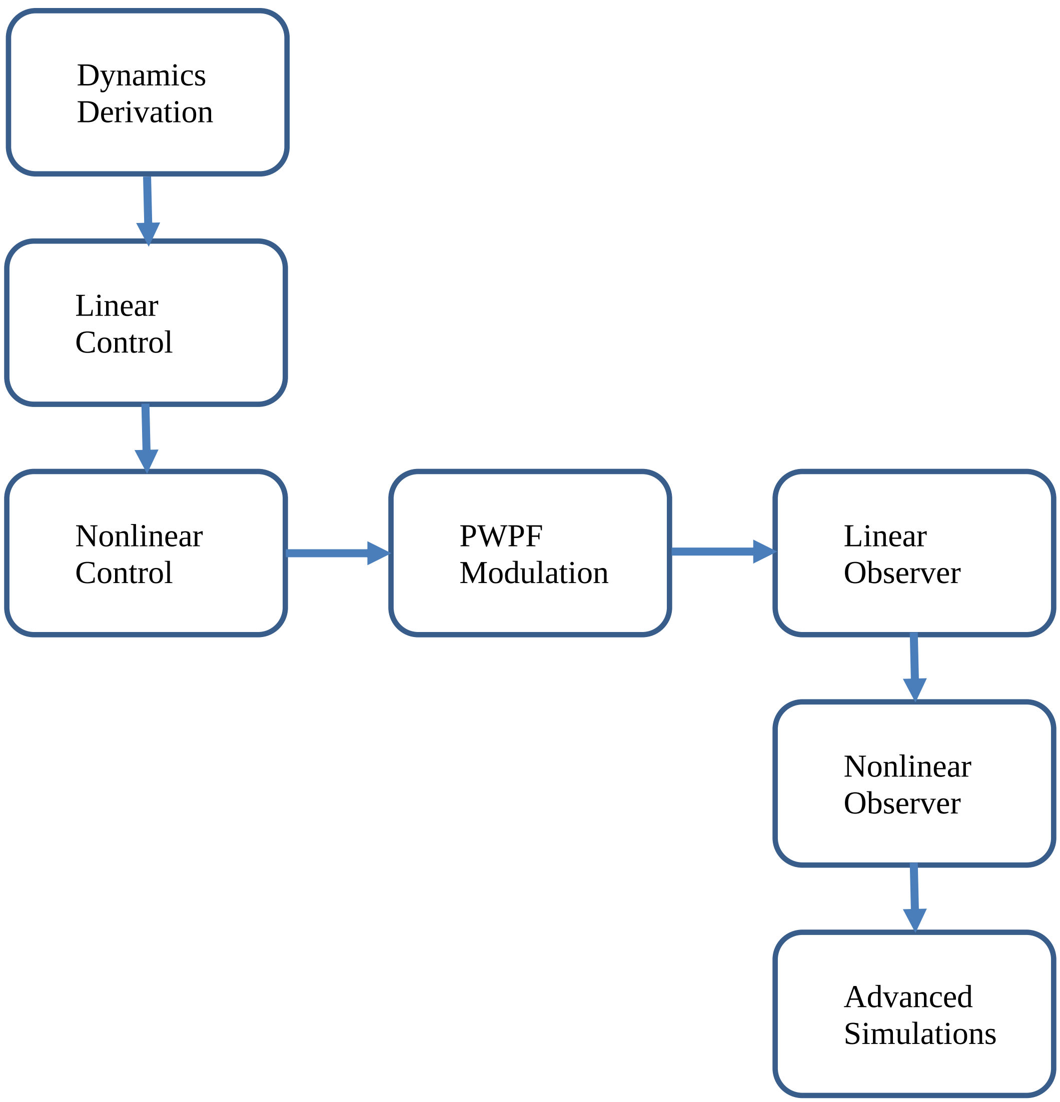

Figure 2.2 Proposed Methodology

Chapter 3 DYNAMICS OF SPACE TETHER SYSTEM

Summary: In this chapter, the space tether system will be simplified to the "dumbbell" model. Dynamic equations of the dumbbell will be derived, and extensions of the model will be briefly discussed. Specifically, emphasis on the applicability to nanosatellites will be analyzed and potential for future work will be outlined. Observability and controllability will be examined to validate the main results presented later in this thesis. Finally, the dynamics of the TSS will be analyzed to gain some useful insights into the system.

3.1 DERIVATION OF THE DUMBBELL MODEL

The dynamics of the deployment of tether system has been studied extensively throughout the literature [76] [30] [77] [78]. However, in practical applications and control law development, the "dumbbell" model of the system is sufficient [29]. In this model, the tether is assumed straight, inextensible and massless. The spacecraft or satellites attached to the ends of tether will be simplified as lumped masses with their attitude dynamics ignored, because the tether length is typically orders of magnitude greater than the dimensions of spacecraft.

Consider the TSS in a circular orbit of Earth shown Figure 3.1. Here, a circular orbit was chosen since it has a stable equilibrium whereas elliptic orbits do not. It is composed of two point masses m_1 and m_2 which are connected by a massless inextensible tether of varying length l orbiting around the Earth. The assumption provides a simple and convenient way of determining the location of the center of mass M of the system.

However, although $m_1, m_2 \gg m_t$, where m_t is the mass of the tether, is a reasonable assumption, the rigidity of the tether requires more justification. In reality, the tether has elastic deformations as it twists, stretches and bends, however, the tension in the tether is relatively small and the resulting elastic potential energy is negligible compared to the kinetic energy of the system. Furthermore, we assume (validated in simulation) that the tether is taut throughout the deployment. Nonetheless, for simplicity and in conjunction with the premise of an active control law where the tension in the tether is maintained, practical dynamics of this system can be derived. For detailed and practical engineering design, an elastic tether should be used and there have been a lot of work in the literature on this subject and is omitted from the scope of this thesis.

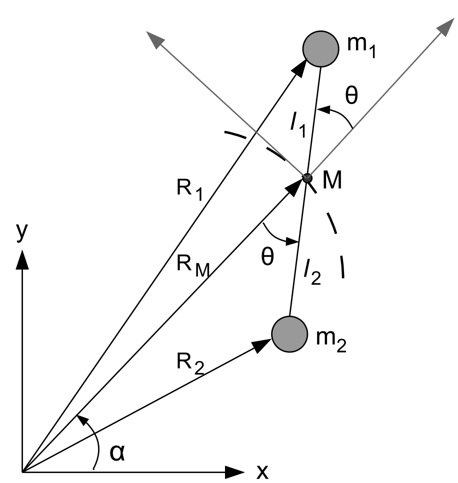

Figure 3.1 Tether Dumbbell Model.

The last assumption is that the out-of-plane libration dynamics is neglected because studies have shown that due to the weak coupling between in-plane and out-of-plane dynamics [32], the latter cannot be controlled through tension, and, relatively small initial conditions will produce relatively small periodic oscillations around the equilibrium point.

There are two main coordinate systems used for the TSS. The most popular choice is Polar coordinates, however, Cartesian coordinates have also been used [26]. This may be attributed to the resemblance of the motion of the TSS system to a simple pendulum. These co-ordinate systems are typically defined in the orbital frame since the main concern is the relative motion of the satellites with respect to the center of mass.

Let $\mathbf{R_1}, \mathbf{R_2}, \mathbf{R_M}$ be the vectors from the center of the Earth to masses m_1, m_2 and the center of mass M respectively. Let α, θ represent the true anomaly of the center of mass motion and the angle the tether makes with respect to the local vertical (angle measures positive in counter-clockwise direction). Finally, let $\boldsymbol{l}_1, \boldsymbol{l}_2$ represent the vectors from the center of mass to each point mass and let $\boldsymbol{l} = \boldsymbol{l}_1 + \boldsymbol{l}_2$ be the total length of the tether.

The dynamics of TSS will be derived by the Lagrange equation. Consider the equations of the form,

$$\frac{d}{dt}\frac{\partial T}{\partial \dot{q}_i} - \frac{\partial T}{\partial q_i} + \frac{\partial V}{\partial q_i} = Q_i \tag{3.1}$$

where T, V are the kinetic and potential energies of the system, $q_i, \dot{q}_i$ are the generalized coordinates and their time derivatives, and Q_i are the generalized forces.

From Figure 3.1, we have the following kinematic relationship

$$\begin{aligned} \mathbf{R_1} &= \left(R_M \cos\alpha + l_1 \cos\left(\alpha+\theta\right)\right) i + \left(R_M \sin\alpha + l_1 \sin\left(\alpha+\theta\right)\right) j \\ \mathbf{R_2} &= \left(R_M \cos\alpha - l_2 \cos\left(\alpha-\theta\right)\right) i + \left(R_M \sin\alpha - l_2 \sin\left(\alpha-\theta\right)\right) j \end{aligned} \tag{3.2}$$

where i, j are the unit vectors along the x, y axes respectively.

Taking the time derivative of above equations yields,

$$\begin{aligned}
\dot{\mathbf{R}}_{\mathbf{1}} &= \left(-R_M\dot{\alpha}\sin\alpha + \dot{l}_1\cos\left(\alpha+\theta\right) - l_1\left(\dot{\alpha}+\dot{\theta}\right)\sin\left(\alpha+\theta\right)\right)i \\
&\quad + \left(R_M\dot{\alpha}\cos\alpha + \dot{l}_1\sin\left(\alpha+\theta\right) + l_1\left(\dot{\alpha}+\dot{\theta}\right)\cos\left(\alpha+\theta\right)\right)j \\
\dot{\mathbf{R}}_{\mathbf{2}} &= \left(-R_M\dot{\alpha}\sin\alpha - \dot{l}_2\cos\left(\alpha-\theta\right) + l_2\left(\dot{\alpha}-\dot{\theta}\right)\sin\left(\alpha-\theta\right)\right)i \\
&\quad + \left(R_M\dot{\alpha}\cos\alpha - \dot{l}_2\sin\left(\alpha-\theta\right) - l_2\left(\dot{\alpha}-\dot{\theta}\right)\cos\left(\alpha-\theta\right)\right)j
\end{aligned} \tag{3.3}$$

The kinetic energy T can be expressed as,

$$\begin{aligned}
T &= \frac{1}{2}\left(m_1\dot{R}_1^2 + m_2\dot{R}_2^2\right) \\
&= \frac{m_1}{2}\left(R_M^2\dot{\alpha}^2 + l_1^2\left(\dot{\alpha}+\dot{\theta}\right)^2 + \dot{l}_1^2 + 2R_M\dot{\alpha}\dot{l}_1\sin\theta + 2R_M\dot{\alpha}l_1\left(\dot{\alpha}+\dot{\theta}\right)\cos\theta\right) \\
&\quad + \frac{m_2}{2}\left(R_M^2\dot{\alpha}^2 + l_2^2\left(\dot{\alpha}-\dot{\theta}\right)^2 + \dot{l}_2^2 + 2R_M\dot{\alpha}\dot{l}_2\sin\theta - 2R_M\dot{\alpha}l_2\left(\dot{\alpha}-\dot{\theta}\right)\cos\theta\right)
\end{aligned} \tag{3.4}$$

The distance to each point mass R_1, R_2 is,

$$\begin{aligned}
R_1 &= \left(R_M + l_1\cos\theta\right)^2 + \left(l_1\sin\theta\right)^2 \\
R_2 &= \left(R_M - l_2\cos\theta\right)^2 + \left(l_2\sin\theta\right)^2
\end{aligned} \tag{3.5}$$

Therefore, the potential energy V can be expressed as,

$$V = -\mu\left(\frac{m_1}{R_1} + \frac{m_2}{R_2}\right) = -\mu\left(\frac{m_1}{\sqrt{R_M^2 + 2l_1R_M\cos\theta + l_1^2}} + \frac{m_2}{\sqrt{R_M^2 - 2l_2R_M\cos\theta + l_2^2}}\right) \tag{3.6}$$

For a circular orbit, the radius to the center of mass R_M is constant. Furthermore, the orbital angular rate $\Omega = \dot{\alpha}$ is constant as well, specifically,

$$\Omega = \sqrt{\frac{\mu}{R_M^3}} \tag{3.7}$$

Therefore, the generalized coordinates for the TSS become,

$$\mathbf{q} = \begin{bmatrix} l_1 & l_2 & \theta \end{bmatrix} \tag{3.8}$$

Before deriving the dynamics equations, it is worthwhile to perform some simplifications on the gravity terms. Consider the partial derivatives of the generalized coordinates with respect to the gravitational potential energy,

$$
\begin{aligned}
\frac{\partial V}{\partial l_1} &= \frac{\mu m_1\left(R_M \cos\theta + l_1\right)}{\sqrt{\left(R_M^2 + 2l_1R_M \cos\theta + l_1^2\right)^3}} \\
\frac{\partial V}{\partial l_2} &= \frac{-\mu m_2\left(R_M \cos\theta + l_2\right)}{\sqrt{\left(R_M^2 - 2l_2R_M \cos\theta + l_2^2\right)^3}} \\
\frac{\partial V}{\partial \theta} &= \frac{-\mu m_1 R_M l_1 \sin\theta}{\sqrt{\left(R_M^2 + 2l_1R_M \cos\theta + l_1^2\right)^3}} + \frac{\mu m_2 R_M l_2 \sin\theta}{\sqrt{\left(R_M^2 - 2l_2R_M \cos\theta + l_2^2\right)^3}}
\end{aligned}
\tag{3.9}
$$

Now consider just the first partial derivative $\partial V / \partial l_1$,

$$
\frac{\partial V}{\partial l_1} = \frac{\mu m_1\left(R_M \cos\theta + l_1\right)}{\sqrt{\left(R_M^2 + 2l_1R_M \cos\theta + l_1^2\right)^3}} = \frac{\mu m_1 R_M\left(\cos\theta + \frac{l_1}{R_M}\right)}{\sqrt{\left(R_M^2\left(1 + 2\frac{l_1}{R_M}\cos\theta + \left(\frac{l_1}{R_M}\right)^2\right)\right)^3}}
$$

Let $a = {l_1}/{R_M}$, then,

$$
\frac{\partial V}{\partial l_1} = \frac{\mu m_1\left(\cos\theta + a\right)}{R_M^2\sqrt{\left(1 + 2a\cos\theta + a^2\right)^3}} \tag{3.10}
$$

Assuming $a \ll 1$, taking the Maclaurin series of (3.10) and substituting (3.7) yield

$$
\frac{\partial V}{\partial l_1} = m_1 R_M \Omega^2\left(\cos\theta + \frac{l_1}{R_M}\left(1 - 3\cos^2\theta\right) + O\left(\frac{l_1}{R_M}\right)^2\right) \tag{3.11}
$$

Proceeding analogously for the other partial derivatives yield,

$$
\begin{aligned}
\frac{\partial V}{\partial l_2} &= m_2 R_M \Omega^2 \left(-\cos\theta + \frac{l_2}{R_M}\left(1 - 3\cos^2\theta\right) + O\left(\frac{l_2}{R_M}\right)^2 \right) \\
\frac{\partial V}{\partial \theta} &= -m_1 R_M l_1 \Omega^2 \sin\theta \left(1 - 3\frac{l_1}{R_M}\cos\theta + O\left(\frac{l_1}{R_M}\right)^2 \right) \\
&\quad + m_2 R_M l_2 \Omega^2 \sin\theta \left(1 + 3\frac{l_2}{R_M}\cos\theta + O\left(\frac{l_2}{R_M}\right)^2 \right)
\end{aligned} \tag{3.12}
$$

After computing the remaining terms of (3.1), assuming no aerodynamic drag forces, the tension in the tether is consistent (i.e., $Q_{l_1} = Q_{l_2} = Q_l$) and, the fact that no torque acts at the point of tether attachment, the dynamics equations of the system becomes,

$$
\begin{aligned}
\ddot{l}_1 &= l_1\left(\dot{\theta}^2 + 2\Omega\dot{\theta} + 3\Omega^2\cos^2\theta\right) + \frac{Q_l}{m_1} \\
\ddot{l}_2 &= l_2\left(\dot{\theta}^2 - 2\Omega\dot{\theta} + 3\Omega^2\cos^2\theta\right) + \frac{Q_l}{m_2} \\
\ddot{\theta} &= \frac{m_1 l_1^2}{\left(m_1 l_1^2 + m_2 l_2^2\right)}\left(-2\frac{\dot{l}_1}{l_1}\left(\dot{\theta} + \Omega\right) - 3\Omega^2\sin\theta\cos\theta \right) \\
&\quad + \frac{m_2 l_2^2}{\left(m_1 l_1^2 + m_2 l_2^2\right)}\left(-2\frac{\dot{l}_2}{l_2}\left(\dot{\theta} - \Omega\right) - 3\Omega^2\sin\theta\cos\theta \right)
\end{aligned} \tag{3.13}
$$

Obviously, these equations describe the relative motion of each mass with respect to the center of mass of the system. Further simplification can be made by assuming $m_1 \gg m_2$. Given that $l = l_1 + l_2$, Eq. (3.13) can be simplified as,

$$
\begin{aligned}
\ddot{l} &= l_1\left(\dot{\theta}^2 + 2\Omega\dot{\theta} + 3\Omega^2\cos^2\theta\right) \\
&\quad + l_2\left(\dot{\theta}^2 - 2\Omega\dot{\theta} + 3\Omega^2\cos^2\theta\right) + \frac{\left(m_1 + m_2\right)Q_l}{m_1 m_2} \\
\ddot{\theta} &= \frac{m_1 l_1^2}{\left(m_1 l_1^2 + m_2 l_2^2\right)}\left(-2\frac{\dot{l}_1}{l_1}\left(\dot{\theta} + \Omega\right) - 3\Omega^2\sin\theta\cos\theta\right) \\
&\quad + \frac{m_2 l_2^2}{\left(m_1 l_1^2 + m_2 l_2^2\right)}\left(-2\frac{\dot{l}_2}{l_2}\left(\dot{\theta} - \Omega\right) - 3\Omega^2\sin\theta\cos\theta\right)
\end{aligned}
\tag{3.14}
$$

Then, the location of the center of mass of this system,

$$
\boldsymbol{R}_{CM} = \frac{m_1\boldsymbol{l_1} + m_2\boldsymbol{l_2}}{\left(m_1 + m_2\right)} \approx \boldsymbol{R}_1 \tag{3.15}
$$

roughly coincides with m_1 (i.e., $l_1 \cong 0 \Rightarrow l_2 \cong l$). Then, Eq. (3.14) is further reduced to,

$$
\begin{aligned}
\ddot{l} &= l\left(\dot{\theta}^2 + 2\Omega\dot{\theta} + 3\Omega^2\cos^2\theta\right) + \frac{\left(m_1 + m_2\right)Q_l}{m_1 m_2} \\
\ddot{\theta} &= -2\frac{\dot{l}}{l}\left(\dot{\theta} + \Omega\right) - 3\Omega^2\sin\theta\cos\theta
\end{aligned}
\tag{3.16}
$$

This is the standard form of the tether dumbbell model for in-plane libration, which is commonly found in the literature. This is also the model used for controller development in this thesis. It is important to note that the dynamics equations in (3.14) represent a system with arbitrary mass ratios. Controllers developed for this system are more general and is left outside the scope of this thesis. Presumably, (3.15) is a key relationship that would be part of the scaling factor from controllers developed in this thesis to the more general case.

3.2 Extensions of Dumbbell Model and Applicability to Tethered Nanosatellites

There are many assumptions made in the derivation of the dumbbell model. By relaxing the assumptions, a more complete model can be obtained however, at the cost of increasing complexity. Standard extensions of the model were discussed in the literature review. If the system is composed of two satellites of comparable masses, Eq. (3.13) would be an appropriate model for controller development. However, if the mass of the tether is now comparable to the satellite masses, then a model that accounts for the variation in center of mass would need to be developed. Similarly, if the length and accordingly cross-sectional area of the tether is significantly large, then atmospheric drag needs to be included. A simplified model of atmospheric drag was studied by Zhe et al. and they showed that a simple controller can effectively stabilize the system with consideration of atmospheric drag [79]. However, it is important to note that atmospheric drag would need to be a function of the deployed tether length which would make controller development much more difficult. Inclusion of these conditions is necessary for a tethered nanosatellite system and is omitted in this thesis and left for future work. Instead, this thesis assumes that the subsatellite is a nanosatellite and the main satellite is orders of magnitude larger in mass. This allows the assumptions in the standard dumbbell to be valid and proceed with the dynamic analysis and controller development.

3.3 DUMBBELL MODEL IN NON-DIMENSIONLESS FORM

The system in Eq. (3.16) can be transformed into a more convenient form suitable for controller development. It is advantageous to convert the system into a non-dimensionless form, develop the controllers then apply appropriate scaling factors to achieve desired results and performance.

Let $m_e = \dfrac{m_1 m_2}{\left(m_1 + m_2\right)}$ be the effective mass of the system, $\alpha = \Omega t$ the true anomaly, and $\xi_0 = {l}/{l_{\max}}$ the dimensionless length of tether where $l_{\max}$ is the maximum desired tether length. Denote $()'$ as the derivate with respect to α . Then, Eq. (3.16) can be rewritten in a dimensionless form as,

$$
\begin{aligned}
\xi_0'' &= \xi_0\left(\left(\theta'+1\right)^2 - 1 + 3\cos^2\theta\right) - \widehat{T} \\
\theta'' &= -2\left(\frac{\xi_0'}{\xi_0}\right)\left(\theta'+1\right) - 3\sin\theta\cos\theta
\end{aligned}
\tag{3.17}
$$

where $\widehat{T} = {Q_l}/{m_e \Omega^2 l_{\max}}$ is the dimensionless tension. In this configuration, the equilibrium point of Eq. (3.17) is the set $\left\{\xi_0, \xi_0', \theta, \theta' \in \mathbf{x} \mid \xi_0 = 1 \wedge \xi_0' = \theta = \theta' = 0\right\}$. Here, $\mathbf{x}$ is the state space of the system. It is also convenient to translate the system such that the origin is the equilibrium point. Define $\xi = \xi_0 - 1$, Eq. (3.17) becomes,

$$
\begin{aligned}
\xi'' &= \left(1+\xi\right)\left(\left(\theta'+1\right)^2 - 1 + 3\cos^2\theta\right) - \widehat{T} \\
\theta'' &= -2\left(\frac{\xi'}{1+\xi}\right)\left(\theta'+1\right) - 3\sin\theta\cos\theta
\end{aligned}
\tag{3.18}
$$

3.4 DUMBBELL MODEL IN STATE-SPACE FORM

Define the state vector in the state space as

$$
\mathbf{x} = \left[\xi \quad \xi' \quad \theta \quad \theta'\right]^T \tag{3.19}
$$

Then, Eq. (3.18) can be expressed as,

$$
\begin{aligned}
\dot{x}_1 &= x_2 \\
\dot{x}_2 &= (1+x_1)\left[(1+x_4)^2 - 1 + 3\cos^2 x_3\right] - \hat{T} \\
\dot{x}_3 &= x_4 \\
\dot{x}_4 &= -2\left(\frac{x_2}{1+x_1}\right)(1+x_4) - 3\sin x_3 \cos x_3
\end{aligned}
\tag{3.20}
$$

Obviously, this system is highly nonlinear and therefore difficult to analyze and develop controllers. Indeed, the system can be linearized in the vicinity of the equilibrium and the model reduces even further to,

$$
\begin{aligned}
\dot{x}_1 &= x_2 \\
\dot{x}_2 &= 3x_1 + 2x_4 - \hat{T} \\
\dot{x}_3 &= x_4 \\
\dot{x}_4 &= -2x_2 - 3x_3
\end{aligned}
\tag{3.21}
$$

The system in both the linear and nonlinear state-space form will be commonly used throughout this thesis in the development of control laws.

3.5 OBSERVABILITY AND CONTROLLABILITY

The tether dumbbell system is clearly a two-degree of freedom, underactuated, and second-order system. Therefore, observability and controllability must first be analyzed. In this thesis, the local behavior will be discussed through linearization as the application of nonlinear tools for this analysis is outside the scope. Consider the system in the following form,

$$
\begin{aligned}
\dot{\mathbf{x}} &= \mathbf{A}\mathbf{x} \\
\mathbf{y} &= \mathbf{C}\mathbf{x}
\end{aligned}
\tag{3.22}
$$

where,

$$\mathbf{A} = \begin{bmatrix} 0 & 1 & 0 & 0 \\ 3 & 0 & 0 & 2 \\ 0 & 0 & 0 & 1 \\ 0 & -2 & -3 & 0 \end{bmatrix}, \mathbf{C} = \begin{bmatrix} 1 & 0 & 0 & 0 \end{bmatrix}$$

and $\mathbf{y}$ is the output vector. Complete observability of the system in Eq. (3.22) can be determined if and only if the observability matrix,

$$\begin{bmatrix} \mathbf{C}^* & | & \mathbf{A}^*\mathbf{C}^* & | & \cdots & | & (\mathbf{A}^*)^{n-1}\mathbf{C}^* \end{bmatrix} \tag{3.23}$$

is of full rank. Here the $(\ )^*$ denotes the conjugate transpose. Proceeding accordingly, the observability matrix for the linearized tether dumbbell system is,

$$\begin{bmatrix} 1 & 0 & 3 & 0 \\ 0 & 1 & 0 & -1 \\ 0 & 0 & 0 & -6 \\ 0 & 0 & 2 & 0 \end{bmatrix}$$

which is obviously of rank 4. Therefore, the system is completely observable. Interestingly, using measurements of $x_1 = \xi$ (length of the tether) alone, we can deduce the remaining states through proper observer design. This is highly advantageous as measurement of the length rate directly may be difficult/noisy and measurements of the libration angle and its rate may be expensive.

Analogously, controllability can be determined if and only if the controllability matrix is of full rank. Consider now an extension of Eq. (3.22) such that the tether system in the form,

$$\begin{aligned} \dot{\mathbf{x}} &= \mathbf{A}\mathbf{x} + \mathbf{B}u \\ \mathbf{y} &= \mathbf{C}\mathbf{x} \end{aligned} \tag{3.24}$$

where,

$$\mathbf{B} = \begin{bmatrix} 0 \\ -1 \\ 0 \\ 0 \end{bmatrix}$$

The controllability matrix can be computed as,

$$\begin{bmatrix} \mathbf{B} & | & \mathbf{AB} & | & \cdots & | & \mathbf{A}^{n-1}\mathbf{B} \end{bmatrix} = \begin{bmatrix} 0 & -1 & 0 & 1 \\ -1 & 0 & 1 & 0 \\ 0 & 0 & 2 & 0 \\ 0 & 2 & 0 & -8 \end{bmatrix} \tag{3.25}$$

which is rank 4 as well, therefore, the system is completely controllable as well.

3.6 DYNAMIC ANALYSIS OF TETHER SPACE SYSTEM

Analysis of the dynamics of the system is crucial in understanding its intrinsic behavior. Again, local behavior will be studied, and the global nonlinear behavior is omitted for future work. The theory of linear systems provides many tools to analyze this system.

Consider the open-loop poles of the system in Eq. (3.21),

$$\begin{aligned} p_1 &= -1.2671 \\ p_2 &= 1.2671 \\ p_3 &= 2.3676i \\ p_4 &= -2.3676i \end{aligned} \tag{3.26}$$

Obviously, the system is unstable because the pole p_2 is in the right-half plane. Furthermore, we have poles p_3 and p_4 that sit on the imaginary axis cause an oscillatory response in the output as shown in Figure 3.2 below. The initial conditions are shown in

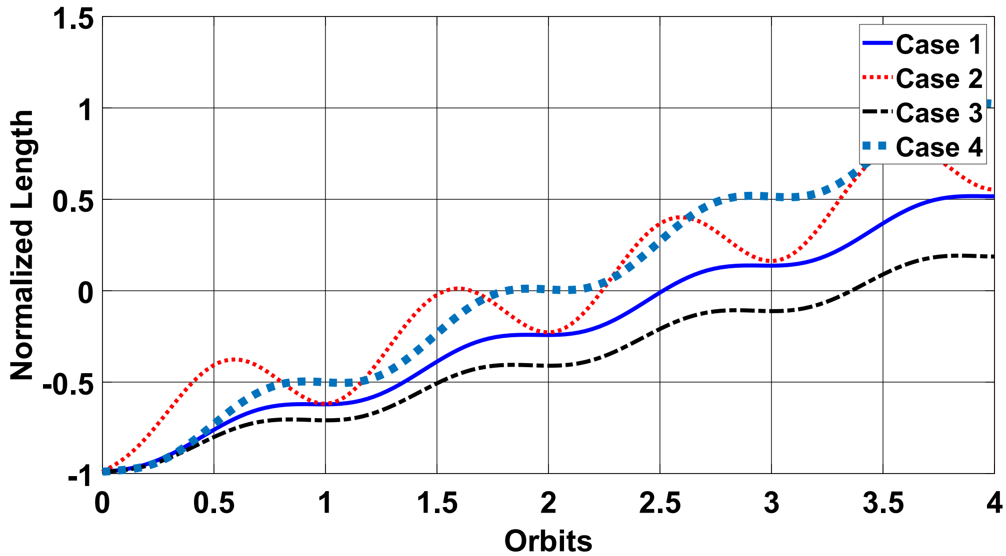

Figure 3.2 Open Loop Response of deployed tether length vs orbit numbers under various initial conditions.

Table 3-1 Initial Conditions for Open Loop Response

Initial Conditions	Case 1	Case 2	Case 3	Case 4
x_{10}	-0.99	-0.99	-0.99	-0.99
x_{20}	0.1	1	1	1
x_{30}	0	0	$\frac{\pi}{4}$	$-\frac{\pi}{8}$
x_{40}	0	0	$\frac{\pi}{4}$	$-\frac{\pi}{4}$

Further examination of the root locus yields greater insight into the system. The system in (3.24) is transformed into the following transfer function,

$$G_p(s) = \frac{Y(s)}{U(s)} = \frac{-s^2-3}{s^4+4s^2-9} \tag{3.27}$$

where $Y(s)$ is the output x_1 (length of tether) and $U(s)$ is the control input. The root locus of (3.27) is plotted in Figure 3.3 below,

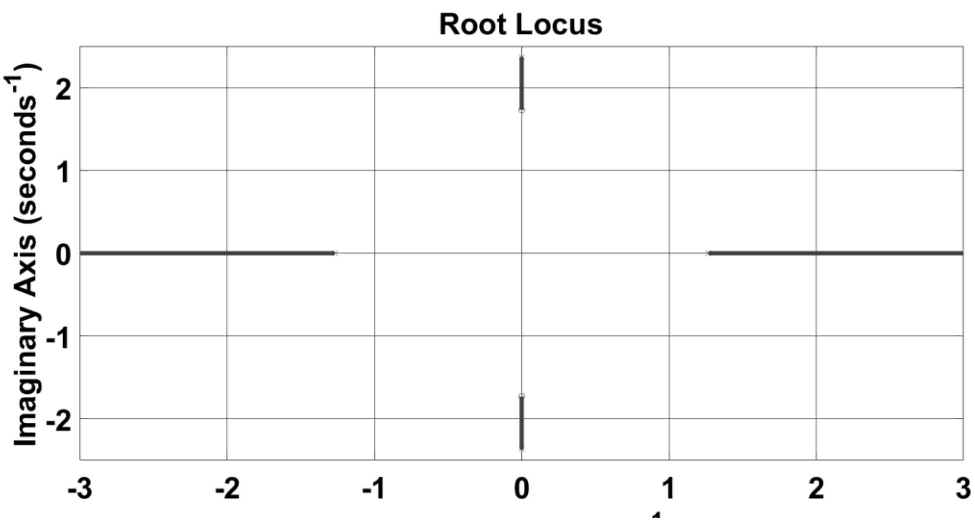

Figure 3.3 Root Locus Plot of Tether Dumbbell System

Given the open-loop system, the root locus indicates the location of the closed loop poles as a function of control gain K. This implies that a proportional control gain would not suffice to stabilize the system. Indeed, a proportional plus a derivative term is necessary to stabilize the tether dumbbell system as this would "shift/pull" the root locus to the left. In the next chapter, it will be shown that a simple PD control is sufficient in controlling the system. Furthermore, the root locus cannot be arbitrarily shifted to the left because of the open-loop zeros on the imaginary axis. This will ultimately result in a pair of dominant closed-loop poles to reside near the imaginary axis which implies a small natural frequency of the system (i.e., a slow-response in the output; slow deployment).

3.7 EQUILIBRIA OF TETHER SYSTEM

Consider Eq. (3.20). The equilibrium of the system can be obtained by solving for the states of the system that yield zero dynamics (i.e., $\dot{x}_1 = \dot{x}_2 = \dot{x}_3 = \dot{x}_4 = 0$). Therefore,

$$\begin{aligned} \dot{x}_1 &= 0 \Rightarrow x_2 = 0 \\ \dot{x}_3 &= 0 \Rightarrow x_4 = 0 \end{aligned} \tag{3.28}$$

Using (3.28) yields

$$\dot{x}_4 = 0 \Rightarrow -3\sin x_3 \cos x_3 = 0 \tag{3.29}$$

which implies $x_3 = \left\{0, \pi/2, \pi, 3\pi/2\right\}$. Finally,

$$\dot{x}_2 = 0 \Rightarrow 3(1 + x_1)\cos^2 x_3 - \hat{T} = 0 \tag{3.30}$$

If $x_3 = 0$ or $x_3 = \pi$, then

$$3x_1 + 3 - T = 0 \tag{3.31}$$

Therefore, the equilibrium length of the tether depends on the final tension. The desired equilibrium is such that $x_1 = 0$ (since the equations of motion were translated), therefore, $T = 3$. However, consider the case when $x_3 = \pi/2$ or $x_3 = 3\pi/2$. This implies that $T = 0$, which although is theoretically possible, infers that the masses have independent motion (i.e., not constrained by the tether) and the tether can be of any length. It can be shown that these equilibria when the tether is horizontal is unstable.

Chapter 4 DEPLOYMENT CONTROL LAW OF TETHERED SPACE SYSTEM

Summary: In this Chapter, the tether deployment problem is introduced followed by a brief overview of deployment mechanisms and measurement systems. Then, linear and nonlinear controllers are developed, followed by a modulation technique (PWPF) that can be used to simplify the actuator. For each controller, case studies are presented and analyzed with a roughly common set of initial conditions to make reasonable comparisons.

4.1 PROBLEM STATEMENT

Consider the forces on the tether system as shown in Figure 4.1.

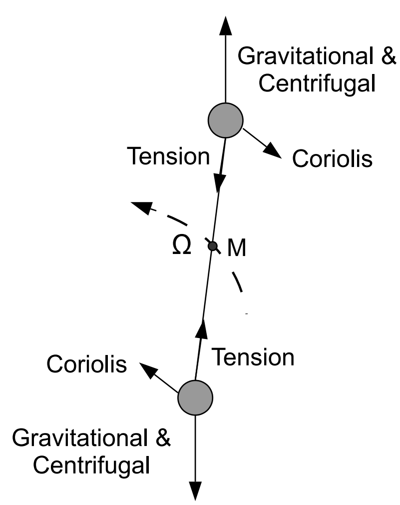

Figure 4.1 Forces on Tether Spacecraft System.

It is important to note that the Coriolis force will be generated during deployment and is proportional to the tether deployment velocity, because the model describes the motion of the system in the orbital (rotating) frame. Neglecting the Coriolis force, the gravitational and centrifugal forces are balanced at the center of mass,

$$\begin{aligned} \frac{GM_e M_M}{R_M^2} &= M_M R_M \omega_M^2 \\ \omega_M^2 &= \frac{GM_e}{R_M^3} \end{aligned} \tag{4.1}$$

where G is the universal gravitational constant, M_e, M_M are the mass of the Earth and mass of the tether system respectively, R_M is the distance from the center of the Earth to the center of mass, and ω_M is the orbital angular velocity of the center of mass M_M. As a result of the tether, the two satellite masses are constrained to have the same orbital angular velocity as the center of mass of the TSS. If the masses were to have independent motion, their orbital angular velocities would be,

$$\begin{aligned} \omega_1^2 &= \frac{GM_e}{\left(R_M + l_1\right)^3} \\ \omega_2^2 &= \frac{GM_e}{\left(R_M - l_2\right)^3} \end{aligned} \tag{4.2}$$

Clearly, the upper mass moves faster than the lower mass of the TSS, This results in a larger centrifugal force at the upper mass (higher altitude) and a smaller centrifugal force at the lower mass (lower altitude). This imbalance, called gravity gradient, yields the balancing tether tension. Furthermore, the resultant force from the tension, centrifugal and gravitational forces yield a resultant torque that attempts to align the tether with the local vertical.

Consider the deployment process in which the tension in the tether is directly controlled. This now implies that we can indirectly control the resultant torque that aligns the tether with the local vertical (i.e., $\theta \to 0$ or $\theta \to \pi$). However, during the deployment process, the Coriolis force causes the tether to move away from the local vertical ($F_c = -2m_i\Omega \times v$; v – tether deployment velocity). Therefore, the tension is sufficient to control both the length of the tether and, the libration angle θ of the tether. However, it is important to note that since the Coriolis force directly depends on the deployment velocity and that the fact that the magnitude of the resultant restoring torque is relatively small, there exists an upper bound on the deployment velocity in order to prevent the tether from wrapping around and/or reaching an undesired equilibrium.

4.2 DEPLOYMENT MECHANISM

The tree structure in Figure 4.2 below depicts the various types of deployment mechanisms. Broadly speaking, they can be categorized into active and passive mechanisms and the deployment is achieved through thrusters or tension control. Indeed, a combination of thrusters and tension control could also be conceived and theoretically would provide the optimal performance. Although conceptually the type of tether used is agnostic to the deployment mechanism, mechanically they would differ significantly.

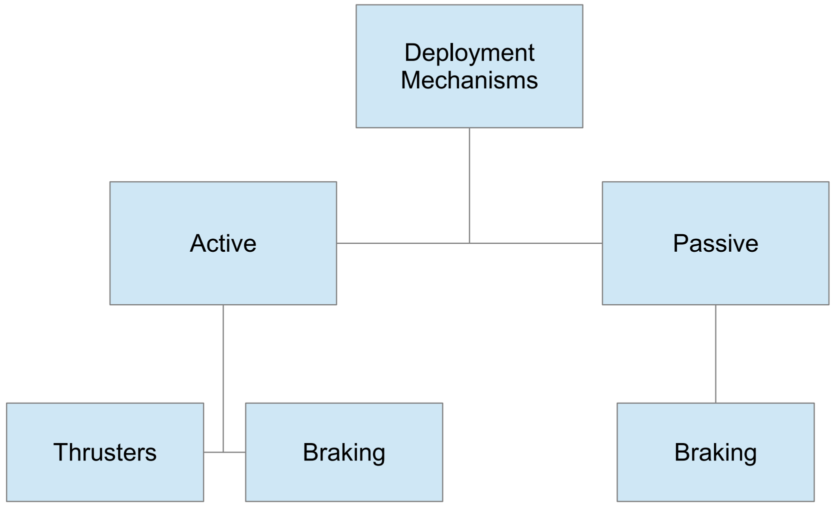

Figure 4.2 Types of Deployment Mechanisms

4.2.1 Actuation with Thrusters

Control of tether deployment has been achieved with the use of thrusters as mentioned in the Introduction in Table 1-1. In this mechanism, thrusters are placed on all three axes to achieve full control of the relative motion of the satellite. There have also been scenarios where thrusters were augmented with tension control to achieve the same objective. The obvious drawback of thrusters is the need for propellant which among others, adds complexity to the assembly, integration and testing (AIT) phase of the mission as well as additional mass and cost. However, depending on the configuration of the thrusters, far superior performance can be achieved in terms of the control objectives and deployment speed/time.

4.2.2 Tension Control Mechanisms

There are two types of tethers that are commonly used, cable and taped. The early developments of tethers and deployment mechanisms were primarily focused on the cable type. Only two missions included closed-loop feedback deployment systems, SEDS-II and YES2 missions. Their deployment mechanisms are depicted in Figure 4.3.

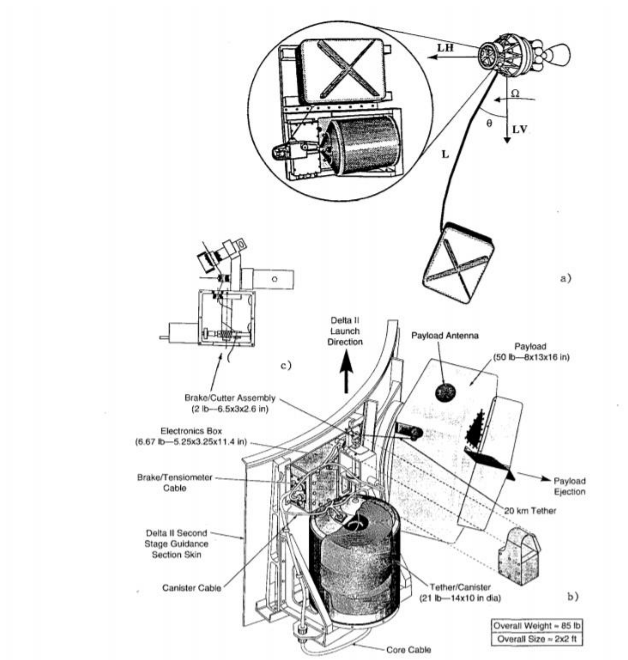

Figure 4.3 SEDS-II Deployment Mechanism [13]

Figure 4.4 YES2 Deployment Mechanism [14]

Interestingly, both the deployers employ the same strategy in which a spring is used to provide an initial impulse and separation velocity, and then a braking mechanism is used to control the deployment process and damp out the kinetic energy provided by the spring. The braking mechanism for the cable type tether is essentially a barber pole in which the number of turns of the tether around the pole controls the friction (braking force) which in turn controls the tension. A closer look at the barber pole braking mechanism for the YES2 mission is shown in Figure 4.5.

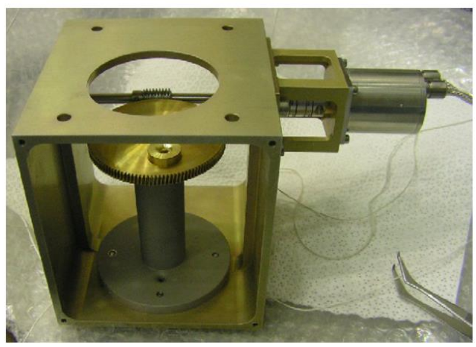

Figure 4.5 YES2 Barber pole [14]

Therefore, the dynamics of the system can be described as in (3.20) and a tension controller can be developed. Then, the tension in the tether is related to the braking force as follows [13],

$$T = \left(T_0 + I\rho\dot{L}^2 A_{rel}^{-E}\right)\exp\left(f\cdot\left|\theta_0 - \theta\right|\right)\exp\left(B\right) \tag{4.3}$$

where T_0 is the minimum tension, I is the inertia of barber pole system, ρ is the linear density of the tether, $\dot{L}$ is the velocity of the tether, $A_{rel} = 1 - A_{sol}L / L_{\max}$, A_{sol} is the tether annulus solidity, L and $L_{\max}$ are the deployed tether length and maximum length of the tether respectively, E is the area exponent, f is the friction coefficient, θ_0 is the null-friction exit angle, θ is the tether libration angle, $B = 2\pi fn$ is the brake parameter and n is the number of turns of brake axle.

The frictional model was developed from experimental data and classical formulas. As such, it carries a significant amount of uncertainty which is unavoidable. Proper characterization of the parameters is required, and practical controllers may include robustness or adaptive terms to increase performance. However, from flight data recorded during these missions, the mechanism performed surprisingly well even under all the uncertainties. This could be largely attributed to the fact that a closed-loop control system was utilized.

A simplified schematic of the YES2 deployment mechanism is shown in Figure 4.6 to get a better understanding of the deployment mechanism. It is important to note that both systems had a tether cut mechanism which is used to sever the tethered payload at the end of deployment which were objectives of the respective missions. However, it has no impact on the deployment process itself.

Yi et al. proposed an adaptive reel mechanism [80]. The mechanism is designed to minimize winding, tumbling and other disturbances experienced during tether deployment and retrieval. The advantage of the reel mechanism is the ability to have positive and negative tether velocities and more general class of controllers are applicable with much faster deployment times. In their paper, their outline the dynamical equations of their mechanism along with some experiments to validate the process.

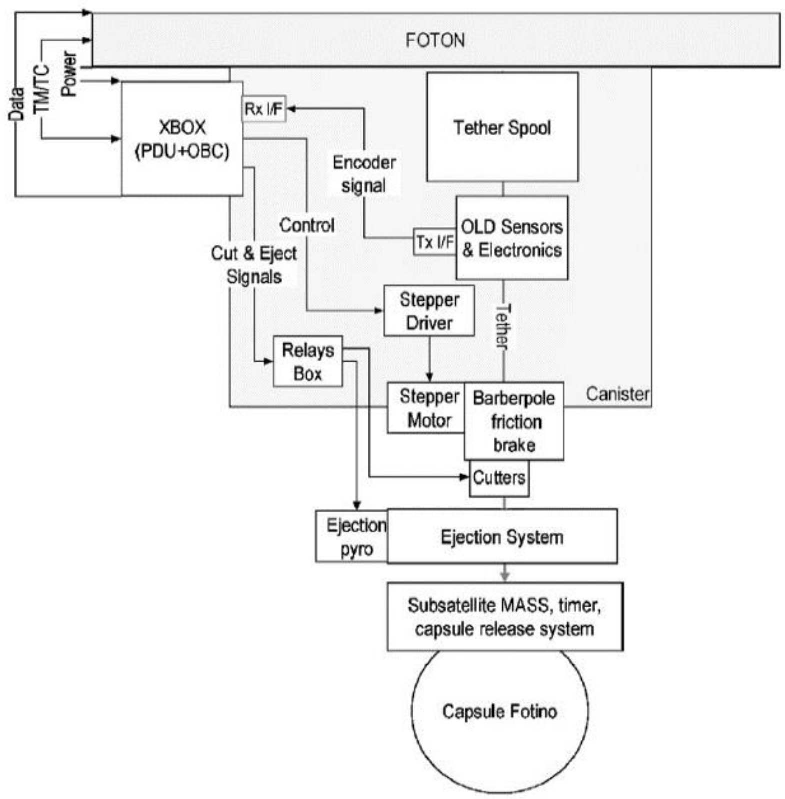

Figure 4.6 YES2 Deployment Schematic Diagram [14]

The tape tether was introduced recently and conceptually, which is very similar to the cable tether. In the tape tether deployment system, there still exists a spring which provides an initial impulse and then a brake is used to control the deployment process. However, the braking mechanism is arguably simpler. Figure 4.7 depicts a braking mechanism for a tape tether. It is important to note that the mechanism shown is actually passive. The top region of folded tether deploys with no control/brake and the final portion is used to slow the tether. However, the brake can be placed at any arbitrary location within the storage box and a stepper motor or solenoid can be used to control the braking force. Indeed, this mechanism suffers similar drawbacks in terms of uncertainty and the need for proper calibration/characterization. Given the success of the alternative mechanism, this design appears promising.

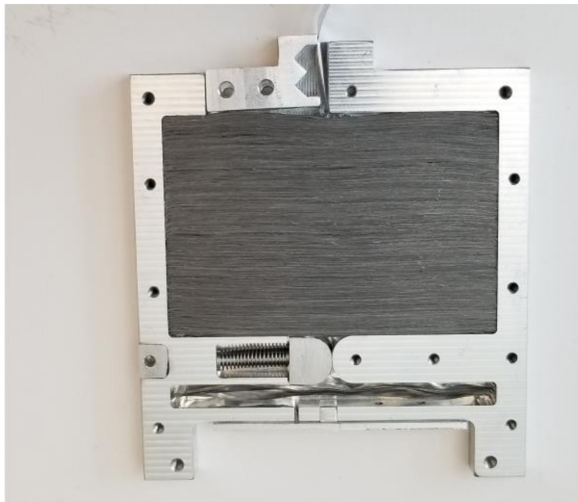

Figure 4.7 Tape Tether Deployment Mechanism.

An important characteristic of these deployment mechanisms is that fundamentally, they do not allow retrieval of the tether. Therefore, the deployment of the tether must be monotonic in length. It is an important property that has been neglected in the literature and previous missions. This thesis aims to directly address this issue within the controller development.

4.3 MEASUREMENT SYSTEMS FOR TETHER DEPLOYMENT

The four states of the tether system are the length, length rate, libration angle and, libration angle rate of the tether. As mentioned earlier, the tether system is observable under the length measurement alone. A simple length measurement system for tape tethers is shown in Figure 4.8.

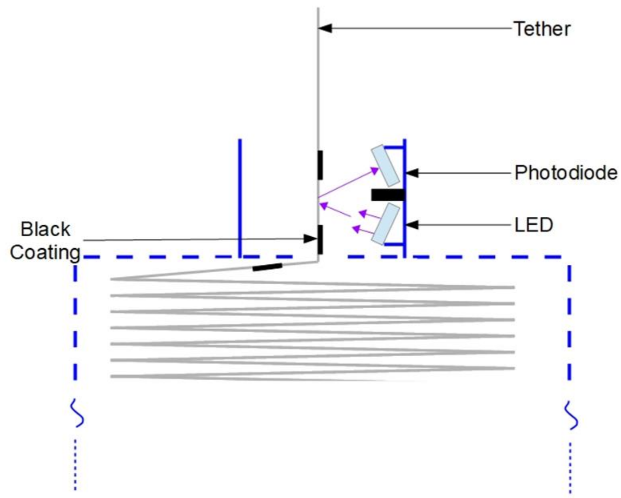

Figure 4.8 Tether Length Measurement System

In this system, a tether made of a highly reflective material such as aluminum is coated with black strips/paint at equally spaced intervals. Then, using a LED and photodiode, we can detect the number of black strips as the tether deploys and infer the total length. Both the hardware and software (computational complexity) are inexpensive, however, the measurements of the length are discrete and appear at non-uniform/time-varying intervals. It can be considered discrete because the rate at which the measurements are collected will be much slower than the desired rate at which the actuators will be controlled. Furthermore, the rate itself is dependent on the tether deployment velocity. If the velocity was constant, the length measurements will arrive at constant intervals. However, the real velocity profile is non-linear and has regions of both acceleration and deceleration. Therefore, the measurements will appear at time-varying intervals.

Although the length measurement is sufficient to estimate the remaining states, more advanced controllers may not perform well with the augmentation of an observer. This is attributed to the insufficient convergence rate of the observer itself. Therefore, it may be necessary to directly measure the remaining states, specifically the libration angle.

Grassi et al. proposed a length measurement system for a cable type tether [81]. They placed IR emitters on the tether spool and IR receivers on the outer canister. As the tether is deployed, the angular rate of the spool is measured, and the length of the deployed tether is inferred.

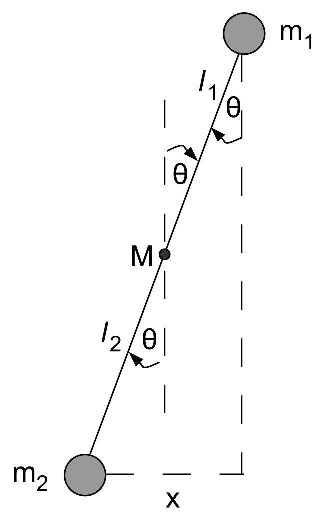

Figure 4.9 Schematic of tether libration angle.

Since the libration angle is measured from the local vertical, its measurement system is generally much more complex and expensive than the length and length rate. Consider the system depicted in Figure 4.9. Assuming that the attitude of the spacecraft can be controlled, we can relate the horizontal distance x to the libration angle θ as follows

$$\theta = \sin^{-1}\left(\frac{x}{l}\right) \tag{4.4}$$

where $l = l_1 + l_2$ is the length of the tether that can be determined from independent measurements. The horizontal distance can be determined via computer vision or differential GPS measurements among other techniques. Computer vision is generally inexpensive in hardware but quite expensive in software/computational complexity. Differential GPS measurements have reciprocal trade-offs since hardware is quite expensive and software is relatively inexpensive. Other techniques based on radar through highly accurate characterization of antenna beam patterns can also be conceived. However, proper trade studies along with verification and validation needs to be conducted to determine feasibility and viability.

4.4 LINEAR CONTROL

4.4.1 Pole Placement

Consider the system in the following form

$$\begin{aligned} \dot{\mathbf{x}} &= \mathbf{A}\mathbf{x} + \mathbf{B}u \\ y &= \mathbf{C}\mathbf{x} \end{aligned} \tag{4.5}$$

where

$$\mathbf{A} = \begin{bmatrix} 0 & 1 & 0 & 0 \\ 3 & 0 & 0 & 2 \\ 0 & 0 & 0 & 1 \\ 0 & -2 & -3 & 0 \end{bmatrix}, \mathbf{B} = \begin{bmatrix} 0 \\ 1 \\ 0 \\ 0 \end{bmatrix}, \mathbf{C} = \begin{bmatrix} 1 & 0 & 0 & 0 \end{bmatrix} \tag{4.6}$$

The tether system can be considered as a Type 0 system [82] since the plant has no integrator (poles at the origin of the s-plane). We can then proceed to design a linear state feedback controller to drive the system to a desired reference in finite time by choosing the feedback law as,

$$u = -\mathbf{K}\mathbf{x} + k_I \xi$$
$$\dot{\xi} = r - \mathbf{C}\mathbf{x} \tag{4.7}$$

This closed loop system can be shown schematically in Figure 4.10.

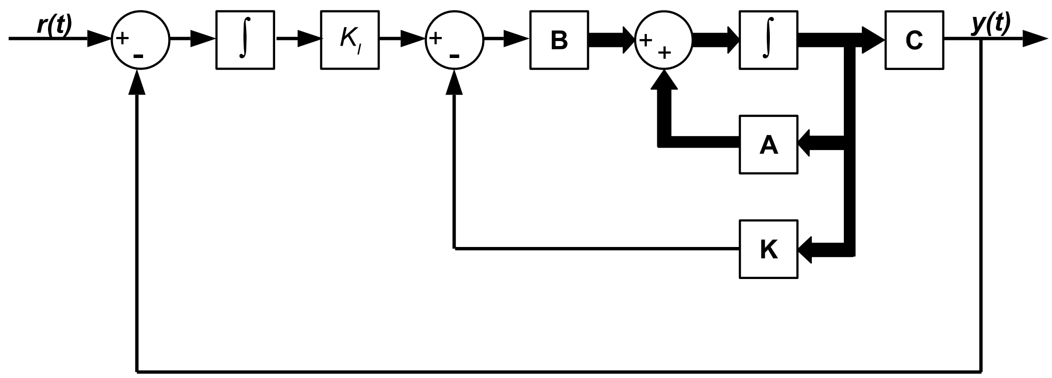

Figure 4.10 Type 1 Servo Block Diagram

which can also be expressed in state-space form as,

$$\begin{bmatrix} \dot{\mathbf{x}} \\ \dot{\xi} \end{bmatrix} = \begin{bmatrix} \mathbf{A} & \mathbf{0} \\ \mathbf{-C} & 0 \end{bmatrix} \begin{bmatrix} \mathbf{x} \\ \xi \end{bmatrix} + \begin{bmatrix} \mathbf{B} \\ 0 \end{bmatrix} u + \begin{bmatrix} \mathbf{0} \\ 1 \end{bmatrix} r \tag{4.8}$$

Define

$$\mathbf{e} = \begin{bmatrix} \mathbf{x} - \mathbf{x}_{ss} \\ \xi - \xi_{ss} \end{bmatrix}, u_e = u - u_{ss} \tag{4.9}$$

where $\mathbf{x}_{ss}, \xi_{ss}$ and u_{ss} are the steady-state values of the state, augmented and control variables respectively. If we assume the reference r is a step input, then, the error dynamics can be written as,

$$\dot{\mathbf{e}} = \hat{\mathbf{A}}\mathbf{e} + \hat{\mathbf{B}}u_e \tag{4.10}$$

with

$$\hat{\mathbf{A}} = \begin{bmatrix} \mathbf{A} & \mathbf{0} \\ \mathbf{-C} & 0 \end{bmatrix}, \hat{\mathbf{B}} = \begin{bmatrix} \mathbf{B} \\ 0 \end{bmatrix} \tag{4.11}$$

By choosing $u_e = -\hat{\mathbf{K}}\mathbf{e}$, where

$$\hat{\mathbf{K}} = \mathbf{K} \quad -k_I \tag{4.12}$$

and choosing $\hat{\mathbf{K}}$ such that $\hat{\mathbf{A}} - \hat{\mathbf{B}}\hat{\mathbf{K}}$ is Hurwitz, the error dynamics will asymptotically approach to zero. Therefore, $\xi \to \xi_{ss} \Rightarrow \dot{\xi} = 0 \Rightarrow y \to r \Rightarrow x_1 \to r$.

Furthermore, given that the system is stable, we can deduce the following,

$$\begin{aligned} &\dot{x}_1 = 0 \Rightarrow x_2 = 0 \\ &\dot{x}_3 = 0 \Rightarrow x_4 = 0 \\ &\dot{x}_4 = 0 \Rightarrow -2x_2 - 3x_3 = 0 \Rightarrow x_3 = 0 \end{aligned} \tag{4.13}$$

Therefore, the system asymptotically reaches the final equilibrium of $\mathbf{x} = \; r \quad 0 \quad 0 \quad 0$.

We can now proceed to designing the state feedback matrix $\hat{\mathbf{K}}$ using the pole-placement method. In general, there are a few approaches that could be used to find the state feedback matrix and the most popular choice is Ackermann's Formula [83]. A necessary and sufficient condition for this approach is that matrix $\mathbf{P}$ is of rank n,

$$\mathbf{P} = \begin{bmatrix} \mathbf{A} & \mathbf{B} \\ \mathbf{-C} & 0 \end{bmatrix} \tag{4.14}$$

For a proof of this method, we refer the reader to [84].

The above pole placement is demonstrated by numerical simulation with the full nonlinear model. The Ackermann's formula is a part of MATLAB's Control Systems Toolbox and can directly be used to find the appropriate state feedback matrix. The parameters of the simulations are detailed in Table 4-1 below.

Table 4-1 Pole-Placement Simulation Parameters

Initial Conditions	Case 1	Case 2	Case 3	Case 4
x_{10}	-0.99	-0.99	-0.99	-0.99
x_{20}	0.1	1	1	1
x_{30}	0	0	$\frac{\pi}{4}$	$-\frac{\pi}{8}$
x_{40}	0	0	$\frac{\pi}{4}$	$-\frac{\pi}{4}$

The simulation results are shown in Figure 4.11 to Figure 4.15. The controller is stable for a wide range of initial conditions and full deployment can be achieved within two orbits. It is worth noting that higher initial velocities x_{20} do not yield faster deployment, as is the case with many of the other controllers which are to be presented later. In fact, for this control, which has a structure similar to a PD controller, increasing the initial velocity results in larger control efforts. Conversely, decreasing the initial velocity below a certain threshold results in a negative control input as illustrated with Case 1 in Figure 4.15. Physically, this can be realized through thrusters or some other force to accelerate the satellite but, this is undesirable in practice. As such, relatively large initial velocities are needed with this controller. To give some context, if we apply the appropriate scaling parameters for a 400 km circular orbit with a 1 km tether, an initial deployment velocity in Cases 2,3 and 4 become 1.13 m/s. There is a correlation between the initial angular displacement and rate (x_{30}, x_{40}) with negative control input, however, it is very small compared to the initial deployment velocity.

Referring to Figure 4.11, there is a considerable amount of overshoot in tether length.

This can only be reduced by modifying the location of closed-loop poles to have a slower response (i.e., slower deployment). A couple disadvantages of overshoot in this context, is that additional length of tether needs to be stored (approx. 50% more) and, the actuator needs to be capable of reeling the tether back in to prevent slack and maintain the appropriate amount of tension.

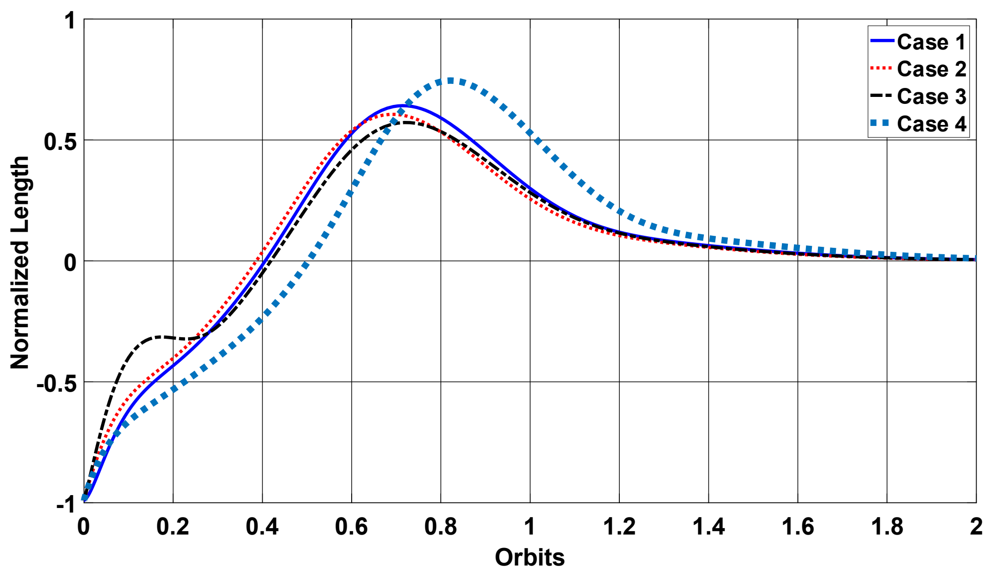

Figure 4.11 Deployment Length vs Time.

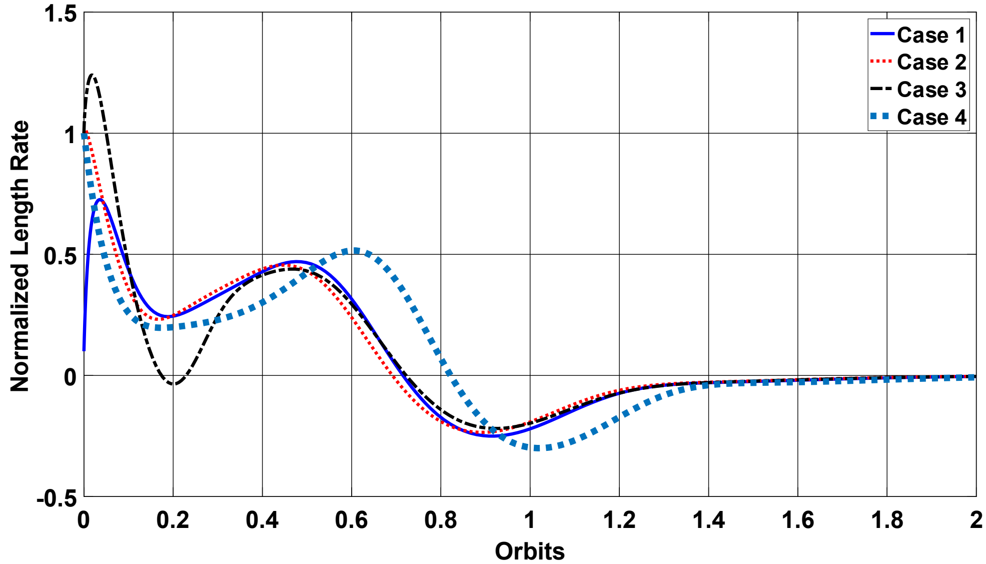

Figure 4.12 Length Rate vs Time.

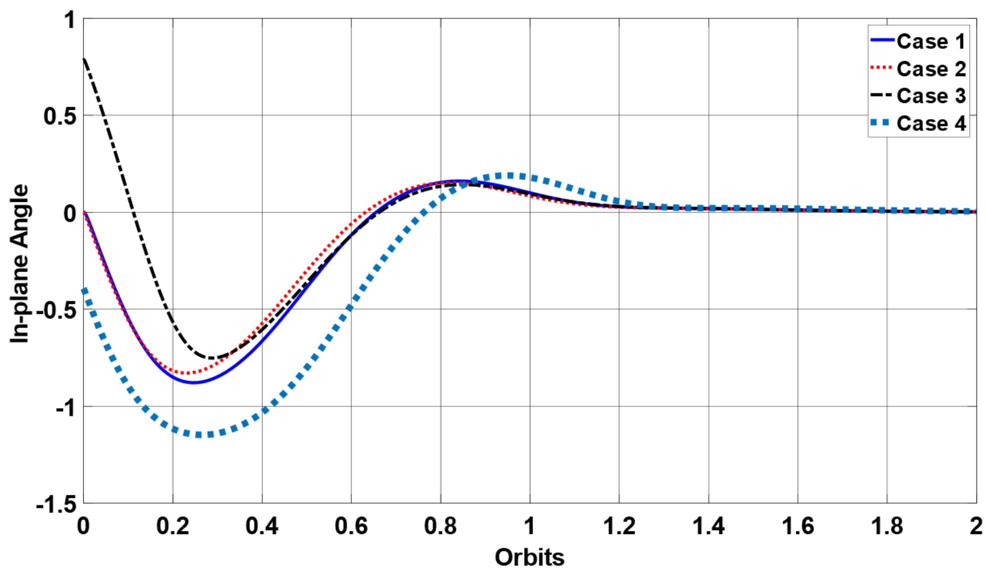

Figure 4.13 In-Plane Angle vs Time

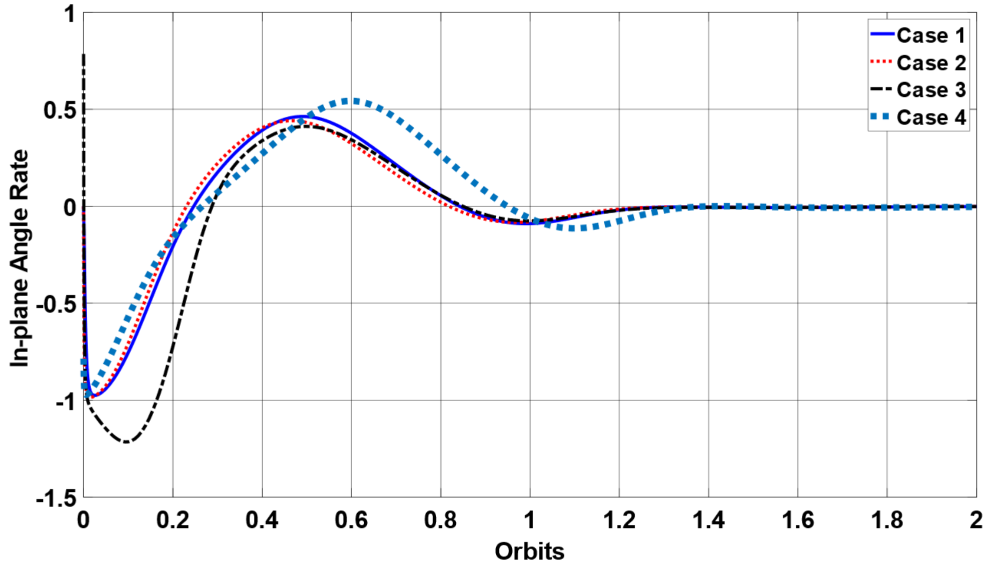

Figure 4.14 In-Plane Angle Rate

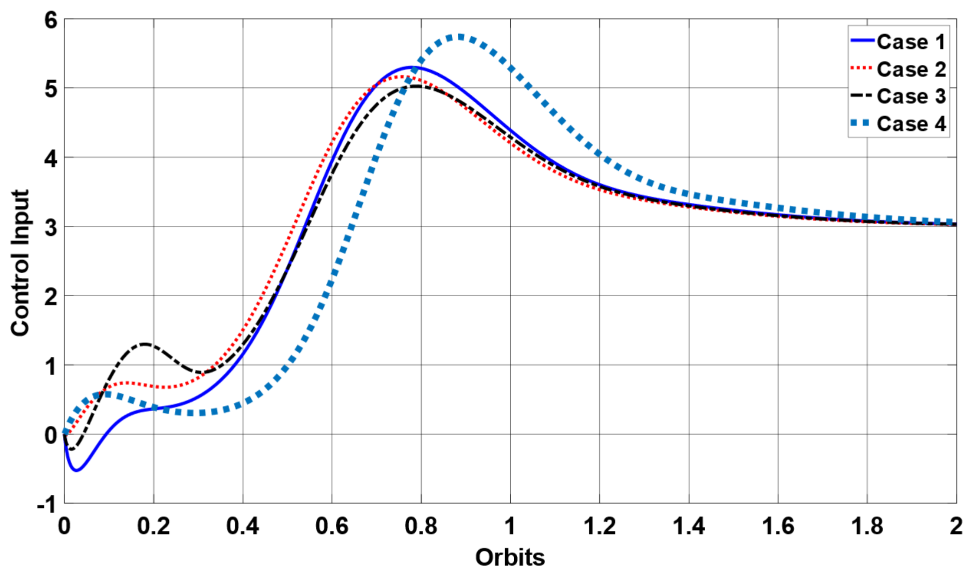

Figure 4.15 Control Input vs Time.

4.4.2 Optimal Gain Selection

The pole-place method is a powerful tool if the dynamics of the system is well-known and well approximated. In the case of the TSS, where there have been numerous assumptions and simplifications, the performance may not be ideal. Another approach, which does not rely heavily on the dynamics model, is to numerically tune the gain parameters to achieve desired performance. The key here is to use the full nonlinear model when tuning the parameters to obtain the best results.

Consider a tension feedback law of the form [34],

$$\widehat{T} = k_1 x_1 + k_2 x_2 + k_3 x_3 + k_4 x_4 + k_5 \tag{4.15}$$

where k_i (i = 1, …, 5) are the control gains to be determined. This controller resembles the structure of a PD controller where $k_1 x_1 + k_3 x_3$ is the proportional term and $k_2 x_2 + k_4 x_4$ is the derivative term, with the desired state as the origin.

Substituting (4.15) into (4.5) yields,

$$\begin{cases} \dot{x}_1 = x_2 \\ \dot{x}_2 = (3 - k_1)x_1 - k_2 x_2 - k_3 x_3 + (2 - k_4)x_4 + 3 - k_5 \\ \dot{x}_3 = x_4 \\ \dot{x}_4 = -2x_2 - 3x_3 \end{cases} \tag{4.16}$$

According to Routh's stability criterion along with the KTC theorem [85], the stable region for the control gains are,

$$\left\{ \forall k_i \in \mathbb{R} : k_1 > 3,\ k_2 > 0,\ k_3 = 0,\ k_4 < \frac{1}{2}(1 + k_1),\ k_5 = 3 \right\} \tag{4.17}$$

It is then necessary to determine the optimal set of control gains within this set.

Denote the ideal system as $\boldsymbol{x}_{ideal}$ and define the cost function as

$$J = \int_0^t (\mathbf{x} - \mathbf{x}_{ideal})^T \mathbf{W} (\mathbf{x} - \mathbf{x}_{ideal}) d\tau \tag{4.18}$$

where $\boldsymbol{W}$ is the weight matrix for each state. By minimizing the cost function subject to constraints (4.17), the optimal set of gains can be determined. There are many search algorithms that could achieve this task and the genetic algorithm was chosen because it has the potential to find a global minima.

The ideal system is chosen such that the transient and steady state response of the system is desirable and is of the same order as the plant to be controlled. For this system, deployment should be achieved within a single orbit with a 2% settling time as shown in Figure 4.16. Then, the ideal system can be defined as,

$$\begin{cases} \dot{x}_1 = x_2 \\ \dot{x}_2 = -1.6211x_1 - 2.5465x_2 \\ \dot{x}_3 = x_4 \\ \dot{x}_4 = -x_3 - x_4 \end{cases} \tag{4.19}$$

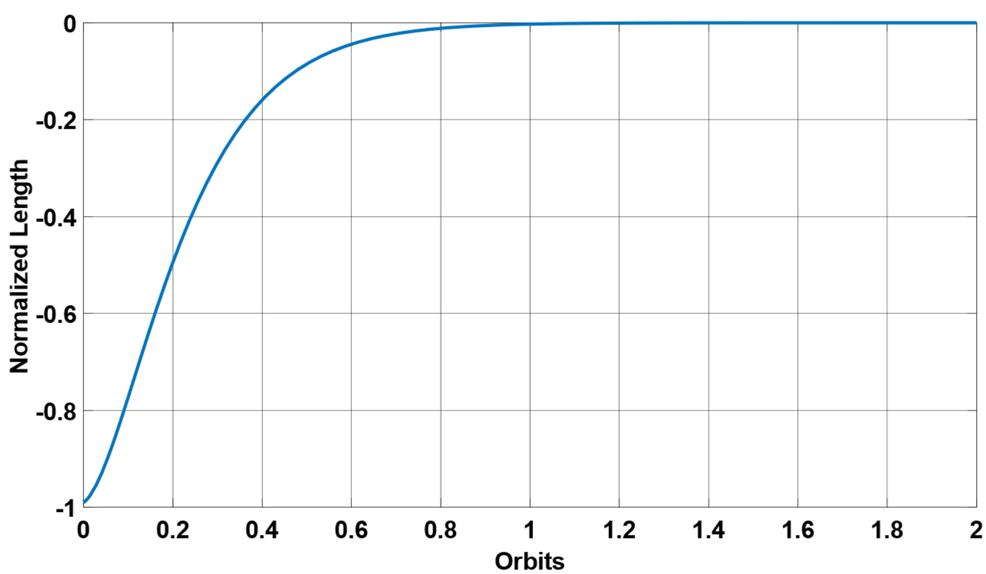

Figure 4.16 Ideal System Length vs Time

The initial condition was identical to Case 1 from Table 4-1. It is important to note that in the ideal system, the libration dynamics has been decoupled from the length dynamics. Although this is not physically accurate, the purpose of this method is to establish a baseline profile for which the deployment process will follow. Also, in the ideal system, the libration dynamics is stable and given the set of initial conditions, the angle and angular rate will remain zero for all time.

Accordingly, the optimal gains are computed via the genetic algorithm,

$$\widehat{T} = 4.8x_1 + 3.4x_2 + 0.4x_4 + 3 \tag{4.20}$$

The above tension controller is implemented in MATLAB again with the use of the full nonlinear model. MATLAB's gamultiobj function was used as the genetic algorithm with the following input parameters (FITNESSFCN, NVARS, A, B, Aeq, beq, LB, UB, options). Where FITNESSFCN is the cost function; NVARS is the number of variables in this 4; A, B, Aeq, beq were not used; LB and UB are the lower and upper bounds respectively and were chosen provided the stability constraints mentioned above; and options is the options structure which is used to plot the results. The same set of initial conditions as found in Table 4-1 were used. The simulation results are shown in Figure 4.17 to Figure 4.21.

The controller can clearly be seen to meet the transient and steady state requirements set out above and match closely to the ideal system even under a range of initial conditions. However, similar to the pole-placement method, the initial deployment velocity plays a critical role in the viability of the controller for nanosatellite application.

There are couple of improvements of this controller over the previous approach as the deployment response is much faster and the overshoot is significantly reduced. If any overshoot is undesirable and the response must be critically, or over- damped, then a constraint can be placed on a state of the system namely, $x_2 \geq 0$ and the genetic algorithm can re-compute the control gains. This constraint on the state of the system is discussed in more detail in the latter sections of this chapter.

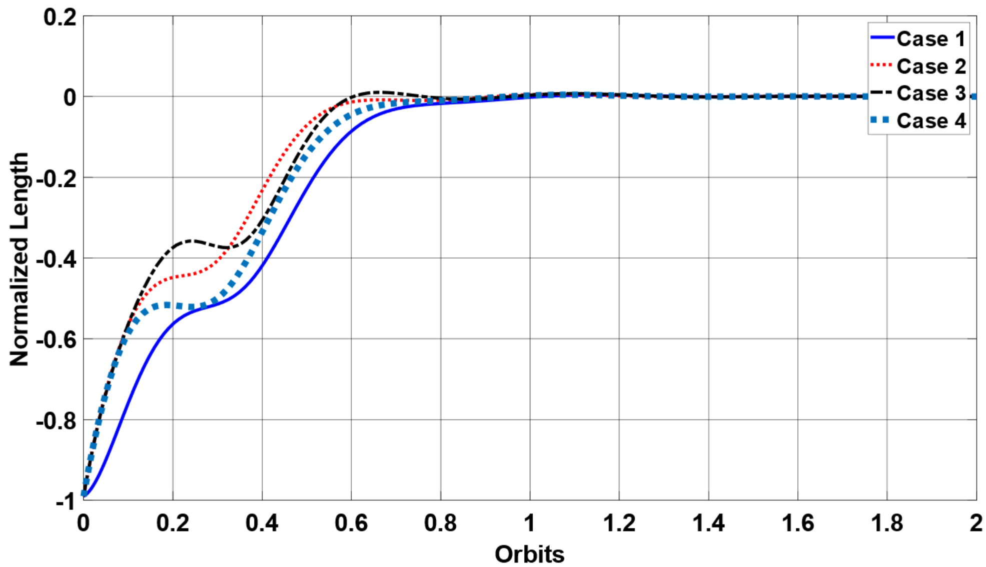

Figure 4.17 Deployment Length vs Time.

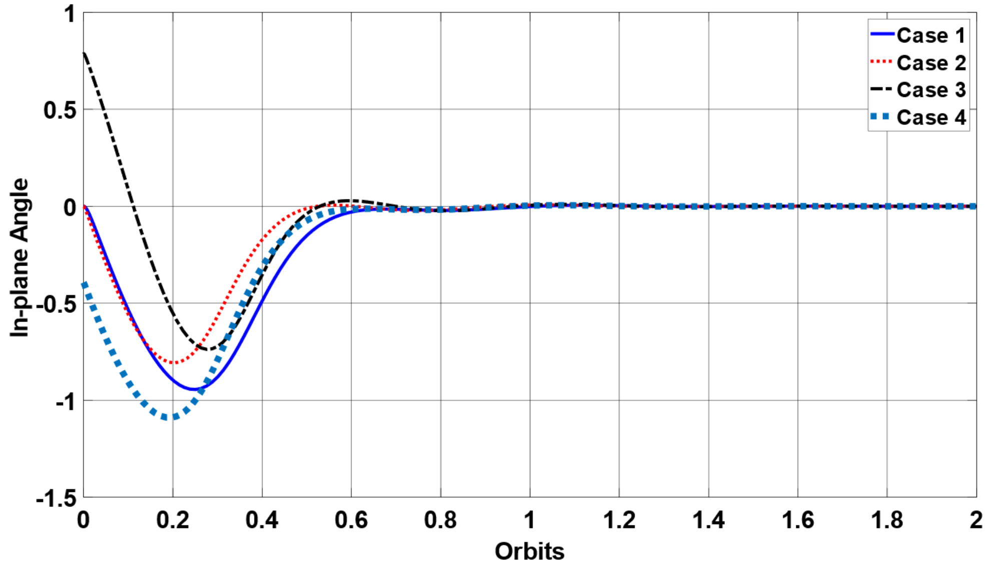

Figure 4.18 In-plane Angle vs Time.

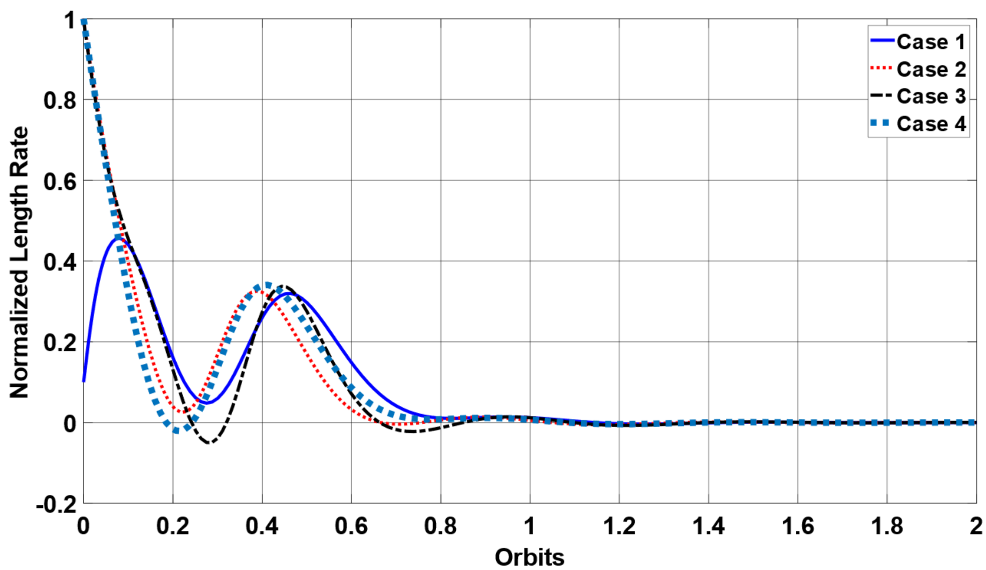

Figure 4.19 Length Rate vs Time.

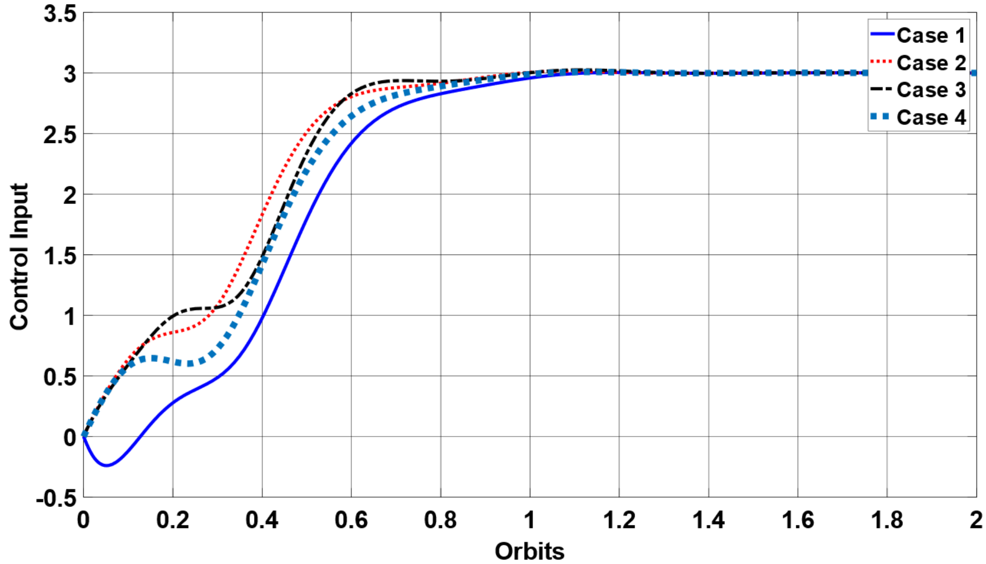

Figure 4.20 Control Input vs Time.

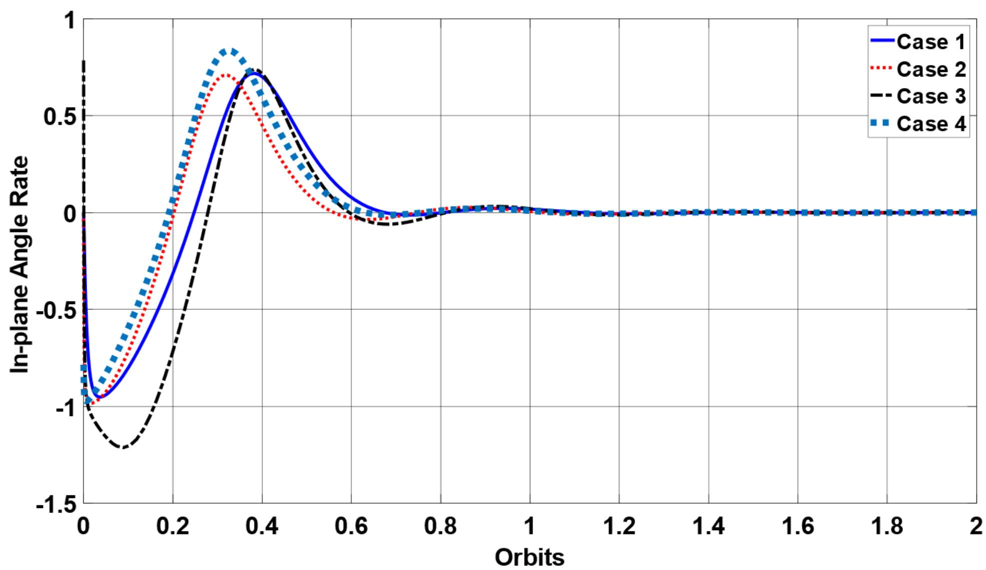

Figure 4.21 In-Plane Angle Rate vs Time.

4.5 NONLINEAR CONTROL - PASSIVITY BASED CONTROL

Linear control is effective for the tether dumbbell system. However, it may not be suitable with the braking mechanism actuator since the deployment must be monotonic. Indeed, proper choice of control gains can achieve monotonicity, but it is not guaranteed especially since the model is linearized. In this section, nonlinear control laws are introduced. A general nonlinear control is developed without the constraint of monotonic deployment, and then manifold based control laws are developed with the constraint directly incorporated into controller development.

Before introducing the monotonic constraint on deployment, a general nonlinear control is introduced. This control can be used in the more general deployment systems in which the tether can be "reeled" back in. Indeed, similar to the linear control, the control gains can be chosen to satisfy the monotonic constraint but is neglected in this section.

4.5.1 Derivation of Control Law

Consider the tether system in the following affine form,

$$\begin{cases} \dot{x} = f(x) + g(x)u \\ y = h(x) \end{cases} \tag{4.21}$$

This system can be considered passive if there exists a positive definite storage function such that

$$V(\varphi(t, x_0, u)) - V(x_0) \leq \int_0^t h(\varphi(\tau, x_0, u))^T u(\tau) d\tau \tag{4.22}$$

where $\varphi(t, x_0, u)$ is the solution of (4.21) with initial condition x_0 and input $u(t)$.

Through feedback passivation and appropriate choices of the output and storage functions, the system in (4.21) can be made passive. Then, we can use the Byrnes-Isidori-Willems Theorem to obtain a passivity-based feedback law which will asymptotically stabilize the equilibrium.

Feedback passivation can be applied through a change of control variables as follows,

$$\widehat{T} = (1+x_1)(1+x_4)^2 + 3(1+x_1)\cos^2 x_3 - 1 - 2\left(\frac{x_4}{1+x_1}\right) 1+x_4 \;\; -W \tag{4.23}$$

where W is the new control input. The dynamics becomes,

$$\begin{cases} \dot{x}_1 = x_2 \\ \dot{x}_2 = -x_1 + 2\left(\dfrac{x_4}{1+x_1}\right) 1+x_4 \;\; +W \\ \dot{x}_3 = x_4 \\ \dot{x}_4 = -2\left(\dfrac{x_2}{1+x_1}\right) 1+x_4 \;\; -3\cos x_3 \sin x_3 \end{cases} \tag{4.24}$$

Choose the storage and output functions as,

$$\begin{cases} V(x) = \dfrac{1}{2} \;\; x_1^2 + x_2^2 + 3\sin^2 x_3 + x_4^2 \\ h(x) = x_2 \end{cases} \tag{4.25}$$

The system becomes passive under $V(x)$ since,

$$\dot{V} = x_2 W \tag{4.26}$$

The system can be considered lossless because it is equality as opposed to an inequality. Now, we can choose a passivity-based feedback (PBF) that will asymptotically stabilize the origin.

Choose the following PBF,

$$W = -\phi(h(x)) = -kx_2 \tag{4.27}$$

This is a valid PBF since, $kx_2^2 > 0$ for all $x \in \mathrm{X}$, and $kx_2^2 = 0$ if and only if $x = 0$ with $k > 0$. The second condition can be shown by applying LaSalle's invariance principle.

Also the system is zero-state detectable under the PBF since, $x_2 = 0$ and $u(t) = 0$ for all $t \geq 0 \Rightarrow \varphi(t, x_0) \rightarrow 0$ as $t \rightarrow \infty$.

The resulting control law can now be expressed by substituting the PBF into (4.23),

$$\widehat{T} = (1+x_1)(1+x_4)^2 + 3(1+x_1)\cos^2 x_3 - 2\left(\frac{x_4}{1+x_1}\right) 1+x_4 \;\; -1+kx_2 \tag{4.28}$$

4.5.2 Case Study

The set of initial conditions for the passivity-based control law is identical to that of the linear controllers except for the initial deployment velocity. Similar to its linear counterparts, the passivity control needs a sufficiently large "push" to achieve deployment in comparable times. If the initial deployment velocity is reduced, the controller produces several oscillations in the early stages of deployment.

From Figure 4.22, the simulation results from Case 1 has the best performance. This is a result of the control gains being "tuned" to this set of initial conditions. This figure depicts the variation in controller performance with the same set of control gains. However, in comparison to the linear control laws, the range of initial conditions did not adversely affect the controller performance. This is largely a result of the libration angle and its rate being used as feedbacks in the control laws. If the initial condition is known relatively accurately, the control gains can be tuned to achieve the desired requirements.

It is also important to note the small number of oscillations of the libration angle and libration angle rate in Figure 4.23 and Figure 4.26. Clearly, the time for the angle and its rate to stabilize is consistent among the range of initial conditions and is much longer than the time to stabilize the length and the length rate. This may be due to the choice of the output, $h(x) = x_2$ the length rate of the tether, being stabilized first and since the libration angle has not reached zero at the same time, there is a small number of damped oscillations at the end.

Table 4-2 Simulation Parameters

Initial Conditions	Case 1	Case 2	Case 3	Case 4
x_{10}	-0.99	-0.99	-0.99	-0.99
x_{20}	4	2	2	2
x_{30}	0	0	$\frac{\pi}{4}$	$-\frac{\pi}{8}$
x_{40}	0	0	$\frac{\pi}{4}$	$-\frac{\pi}{4}$

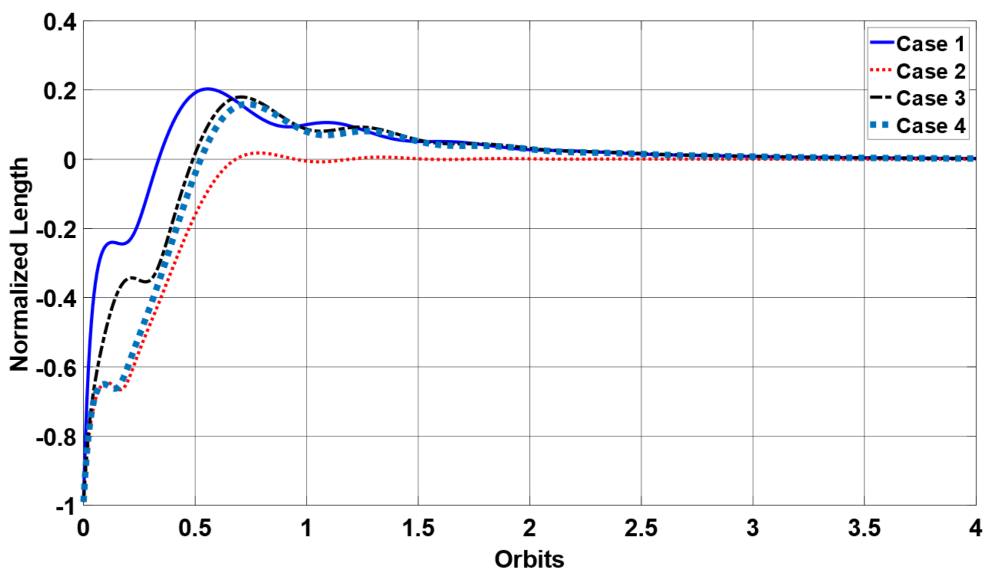

Figure 4.22 Deployment Length vs Time

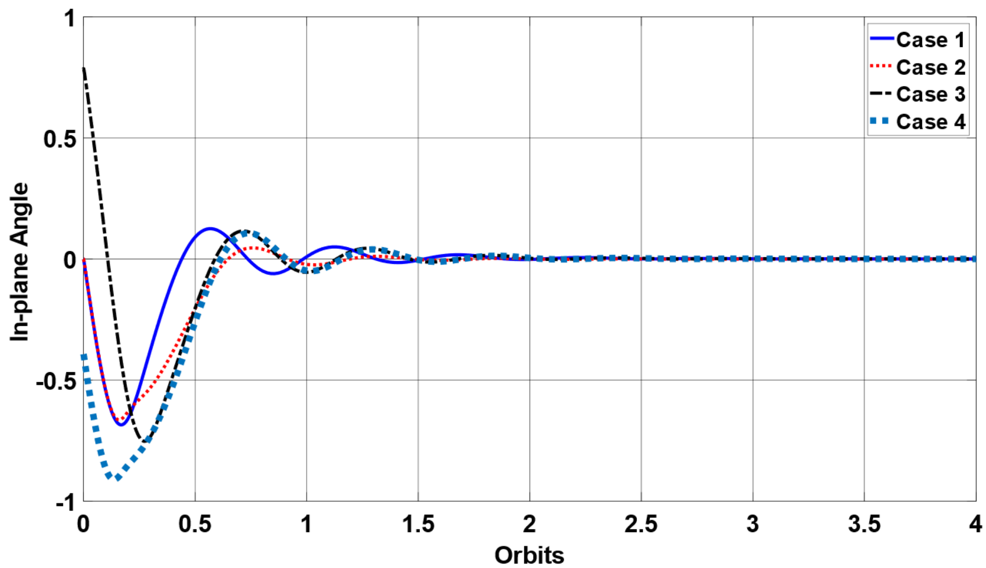

Figure 4.23 In-plane Angle vs Time.

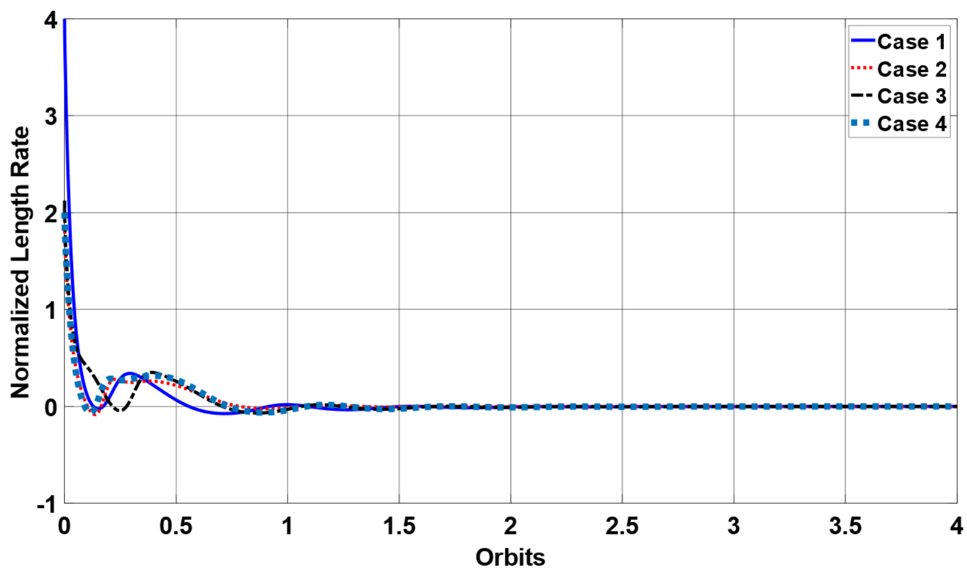

Figure 4.24 Length Rate vs Time.

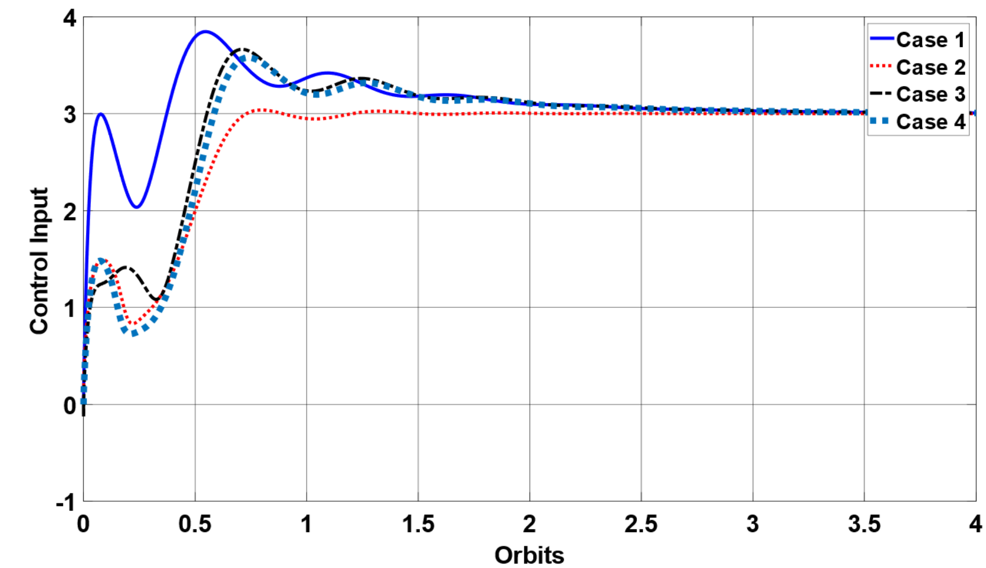

Figure 4.25 Control Input vs Time.

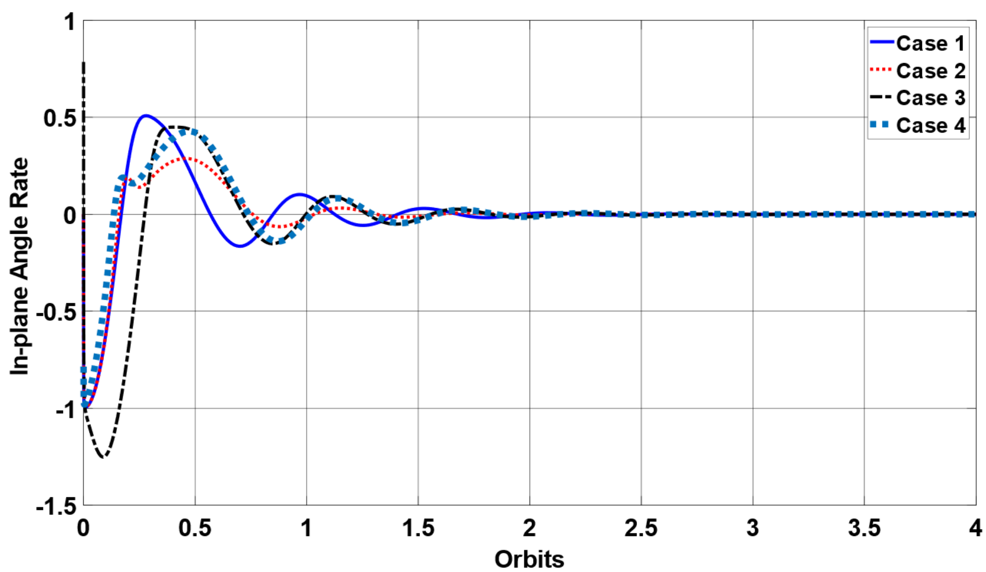

Figure 4.26 In-plane Angle Rate vs Time.

4.6 CONTROL LAWS WITH MONOTONIC DEPLOYMENT

The monotonic tether deployment requires a non-negative tether deployment velocity, such that,

$$\forall \mathbf{x} : x_2 \geq 0 \tag{4.29}$$

The constraint of non-negative tether deployment velocity can be explicitly satisfied by transferring (4.29) into an invariance property of the control system.

Theorem: For a dynamic system $\dot{\mathbf{x}} = \mathbf{f(x)}$. Let $\varphi : \boldsymbol{\chi} \to \mathbb{R}$ be C^1 and let $\Psi = \{ \mathbf{x} \in \boldsymbol{\chi} : \varphi(\mathbf{x}) \leq 0 \}$. Suppose for all $\mathbf{x} \in \mathbb{R}^n$, such that $\varphi(\mathbf{x}) = 0$ and $d\varphi_x \neq 0$, then, Ω is positively invariant if and only if $L_f \varphi(\mathbf{x}) \leq 0$ at the boundary $\forall \mathbf{x} \in \mathbb{R}^n \quad \varphi(\mathbf{x}) = 0$.

Define $\varphi(\mathbf{x}) = -x_2$. Then, the constraint on the non-negative tether deployment velocity in (4.29) can be replaced by the non-negative Lie derivative of $\varphi(\mathbf{x})$ with respect to $\mathbf{F}(\mathbf{x},u)$ in (4.21) at the boundary $\varphi(\mathbf{x}) = 0$, such that,

$$L_F \varphi(\mathbf{x}) = -u\big|_{\varphi=0} \leq 0 \quad \text{or} \quad u\big|_{\varphi=0} \geq 0 \tag{4.30}$$

4.6.1 Approach I

4.6.1.1 Manifold Selection

Assume the tethered space system (TSS) is subject to a new control input $u = (1+x_1)\left[(1+x_4)^2 - 1 + 3\cos^2 x_3\right] - \hat{u} \in \mathbf{R}$ and the output state (y) is the tether length such as $y = x_1 = h(\mathbf{x}) \in \boldsymbol{R}$. The SIMO system in (4.21) is transformed to the following affine control system, such that,

$$\begin{cases} \dot{\mathbf{x}} = \mathbf{f(x)} + \mathbf{g(x)}u = \mathbf{F}(\mathbf{x}, u) \\ y = h(\mathbf{x}) \end{cases} \tag{4.31}$$

where

$$\mathbf{f(x)} = \begin{bmatrix} x_2 \\ 0 \\ x_4 \\ -2\dfrac{x_2}{1+x_1}(1+x_4) - \dfrac{3}{2}\sin 2x_3 \end{bmatrix}, \quad \mathbf{g(x)} = \begin{bmatrix} 0 \\ 1 \\ 0 \\ 0 \end{bmatrix}$$

Then, the TSS is transferred to a single-input-single-output (SISO) system.

Accordingly, the Lie derivatives of output state $h(\mathbf{x})$ and function $\boldsymbol{g}(\mathbf{x})$ of TSS are,

$$\begin{cases} L_f h(\mathbf{x}) = \dfrac{\partial h(\mathbf{x})}{\partial \mathbf{x}} \cdot \mathbf{f(x)} = x_2, \quad L_f^2 h(\mathbf{x}) = \dfrac{\partial (L_f h(\mathbf{x}))}{\partial \mathbf{x}} \cdot \mathbf{f(x)} = 0 \\ L_g h(\mathbf{x}) = \dfrac{\partial h(\mathbf{x})}{\partial \mathbf{x}} \cdot \mathbf{g(x)} = 0, \\ L_g L_f^0 h(\mathbf{x}) = L_g h(\mathbf{x}) = 0, \;\; L_g L_f^1 h(\mathbf{x}) = \dfrac{\partial (L_f h(\mathbf{x}))}{\partial \mathbf{x}} \cdot \mathbf{g(x)} = 1 \neq 0 \end{cases} \tag{4.32}$$

Obviously, the affine control system has the relative degrees of $\rho = 2$ over $\boldsymbol{R}^2$. Thus, the dynamic system in (4.31) can be segregated into two subsystems, with x_1, x_2 describing the dynamics of tether length (defined as external dynamics) and x_3, x_4 describing the dynamics of libration angle (defined as internal dynamics), such that,

$$\begin{cases} \ddot{\mathbf{y}} = L_f^2 h(\mathbf{x}) + L_g L_f h(\mathbf{x}) u \\ \dot{\boldsymbol{\eta}} = Q(\boldsymbol{\xi}, \boldsymbol{\eta}) \end{cases} \tag{4.33}$$

where $[x_1, x_2]^T = [h(\mathbf{x}), L_f h(\mathbf{x})]^T = [\xi_1, \xi_2] = \boldsymbol{\xi} \in \mathbf{R}^2$ and $[x_3, x_4]^T = [\eta_1, \eta_2]^T = \boldsymbol{\eta} \in \mathbf{R}^2$ denote the external and internal states of the SISO system.

Consider a control strategy where a braking force is applied such that the external states (tether deployment length and velocity) reach a zero-equilibrium state $[x_1, x_2]^T = \boldsymbol{\xi} = \mathbf{0}$. Then, the internal dynamics is reduced to the zero dynamics $\dot{\boldsymbol{\eta}} = \mathbf{Q}(\mathbf{0}, \boldsymbol{\eta})$, such that,

$$\dot{x}_3 = x_4, \quad \dot{x}_4 = -\frac{3}{2}\sin 2x_3 \tag{4.34}$$

The stability for the tether deployment control requires the zero dynamics $\dot{\boldsymbol{\eta}} = \mathbf{Q}(\mathbf{0}, \boldsymbol{\eta})$ stable or critically stable at the zero equilibrium [86]. Considering that the eigenvalues of the linearized zero dynamics of (4.34) near the zero equilibrium are $\pm\sqrt{3}i$, respectively, the internal dynamics is critically stable. Thus, the TSS is controllable with only tension control input and the stable tether length deployment is achievable.

It is well-known that the libration motion of TSS is induced by the Coriolis force. This force is proportional to the tether deployment velocity x_2. As the tether deployment completes, the Coriolis force approaches to zero. Thus, it is intuitive to introduce x_2 as a pseudo-control input to the internal dynamics $\dot{\boldsymbol{\eta}} = \mathbf{Q}(\boldsymbol{\xi}, \boldsymbol{\eta})$, such that,

$$\begin{aligned} \dot{x}_3 &= x_4 \\ \dot{x}_4 &= -2\left(\frac{x_2}{1+x_1}\right) - \frac{3}{2}\sin 2x_3 \end{aligned} \tag{4.35}$$

Assume a manifold $s_1 = x_2 - p_1 x_4 = 0$ with $p_1 > 0$ to link the tether deployment velocity with the libration angular velocity. Obviously, the libration angular velocity approaches to zero at the end of tether deployment process ($x_2 = 0$). Substituting the manifold s_1 into (4.35) and then linearizing it near the zero-equilibrium state yield

$$\begin{aligned} \dot{x}_3 &= x_4 \\ \dot{x}_4 &= -3x_3 - 2p_1 x_4 \end{aligned} \tag{4.36}$$

The corresponding eigen values of (4.36) are $\lambda = -p_1 \pm \sqrt{p_1^2 - 3}$. Thus, the control law x_2 derived from the manifold $s_1 = x_2 - p_1 x_4 = 0$ is stable because of $\mathrm{Re}(\lambda) < 0$ for all $p_1 > 0$.

Now introduce the following manifolds,

$$\begin{aligned} s_1 &= x_2 - p_1 x_4 = 0 \\ s_2 &= c x_1 + x_2 = 0 \end{aligned} \tag{4.37}$$

where c is a positive constant. It can be seen that the s_1 yields an equilibrium state set $x \in \chi : x_2 = x_3 = x_4 = 0$, while the s_2 drives the state x_1 to the zero-equilibrium state.

4.6.1.2 Control Law Derivation

Thus, a direct Lyapunov-type control law can be designed by defining a Lyapunov function candidate as,

$$V = \frac{1}{2} S^2 \tag{4.38}$$

where $S = \alpha s_1 + s_2$ and α is a positive constant.

The derivative of the Lyapunov function yields

$$\begin{aligned} \dot{V} &= S\dot{S} = (\alpha s_1 + s_2)(\alpha \dot{s}_1 + \dot{s}_2) \\ &= \left[\, 1+\alpha \;\; x_2 - \alpha p_1 x_4 + c x_1 \right]\left[\, 1+\alpha \;\; u - \alpha p_1 \dot{x}_4 + c x_2 \right] \end{aligned} \tag{4.39}$$

Define the control law as

$$u = \frac{1}{1+\alpha} \;\; \alpha p \dot{x}_4 - c x_2 - k_1 \left[\, 1+\alpha \;\; x_2 - \alpha p_1 x_4 + c x_1 \right] \tag{4.40}$$

where k_1 is a positive constant.

Substituting (4.40) into (4.39) yields

$$\dot{V} = -k_1\left[\, 1+\alpha \;\; x_2 - \alpha p_1 x_4 + c x_1 \right]^2 < 0$$

Thus, the control law is stable.

In order to show the stability of equilibrium state under this new control law, we follow a similar approach as demonstrated by the authors in [52]. Consider the dynamics on the manifold S ,

$$\begin{aligned}
&\dot{S} = \alpha \dot{s}_1 + \dot{s}_2 = 0 \\
&\dot{S} = \alpha \;\; \dot{x}_2 - p\dot{x}_4 \;\; + c\dot{x}_1 + \dot{x}_2 = 0 \\
&\dot{x}_2 = \left(\frac{1}{1+\alpha}\right) \;\alpha p \dot{x}_4 - c\dot{x}_1
\end{aligned} \tag{4.41}$$

Substituting these dynamics into (4.31) and linearizing about the equilibrium point yields,

$$\begin{bmatrix} \dot{x}_1 \\ \dot{x}_2 \\ \dot{x}_3 \\ \dot{x}_4 \end{bmatrix} = \begin{bmatrix} 0 & 1 & 0 & 0 \\ 0 & \dfrac{-2\alpha p - c}{1+\alpha} & \dfrac{-3\alpha p}{1+\alpha} & 0 \\ 0 & 0 & 0 & 1 \\ 0 & -2 & -3 & 0 \end{bmatrix} \begin{bmatrix} x_1 \\ x_2 \\ x_3 \\ x_4 \end{bmatrix} \tag{4.42}$$

Let $a = \dfrac{-2\alpha p - c}{1+\alpha}$ and $b = \dfrac{-3\alpha p}{1+\alpha}$. Obviously both $a, b < 0$ since α, p and c are all positive. Notice how the x_1 dynamics are decoupled from the rest of the system. Therefore, we can focus on the stability of the reduced system namely x_2, x_3 and x_4. The associated eigenvalue equation becomes,

$$-\lambda^3 + a\lambda^2 - 3\lambda + 3a - 2b = 0$$

It can be shown that $\mathrm{Re}(\lambda_{1,2,3}) < 0$ for all $a, b < 0$. Therefore, $x_2, x_3, x_4 \to 0$ and from the manifold S, $x_1 \to 0$. Thus, the equilibrium state is stable under the dynamics on the manifold.

4.6.1.3 Proof of Non-Negative Length Rate

From (4.40) the Lie derivative at the boundary $\varphi(\mathbf{x}) = -x_2 = 0$ and the manifold $s_1 = 0 \Rightarrow x_4 = x_2 = 0$ becomes

$$u\big|_{\varphi=0} = \frac{1}{(1+\alpha)}\left(-\frac{3}{2}\alpha p_1 \sin 2x_3 - k_1 c x_1\right) \tag{4.43}$$

Thus, under the following conditions, (i) $-1 < x_1 \leq 0$, and (ii) $-\pi/2 \leq x_3 \leq 0 \;\Rightarrow\; \sin 2x_3 \leq 0$, (4.43) becomes $u\big|_{\varphi=0} \geq 0$ and the positive invariant condition is satisfied. Condition (i) is a direct implication of (4.29) as an overshoot in length violates the constraint and can be resolved through appropriate choice of control gains. Also, consider the fact that the libration angle is induced by the Coriolis force in the negative direction of x_3, which is generated by a positive tether length deployment velocity. As the $x_2 \Rightarrow 0$, the libration angle will approach to zero under the restoring gravity torque. Thus, it is reasonable to assume the libration angle satisfies Condition (ii). Accordingly, Now, it is proved that the constraint of non-negative tether deployment velocity $\forall \mathbf{x} : x_2 \geq 0$ is explicitly satisfied by the proposed control law.

4.6.1.4 Case Study

It appears that the natural motion/physics of the system is exploited by this control law as described in the justification for the choice of manifold and the proof of nonnegative length rate. The initial libration angle rate is a result of the Coriolis torque, which is proportional to the positive tether deploying velocity, being more dominant than the restoring torque of gravity-gradient. However, halfway through the deployment, when the length rate peaks, the gravity-gradient becomes dominant and the libration angle rate becomes positive and gradually approaches to zero along the control manifold. This also results in the controller accelerating the length very slowly in the beginning of deployment, which results in a reduced libration angular rate and angle as seen in Figure 4.29 and Figure 4.30. Furthermore, Condition (ii) used to prove the nonnegative length rate is also shown to be satisfied in Figure 4.28. From Figure 4.28 and Figure 4.30, the manifold selection of $x_2 = px_4$ can be seen. Here $p < 1$ and a scaled down version of the length rate is seen in the libration angle rate. The controller can converge to the manifold just after an orbit.

This gives rise to the smooth deployment profile and significantly large penalties for large initial deployment velocities such as that seen in Figure 4.28 in case 2. The large penalty is a result of the controller trying to drive the system toward the manifold. The penalization of large initial “push” is contrary to the previous control laws that have been introduced so far as they relied on these initial conditions to achieve fast deployment. It is also for this reason that the deployment time is relatively much longer and cannot be optimized much further. However, in practical implementations, this is a desirable property especially in the context of nanosatellites as a large force is not required.

This control law is more sensitive to the initial conditions, as the performance of the controller is dependent on the initial conditions. More precisely, the controller performance is dictated by the initial distance of the system from the manifold. Since the first objective of the controller is to drive the system to the manifold and then along the manifold to the equilibrium. Case 3 is interesting because the initial conditions allowed the system to begin very close to the manifold and was able to converge very quickly, allowing for faster deployment as well.

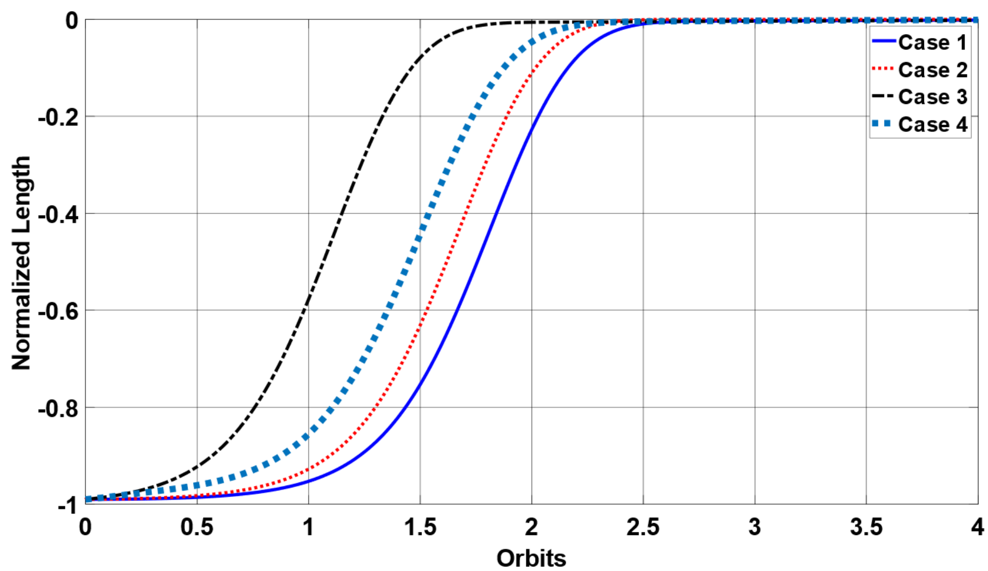

Figure 4.27 Nondimensional length vs Time.

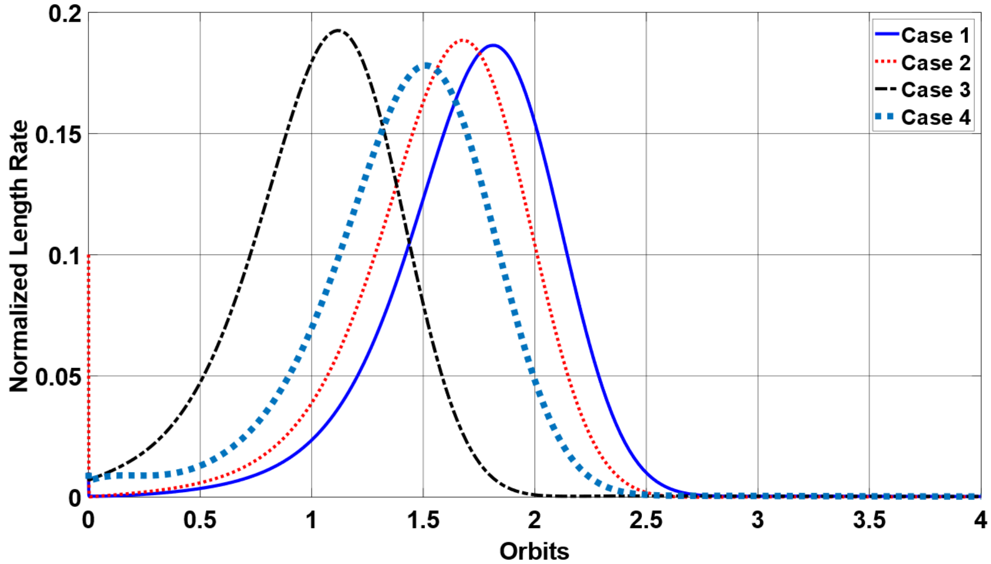

Figure 4.28 Nondimensional Length Rate vs Time.

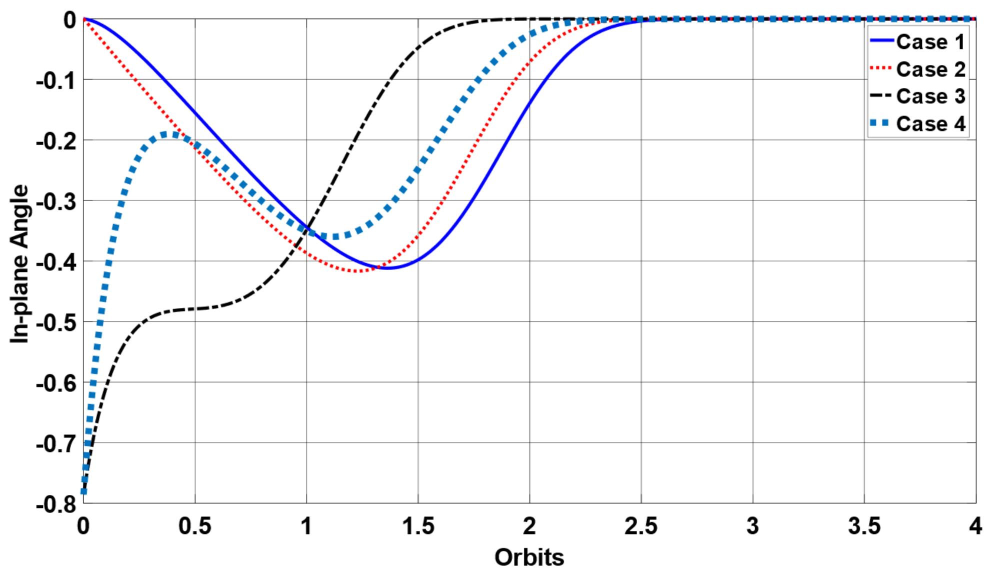

Figure 4.29 In-plane Angle vs Time.

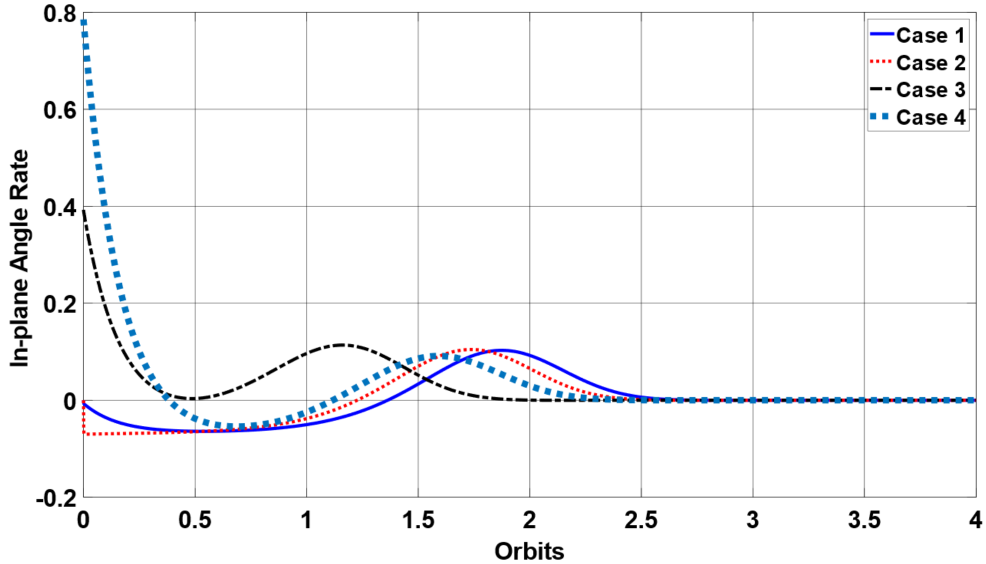

Figure 4.30 In-plane Angle Rate vs Time

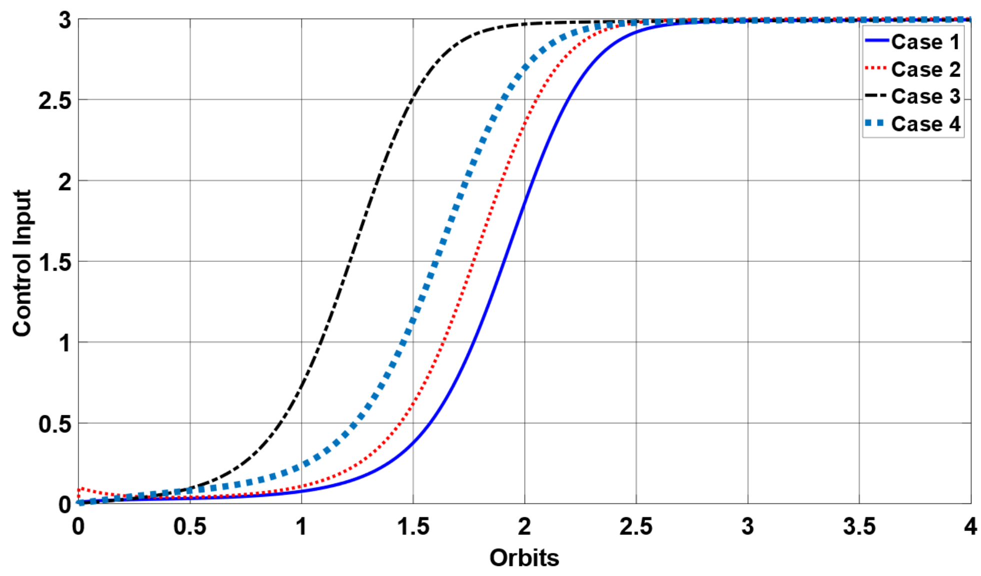

Figure 4.31 Control Input vs Time

4.6.2 Approach II

4.6.2.1 Control Law Derivation

The second control law is derived based on the theory of nonholonomic/holonomic system [87] - [88].

Define a new set of state,

$$\mathbf{q} = x_1 \; x_3 {}^{T} \tag{4.44}$$

Then, the system equations in (4.31) can be rewritten in the matrix form,

$$\mathbf{M\ddot{q}} + \mathbf{n(q, \dot{q})} = \mathbf{B}\hat{u} \tag{4.45}$$

where

$$\mathbf{M} = \begin{bmatrix} 1 & 0 \\ 0 & 1 \end{bmatrix}, \ \mathbf{B} = \begin{bmatrix} -1 \\ 0 \end{bmatrix}, \quad \mathbf{n}(\mathbf{q}, \dot{\mathbf{q}}) = \begin{bmatrix} -\ 1 + x_1 \ \left[\ 1 + x_4 \ {}^2 - 1 + 3\cos^2 x_3 \right] \\ 2\left(\dfrac{x_2}{1 + x_1}\right) 1 + x_4 \ + \dfrac{3}{2}\sin 2x_3 \end{bmatrix}$$

Further define a manifold $x_2 + p_2 x_4 = 0$. Then, the velocity of state can be replaced by a new scalar velocity v as

$$\mathbf{q} = \mathbf{G}v \tag{4.46}$$

where $\mathbf{G} = [p_2, -1]^T$.

Left-multiplying (4.45) by $\mathbf{G}^T$ yields a reduced order dynamic system about the manifold

$$\tilde{\mathbf{M}}\ddot{v} + \tilde{\mathbf{n}}(\mathbf{q}, v) = \tilde{\mathbf{B}}\hat{u} \tag{4.47}$$

where

$$\tilde{\mathbf{M}} = \mathbf{G^T M G}$$
$$\tilde{\mathbf{n}}(\mathbf{q}, v) = \mathbf{G^T M G}v + \mathbf{G^T n}(\mathbf{q}, \mathbf{G}v)\,.$$
$$\tilde{\mathbf{B}} = \mathbf{G^T B}$$

Thus, an invertible feedback law can be designed to stabilize this system by

$$\hat{u} = \frac{1}{\tilde{\mathbf{B}}}\left[\tilde{\mathbf{M}}a + \tilde{\mathbf{n}}\;\; \mathbf{q}, v\;\;\right] \tag{4.48}$$

where $a = \dot{\nu}$ is the acceleration, which is a new tension control input to TSS.

Consider a direct Lyapunov-based control law by defining a Lyapunov function candidate as,

$$V = \frac{1}{2}\;\; \mathbf{q}^T\mathbf{q} + \nu^2 \tag{4.49}$$

The stability requirement ($\dot{V} < 0$) leads to a control law as,

$$a = -\mathbf{q}^T\mathbf{G} - k_2\nu \tag{4.50}$$

where $k_2 > 0$ is the control gain.

Substituting (4.50) into the invertible feedback law (4.48), yields,

$$\hat{u} = \frac{1}{p_2}\left\{\begin{array}{l} -\dfrac{2x_2}{p_2(1+x_1)}\;\; x_2 - p_2\;\; + \dfrac{3}{2}\sin 2x_3 - \;\; p_2^2 + 1\;\left[-p_2x_1 + x_3 - k_2\dfrac{x_2}{p_2}\right]\Bigg] \\ +p_2\;\; 1 + x_1\;\left[\left(\dfrac{x_2}{p_2} - 1\right)^2 - 1 + 3\cos^2 x_3\right] \end{array}\right\} \tag{4.51}$$

4.6.2.2 Proof of Non-Negative Length Rate

Define $\varphi(\mathbf{x}) = -x_2$. The Lie derivative of $\varphi(x)$ with respect to **F** in (4.31) at the boundary $\varphi(\mathbf{x}) = -x_2 = 0$ and the manifold $x_2 + p_2x_4 = 0 \Rightarrow x_4 = x_2 = 0$ becomes

$$L_F\varphi(\mathbf{x})\big|_{\varphi=0} = \frac{3}{2p_2}\sin 2x_3 + \frac{p_2^2+1}{p_2}\;\; p_2x_1 - x_3 \tag{4.52}$$

Based on the same consideration in the Approach I, we have $-1 < x_1 \le 0$ and $-\pi/2 \le x_3 \le 0$. Thus, the Lie derivative of $\varphi(\mathbf{x})$ with respect to $\mathbf{F}(\mathbf{x},u)$ will satisfy the positive invariant condition $L_F\varphi(\mathbf{x})\big|_{\varphi=0} \leq 0$, if we impose the extra conditions $p_2 > 0$ and $p_2 x_1 - x_3 \leq 0$ on the controller. Accordingly, the control law in (4.51) is stable and complies explicitly with the constraint of non-negative tether deployment velocity.

4.6.2.3 Case Study

An important distinction between the manifold chosen for this control law versus the previous control law is the sign change. In this new controller, the manifold is defined as $x_2 = -px_4$. This allows the control to initially align with Coriolis force and allows the length rate to increase immediately, whereas the previous controller waited for the signs of the length rate and libration angle rate to equalize before accelerating the tether length. Overall, this controller still penalizes large initial length rates but starts accelerating the tether much quicker, see Figure 4.33. This results in slightly better performance. Furthermore, this results in a much larger libration angle as compared to the previous controllers.

Interestingly, this controller is not as sensitive its initial conditions and a constant set a gain yield similar performance over a range of initial conditions. Finally, the constraint of nonnegative length rate is satisfied from Figure 4.33 and the assumed conditions of bounded length and libration angle can be seen in Figure 4.32 and Figure 4.34.

However, it is important to note that one of the initial conditions (Case 4), explicitly violates the assumed condition, $-\pi/2 \leq x_3 \leq 0$, yet the controller is still able to maintain a nonnegative length rate. We can conclude that this condition is sufficient but not necessary.

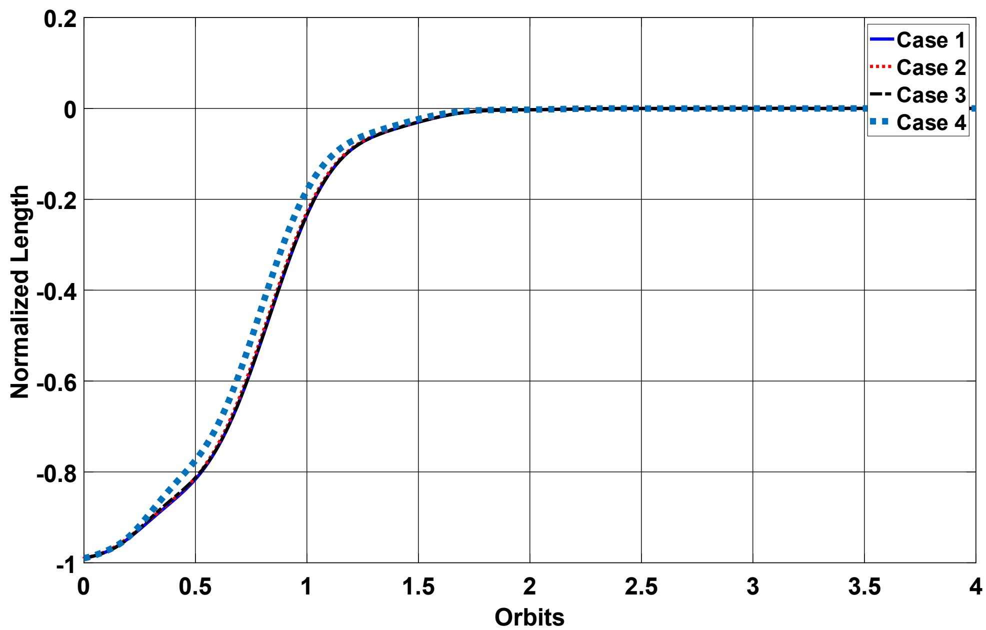

Figure 4.32 Nondimensional Length vs Time.

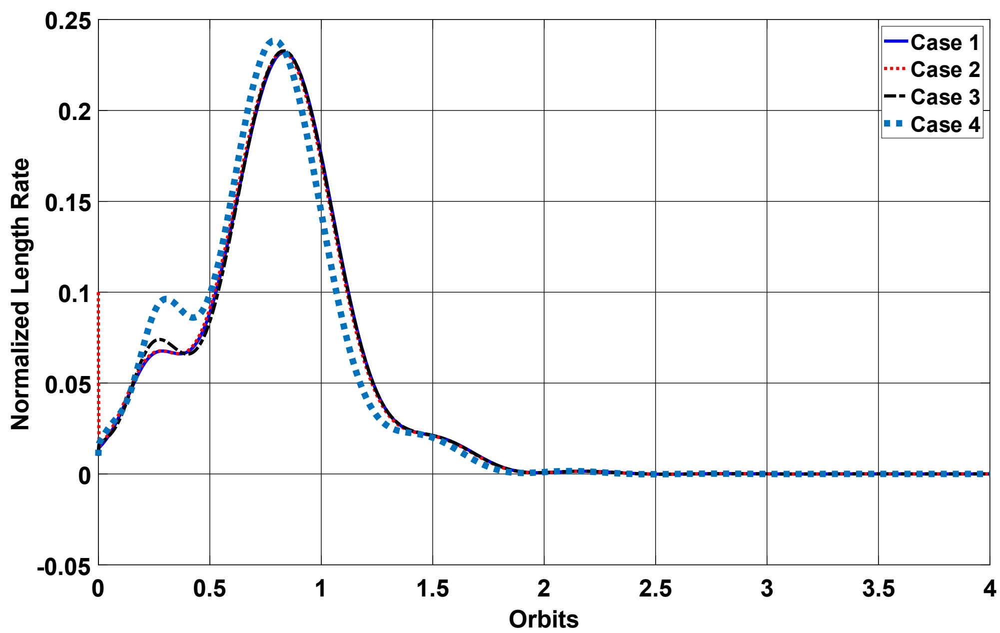

Figure 4.33 Nondimensional Length Rate vs Time.

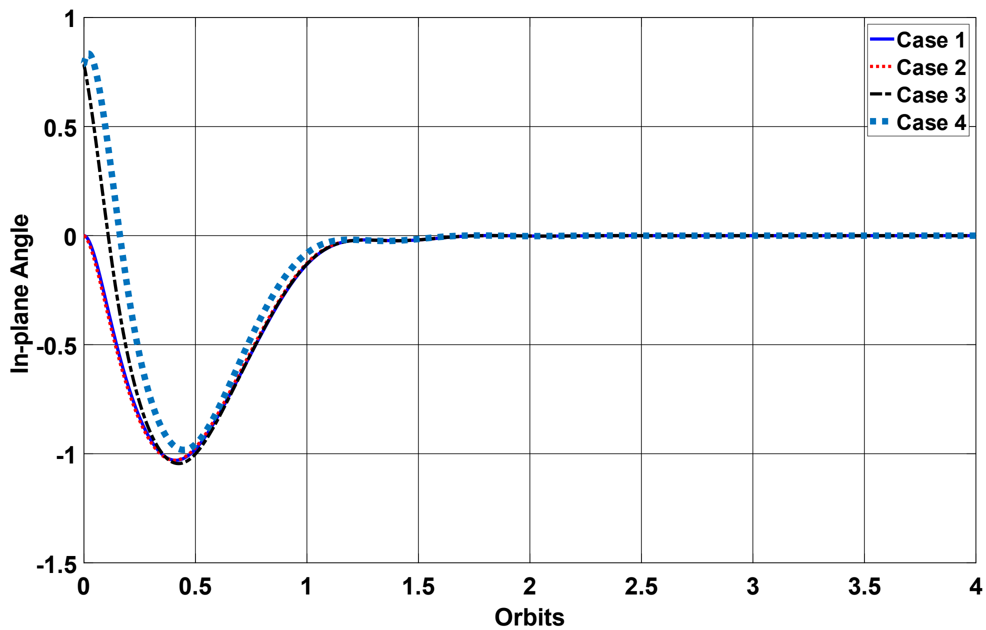

Figure 4.34 In-plane Angle vs Time.

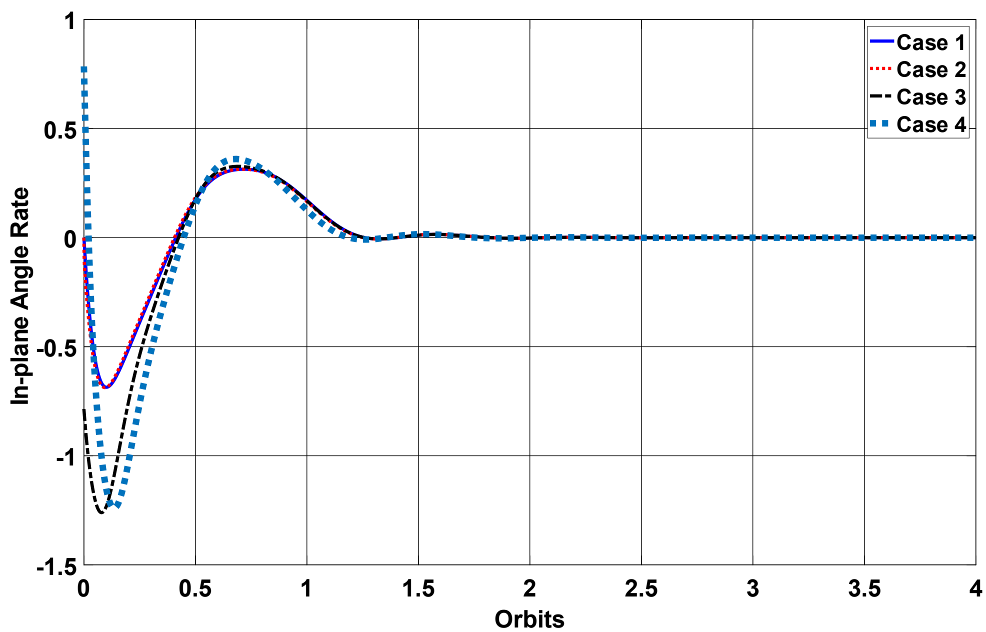

Figure 4.35 In-plane Angle Rate vs Time.

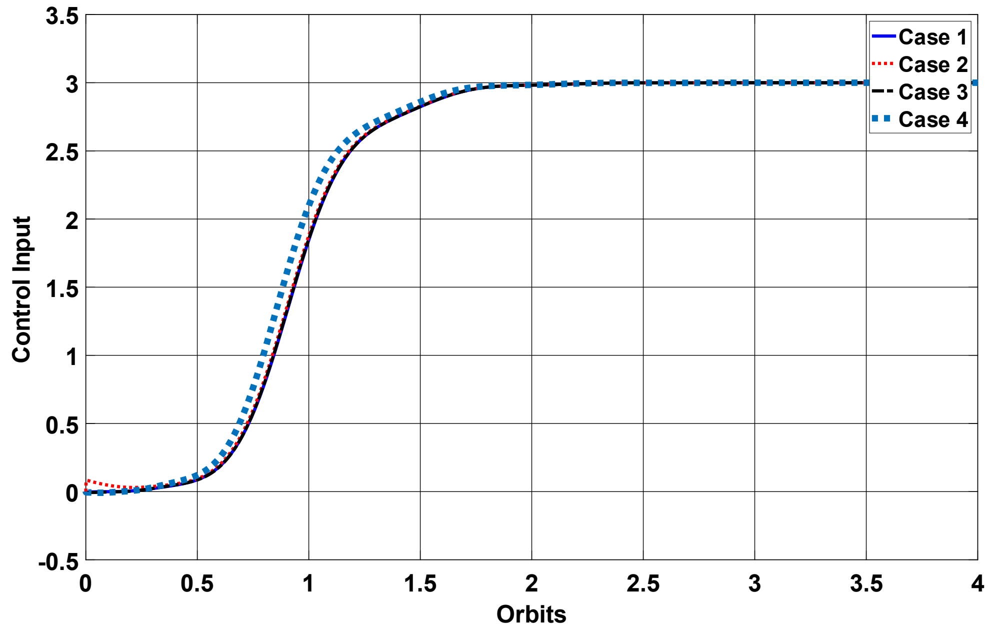

Figure 4.36 Control Input vs Time.

4.7 PULSE WIDTH PULSE FREQUENCY MODULATION FOR MONATOMIC DEPLOYMENT

Consider the braking mechanism as described in Section 4.2. From the controllers that have been presented so far, the control input follows a nonlinear profile that may be difficult/expensive to replicate. Instead, the continuous actuation mechanism can be simplified with an on-off braking system that can be simply constructed by a solenoid or stepper motor to actuate the brakes at two states "on" or "off". Thus, we can replace a continuous time control input by a discretized "on-off\bang-bang" control. In fact, there exists methods that can transform continuous-time signals into discretized pulsed signals with fixed amplitude but varying pulse width and pulse frequency (PWPF) [89] [90] [91]

[15].

Consider the block diagram in Figure 4.37, the error signal is fed through a low-pass filter to smooth out the signal, and then through a Schmitt trigger. The Schmitt trigger has on/off thresholds U_{on}, U_{off}, and outputs a constant magnitude U_m.

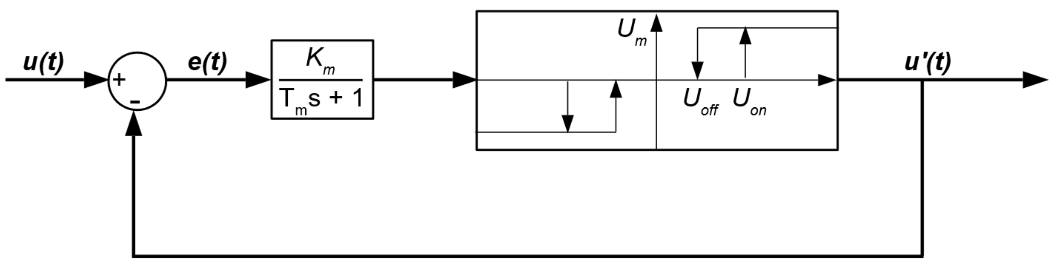

Figure 4.37 PWPF Block Diagram.

The modulation frequency f and duty cycle D can be computed from these external parameters as follows [92] [93],

$$
\begin{aligned}
f &= \frac{1}{T_{on} + T_{off}} \\
D &= \frac{1 + \ln\left(1 + \frac{b}{c}\right)}{\ln\left(1 + \frac{b}{1-c}\right)}
\end{aligned}
\tag{4.53}
$$

where

$$
\begin{aligned}
T_{on} &= -T_m \ln\left(1+\frac{U_{on}-U_{off}}{K_m\left(\hat{e}-U_M\right)-U_{on}}\right) \\
T_{off} &= -T_m \ln\left(1-\frac{U_{on}-U_{off}}{K_m\hat{e}-U_{off}}\right) \\
b &= \frac{U_{on}-U_{off}}{K_m\left(E_s-E_d\right)} \\
c &= \frac{\hat{e}-E_d}{E_s-E_d} \\
E_d &= \frac{U_{on}}{K_m} \\
E_s &= U_m+\frac{U_{off}}{K_m}
\end{aligned}
\tag{4.54}
$$

4.7.1 Case Study

The goal is then to design the filter, on/off thresholds and the output magnitude to achieve desired performance.

A simple linear control in Section 4.4.2 and the passivity based nonlinear control in Section 4.5 were used to illustrate the effectiveness of the PWPF method. The initial conditions and control gains were kept the same to be consistent with the results presented in their respective sections. Furthermore, the results have been normalized as described in Section 3.3. Figure 4.38 and Figure 4.40 clearly show that the controller can converge to the desired equilibrium and the performance of the controller has not been adversely affected. Figure 4.39 and Figure 4.41 depicts the response of the system without PWPF modulation. Clearly the discrepancy between the response with and without the PWPF is negligible. Figure 4.42 shows the PWPF modulated control input. The figure appears to show spikes because of the sampling rate of the simulation. In fact, the minimum pulse width of the signal is 0.0001 orbits, which translates to 0.5 seconds for a LEO orbit around 400km. This minimum pulse width can be controlled based on mission/system requirements by adjusting the PWPF parameters.

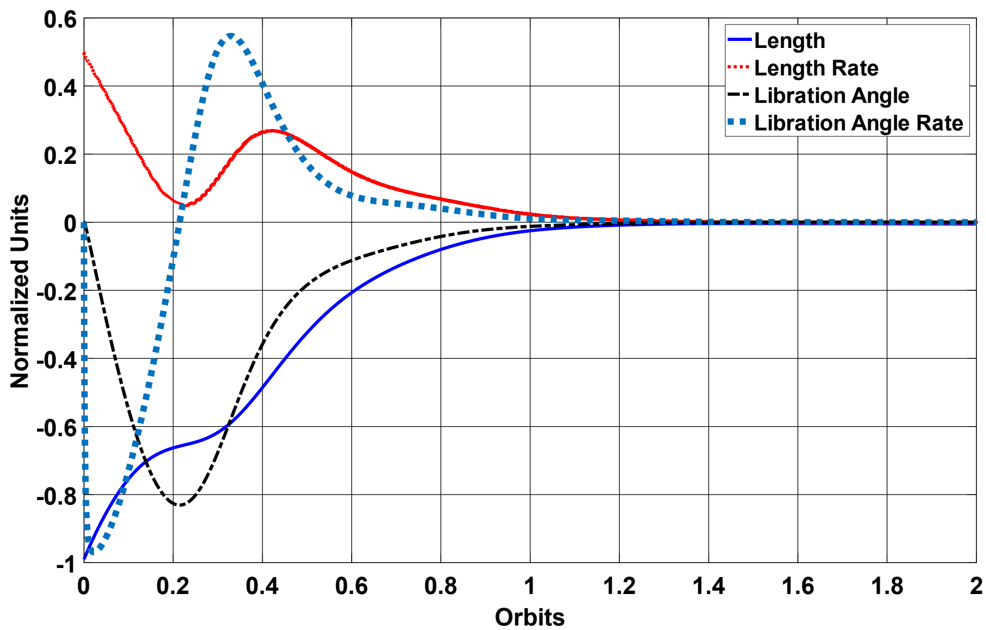

Figure 4.38 System Response with Linear control and PWPF modulation.

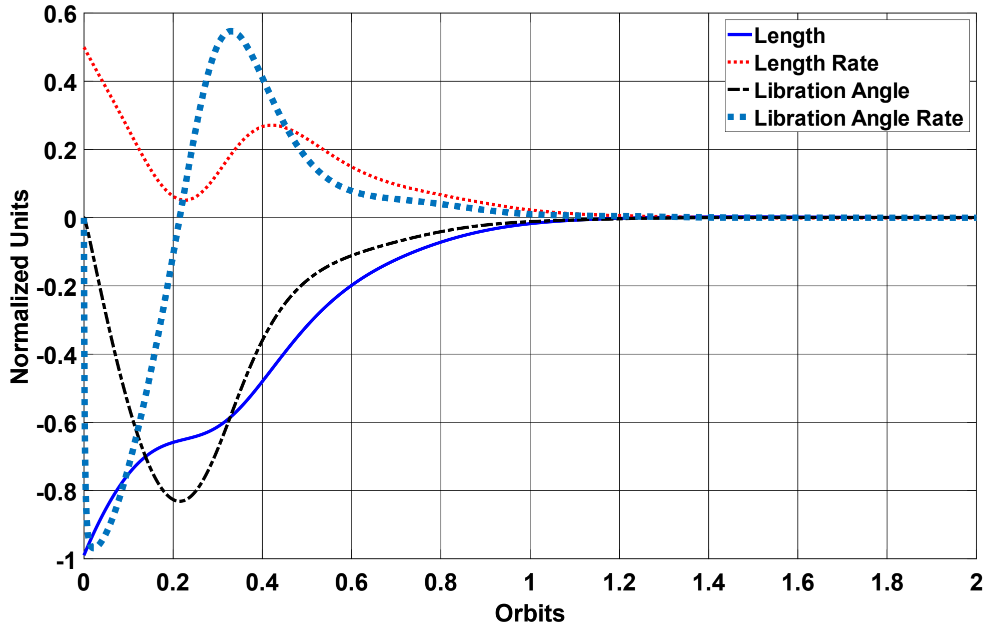

Figure 4.39 System Response with Linear Control and without PWPF modulation

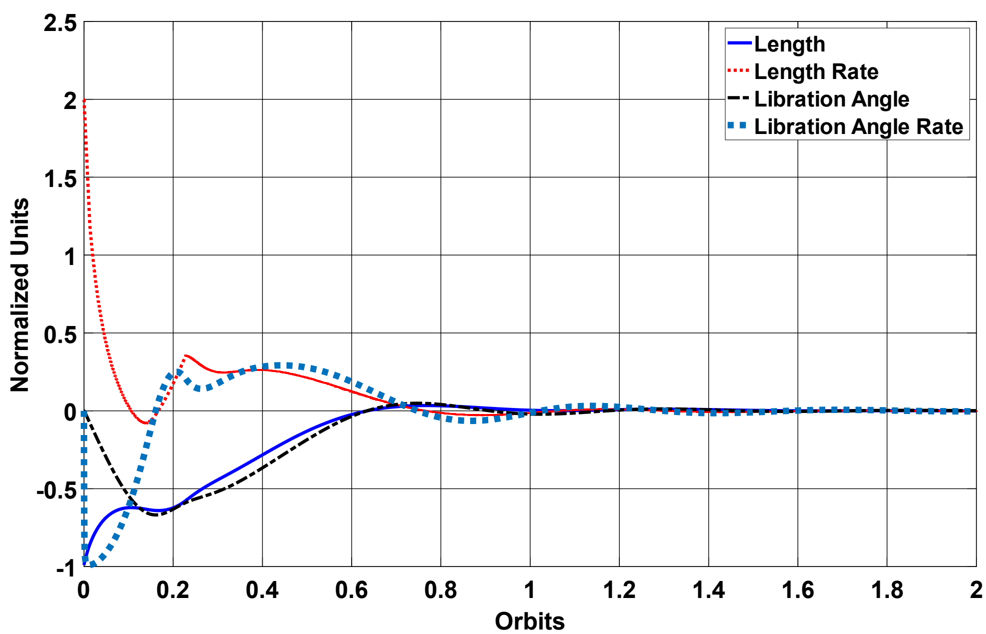

Figure 4.40 System Response with Nonlinear control and PWPF modulation.

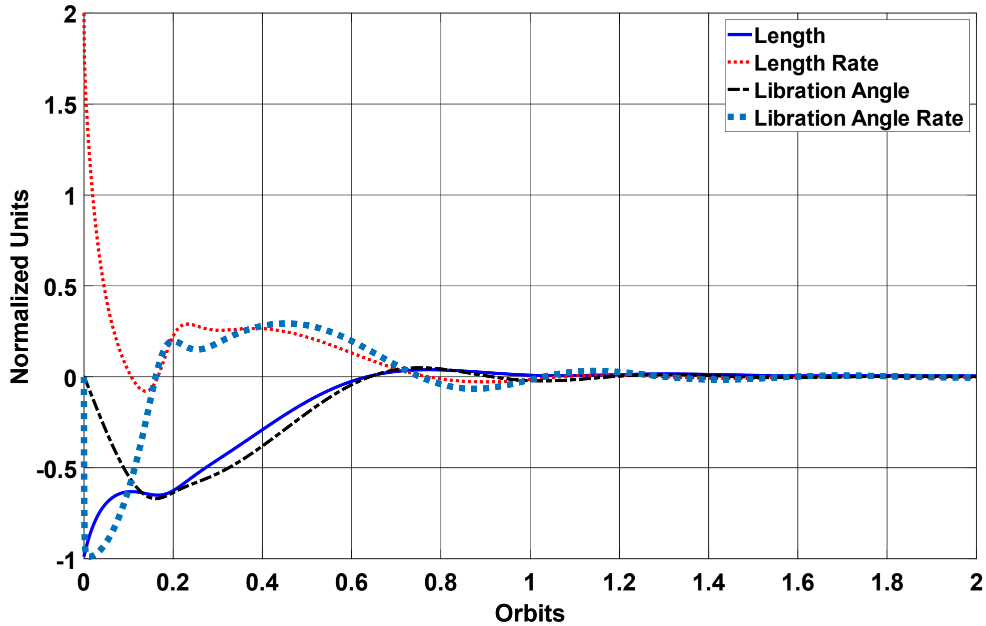

Figure 4.41 System Response with Nonlinear control and without PWPF modulation .

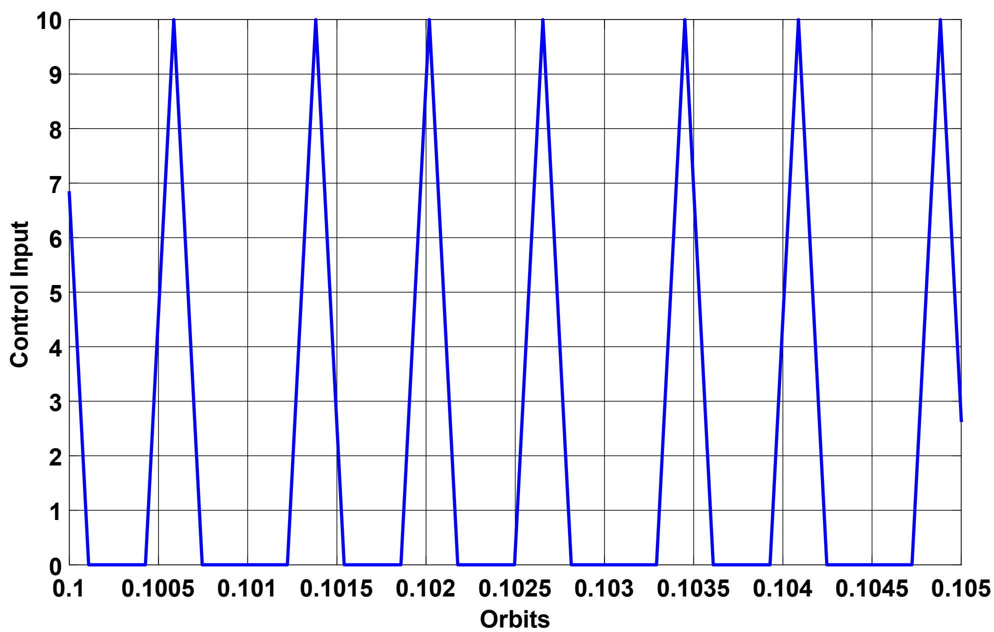

Figure 4.42 PWPF Modulated Control Input

Chapter 5 OBSERVERS FOR TETHERED SPACE SYSTEM

Summary: In this chapter, the concept and application of observers for the TSS are introduced. The need for observers arises from the limited resources available on nanosatellites. Then, linear and nonlinear observers are derived and compared. Finally, similar to the controller development, case studies for each observer are presented and analyzed.

5.1 INTRODUCTION

As discussed earlier, the tether dumbbell system is observable with the measurement of the length of the tether alone. It is advantageous to only collect this measurement and estimate the remaining states if needed. In some of the linear control laws, the feedback was limited to the length and length rate. However, the nonlinear counterparts required all states for feedback. In this chapter, a simple linear observer is designed to handle nominal cases where the measurements are assumed to be continuous and then a nonlinear observer is designed to handle scenarios where the measurements are discrete and appear at time-varying intervals. Arguably, since the length is measured, the length rate can be numerically computed, however, it will be very noisy especially for the proposed length measurement system in this thesis. It will result in zero speed at times between measurements and then spikes/jumps at the time of measurements. The proposed observer addresses this limitation by providing a smooth estimation of the speed of the tether.

5.2 LINEAR OBSERVER

Linear observers are powerful tools in control theory that permit the use of full-state feedback controllers with noisy and limited measurements of the system. Given the surprisingly pleasant performance of linear controllers for the tethered system, this section will design and analyze the performance of a linear observer. For this observer, it is assumed that the measurement is continuous.

Consider the observer system shown in Figure 5.1. The observer dynamics can be described as,

$$\dot{\tilde{\mathbf{x}}} = \mathbf{A}\tilde{\mathbf{x}} + \mathbf{B}u - \mathbf{K}_{\mathbf{obs}}(y - \mathbf{C}\tilde{\mathbf{x}}) \tag{5.1}$$

where $\tilde{\mathbf{x}}$ is the observed state and $\mathbf{K}_{\mathbf{obs}}$ is the observer gain to be designed. Now consider the observer error dynamics,

$$\dot{\mathbf{x}} - \dot{\tilde{\mathbf{x}}} = \mathbf{A}\mathbf{x} - \mathbf{A}\tilde{\mathbf{x}} - \mathbf{K}_{\mathbf{obs}}(\mathbf{C}\mathbf{x} - \mathbf{C}\tilde{\mathbf{x}}) = (\mathbf{A} - \mathbf{K}_{\mathbf{obs}}\mathbf{C})(\mathbf{x} - \tilde{\mathbf{x}}) \tag{5.2}$$

where the output $\mathbf{y} = \mathbf{C}\mathbf{x}$. Therefore, the observer design essentially becomes choosing the observer gain matrix $\mathbf{K}_{\mathbf{obs}}$ such that the matrix $\mathbf{A} - \mathbf{K}_{\mathbf{obs}}\mathbf{C}$ is Hurwitz. Similar to the design of linear controllers, there are many approaches to choosing the observer gain matrix. For simplicity, the pole-placement method is chosen and since the system is fully observable, arbitrary placement of the observer pole is possible.

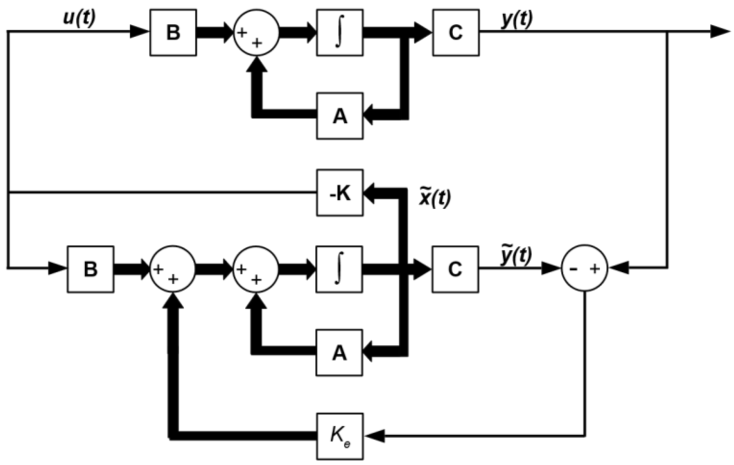

Figure 5.1 Observer State Feedback Block Diagram.

Interestingly, the effects and therefore choice of the observer poles is independent of the choice of the state feedback control gain matrix. Consider the dynamics of the system,

$$\begin{aligned}\dot{\mathbf{x}} &= \mathbf{Ax} + \mathbf{B}u \\ y &= \mathbf{Cx}\end{aligned} \tag{5.3}$$

The state feedback for this system is,

$$u = -\mathbf{K}\tilde{\mathbf{x}}$$

The dynamics of the system is now,

$$\dot{\mathbf{x}} = \mathbf{Ax} - \mathbf{BK}\tilde{\mathbf{x}} \tag{5.4}$$

Now add and subtract $\mathbf{BKx}$ to (5.4) to yield,

$$\dot{\mathbf{x}} = (\mathbf{A} - \mathbf{BK})\mathbf{x} + \mathbf{BK}(\mathbf{x} - \tilde{\mathbf{x}}) \tag{5.5}$$

Define $\mathbf{e} = \mathbf{x} - \tilde{\mathbf{x}}$ and note (5.2) can be expressed as,

$$\dot{\mathbf{e}} = (\mathbf{A} - \mathbf{K_{obs}C})\mathbf{e} \tag{5.6}$$

Combining the system dynamics (5.5) and the observer dynamics (5.6) yields,

$$\begin{bmatrix} \dot{\mathbf{x}} \\ \dot{\mathbf{e}} \end{bmatrix} = \begin{bmatrix} \mathbf{A} - \mathbf{BK} & \mathbf{BK} \\ \mathbf{0} & \mathbf{A} - \mathbf{K_{obs}C} \end{bmatrix} \begin{bmatrix} \mathbf{x} \\ \mathbf{e} \end{bmatrix} \tag{5.7}$$

The characteristic equation of this system is,

$$\left| s\mathbf{I} - \mathbf{A} + \mathbf{BK} \right| \left| s\mathbf{I} - \mathbf{A} + \mathbf{K_{obs}C} \right| \tag{5.8}$$

Clearly, the poles contributed by the controller and observer are independent of each other which implies that they can be designed separately without knowledge of the other. However, this does not guarantee that the performance of the controller with the observer will meet the desired requirements. This can be attributed to the fact that the observer needs some time to converge to the actual states. During this period, in which the controller although bounded and stable, may not perform as designed. It is important to note that the order of the system has now increased from $n \to 2n$.

5.2.1 Case Study

The observer was designed using the pole-placement method where the closed-loop poles were arbitrarily chosen as,

$$p_1 = -5, p_2 = -3, p_3 = -2 + 3i, p_4 = -2 - 3i \tag{5.9}$$

This resulted in the following observer gain matrix,

$$K = \begin{bmatrix} 12 \\ 56 \\ -6 \\ 40 \end{bmatrix} \tag{5.10}$$

Although the observer was designed using the linear system, the results were simulated using the full nonlinear system and the passivity based nonlinear control law presented in

Section 4.5. This controller was chosen since it required full-state feedback and had the optimum performance compared to the other nonlinear controllers. As seen in Figure 5.2, the observer state feedback performs well as all states converge to the equilibrium within two orbits. As mentioned before, the results have been normalized as in Section 3.3.

The observer error was also analyzed under varying initial conditions Table 5-1. Case 1 was identical to the case used in Section 4.5.2 without the presence of the observer as a benchmark and the remaining two cases were used to illustrate the rate of convergence of the observer. Clearly the large change in initial conditions did not greatly affect the performance of the observer as the error still converged in 0.6 orbits. It is important to note that although the closed-loop poles of the observer were arbitrarily chosen, other choices only yielded marginal improvements in the performance of the observer. This is probably a result of the fidelity of the model since a linear approximation is used to estimate the nonlinear behavior.

Finally, as mentioned earlier, although the controller and observer can be designed independently without knowledge of the other, the controller performance with the observer is not guaranteed. This is evident in Figure 5.6 where the controller without the observer can achieve deployment within an orbit and with the observer requires more than two orbits. However, it is possible to achieve slightly better performance with modified gains.

Table 5-1 Linear Observer Initial Conditions

Initial Conditions	Case 1	Case 2	Case 3

x_{10}	-0.99	-0.99	-0.99
x_{20}	2	1	1
x_{30}	0	0	$-\pi/4$
x_{40}	0	0	$-\pi/8$

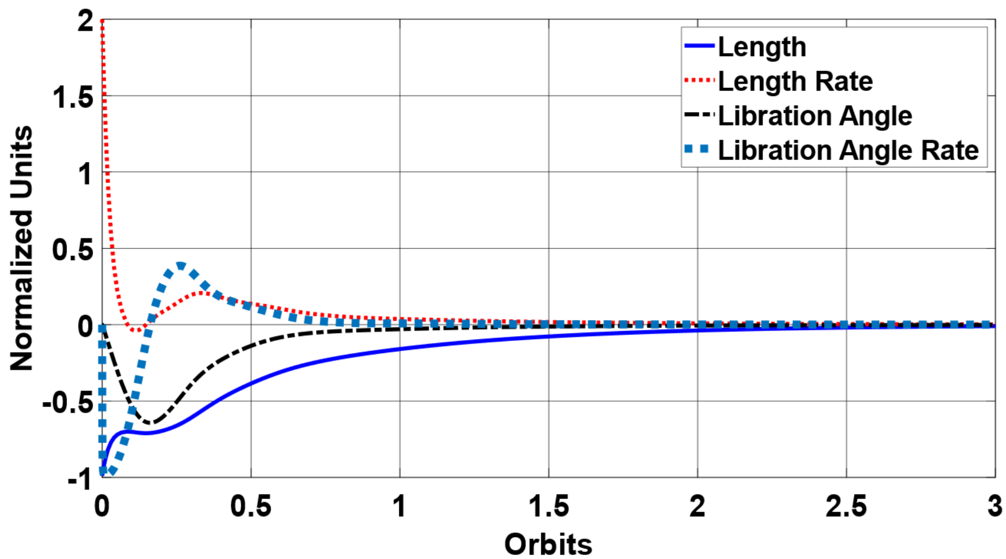

Figure 5.2 Results of nonlinear control with observer.

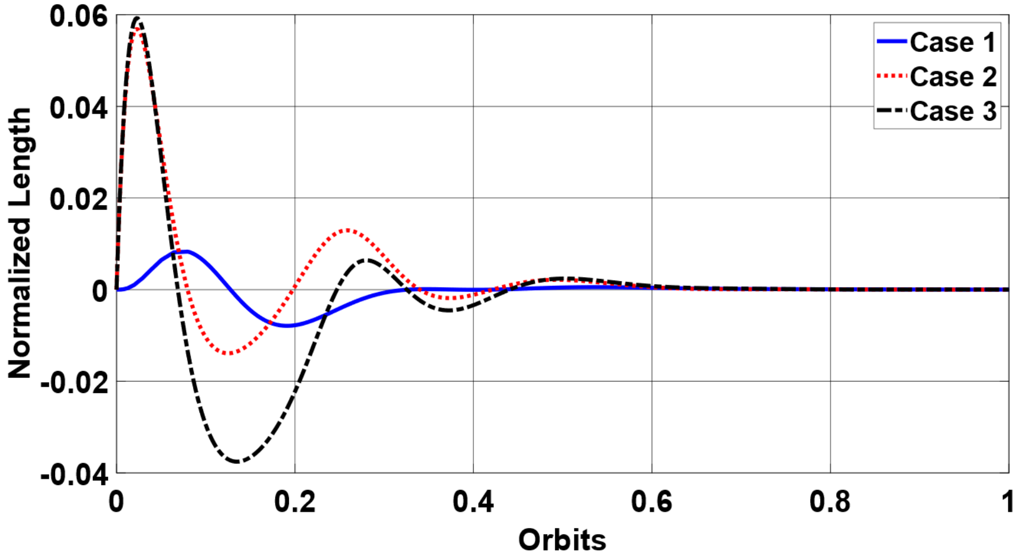

Figure 5.3 Observer error length.

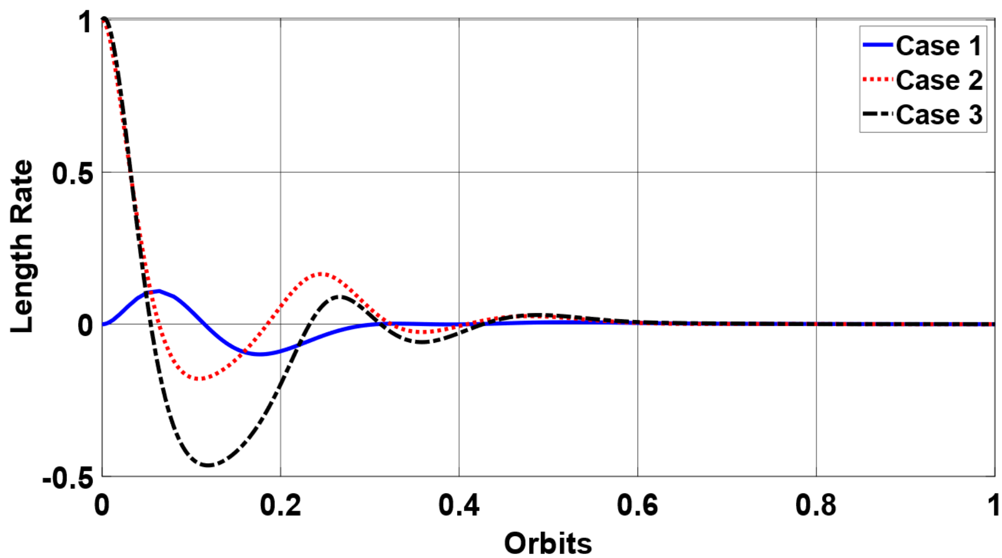

Figure 5.4 Observer error of normalized length rate.

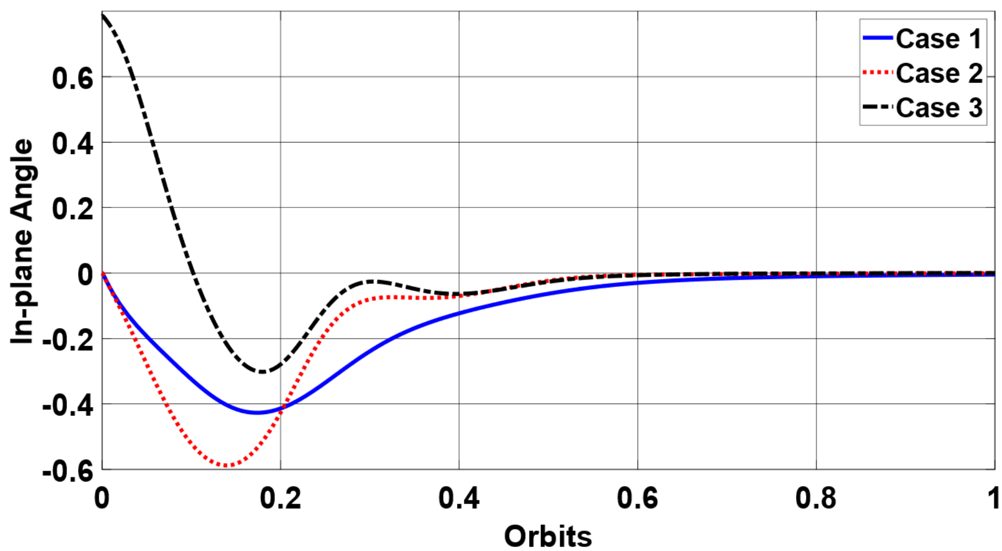

Figure 5.5 Observer error in-plane angle.

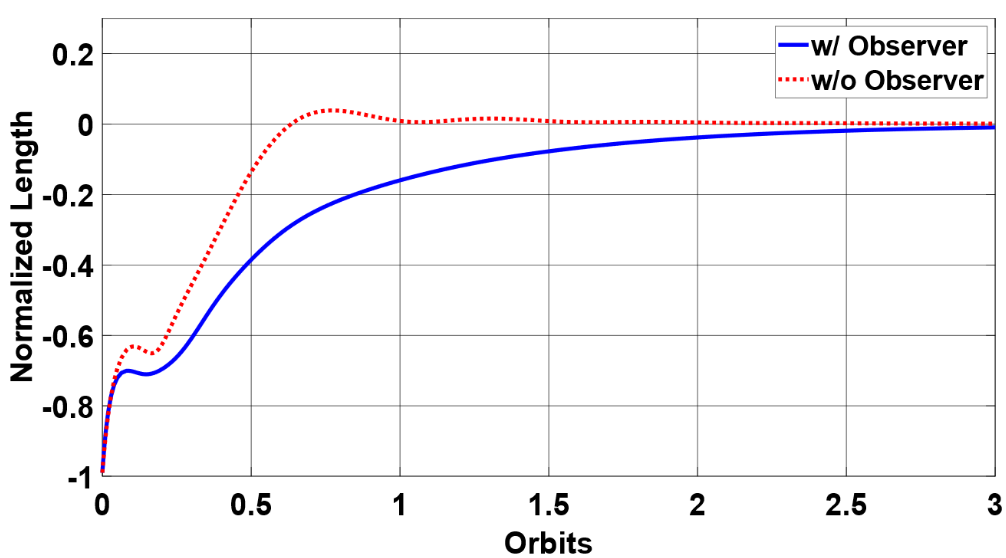

Figure 5.6 Comparison with and without observer.

5.3 NONLINEAR OBSERVER

Continuous-time observers have been extensively studied throughout the literature [94]

[95] [96] [97] [98]. In many practical implementations where the sampling rate of measurements is sufficiently high, these observers provide the ideal solution because of their simplicity. There are instances however, where the sampling rate of measurements cannot meet the desired requirements, and/or they are not guaranteed to occur in constant intervals. Thus, continuous-discrete time observers were introduced to compensate for these irregularities [99] [100] [101]. The basic principle is that continuous predictions are made between $t_k \le t \le t_{k+1}$ and at t_{k+1}, measurements are sampled, and predictions are updated.

The class of nonlinear systems applicable to the observer can be described as,

$$\begin{aligned} \dot{\mathbf{x}}(t) &= \mathbf{A}\mathbf{x}(t) + \mathbf{f}\left(u(t), \mathbf{x}(t)\right) \\ y(t_k) &= \mathbf{C}\mathbf{x}\left(t_k\right) \end{aligned} \tag{5.11}$$

where,

$$\begin{aligned} &\mathbf{x} = \begin{pmatrix} \mathbf{x}^1 \\ \vdots \\ \mathbf{x}^{q-1} \\ \mathbf{x}^q \end{pmatrix} \in \mathbb{R}^n \qquad \mathbf{f}\left(u, \mathbf{x}\right) = \begin{pmatrix} \mathbf{f}^1(u, \mathbf{x}^1) \\ \vdots \\ \mathbf{f}^{q-1}(u, \mathbf{x}^1, \dots, \mathbf{x}^{q-1}) \\ \mathbf{f}^q(u, \mathbf{x}) \end{pmatrix} \\ &\mathbf{A} = \begin{pmatrix} \mathbf{0}_p & \mathbf{I}_p & & \mathbf{0}_p \\ \vdots & \ddots & \ddots & \\ \vdots & & \ddots & \mathbf{I}_p \\ \mathbf{0}_p & \mathbf{0}_p & \cdots & \mathbf{0}_p \end{pmatrix} \qquad \mathbf{C} = \begin{pmatrix} \mathbf{I}_p & \mathbf{0}_p & \cdots & \mathbf{0}_p \end{pmatrix} \end{aligned} \tag{5.12}$$

Here, $\mathbf{x}^i \in \mathbb{R}^p$ are the state variables, $u \subset \mathbb{R}^s$ is the control input with $s \le n$, and $y \in \mathbb{R}^p$ are the system outputs that are sampled at $0 \le t_k \le \infty$ with time-varying intervals $\tau_k = t_{k+1} - t_k$. The functions f^i, are assumed to be globally Lipschitz with respect to x uniformly in u and the main assumption here is that $\mathbf{f}$ has a triangular structure. Therefore, if the system is not of this form, then there needs to exist a diffeomorphism that puts the system into the desired form. Indeed, in general, the transformation in (5.13) may be used but, the inverse may not be trivial and in general, may not be unique.

$$\mathbf{T(x)} = \begin{pmatrix} h(\mathbf{x}) \\ L_f h(\mathbf{x}) \\ \vdots \\ L_f^{r-1} h(\mathbf{x}) \end{pmatrix} \tag{5.13}$$

where $h \subset \mathbb{R}^p$ and r is the relative degree of the system. However, through a slightly different perspective, we propose to relax the assumption of a triangular structure on $\mathbf{f}$ so that the observer is applicable to a wider class of nonlinear systems.

Consider the same system as in (5.11) now with the following function $\mathbf{f}$,

$$\mathbf{f} = \begin{pmatrix} \mathbf{f}^1(u,\mathbf{x}) \\ \vdots \\ \mathbf{f}^{q-1}(u,\mathbf{x}) \\ \mathbf{f}^q(u,\mathbf{x}) \end{pmatrix} \tag{5.14}$$

Then, the following candidate observer is applicable to this system as well.

$$\dot{\hat{\mathbf{x}}} = \mathbf{A}\hat{\mathbf{x}}(t) + \mathbf{f}\left(u(t), \hat{\mathbf{x}}(t)\right) - \theta \mathbf{\Delta}_\theta^{-1} \mathbf{K} e^{-\theta \mathbf{K}^1 (t - t_k)} \left(\mathbf{C}\hat{\mathbf{x}}(t_k) - \mathbf{y}(t_k)\right) \tag{5.15}$$

where $\hat{\mathbf{x}} = \left(\hat{\mathbf{x}}^{1^T} \ldots \hat{\mathbf{x}}^{q^T}\right)^T$ are the state estimates, $\mathbf{K} = \left(\mathbf{K}^{1^T} \ldots \mathbf{K}^{q^T}\right)^T$ is the gain matrix where $\mathbf{K}^i$ is a $p \times p$ matrix that is designed such that $\bar{\mathbf{A}} = \mathbf{A} - \mathbf{KC}$ is Hurwitz and $\mathbf{\Delta}_\theta$ is defined as follows with $\theta \geq 1$.

$$\mathbf{\Delta}_\theta = diag\begin{pmatrix} \mathbf{I}_p & \frac{1}{\theta}\mathbf{I}_p & \cdots & \frac{1}{\theta^{q-1}}\mathbf{I}_p \end{pmatrix} \tag{5.16}$$

To see that this observer is applicable to the wider class of nonlinear systems, we must carefully review the proof of this observer in detail which essentially extends upon the traditional continuous-time observer to allow for bounded and irregular sampling intervals [102]. It can be seen that by simply replacing the Lipschitz constant, the proof is still valid. Consider the following,

$$\mathbf{f}(u,\mathbf{x}) = \begin{pmatrix} \mathbf{f}^1(u,\mathbf{x}) \\ \vdots \\ \mathbf{f}^{q-1}(u,\mathbf{x}) \\ \mathbf{f}^q(u,\mathbf{x}) \end{pmatrix} = \begin{pmatrix} \mathbf{f}^1(u,\mathbf{x}) \\ \vdots \\ 0 \\ 0 \end{pmatrix} + \begin{pmatrix} 0 \\ \vdots \\ \mathbf{f}^{q-1}(u,\mathbf{x}) \\ 0 \end{pmatrix} + \cdots + \begin{pmatrix} 0 \\ \vdots \\ 0 \\ \mathbf{f}^q(u,\mathbf{x}) \end{pmatrix} \tag{5.17}$$

Then, according to the Lipschitz condition,

$$\begin{aligned} \left\| \mathbf{f}(u,\mathbf{x}) - \mathbf{f}(u,\overline{\mathbf{x}}) \right\| &\le \left\| \begin{matrix} \mathbf{f}^1(u,\mathbf{x}) - \mathbf{f}^1(u,\overline{\mathbf{x}}) \\ \vdots \\ 0 \\ 0 \end{matrix} \right\| + \left\| \begin{matrix} 0 \\ \vdots \\ \mathbf{f}^{q-1}(u,\mathbf{x}) - \mathbf{f}^{q-1}(u,\overline{\mathbf{x}}) \\ 0 \end{matrix} \right\| + \cdots \\ &\quad + \left\| \begin{matrix} 0 \\ \vdots \\ 0 \\ \mathbf{f}^q(u,\mathbf{x}) - \mathbf{f}^q(u,\overline{\mathbf{x}}) \end{matrix} \right\| \\ &\le \sum_i L^i \left\| \mathbf{x} - \overline{\mathbf{x}} \right\| \end{aligned} \tag{5.18}$$

where L^i is the associated Lipschitz constant for each $\mathbf{f}^i$. Thus, choosing the appropriate Lipschitz constant $\hat{L} > \sum_i L^i$ permits the use of this observer to this extended class of nonlinear systems.

5.3.1 Case Study

Consider the following transformation,

$$\mathbf{z} = \begin{bmatrix} z_1 \\ z_2 \\ z_3 \\ z_4 \end{bmatrix} = \begin{bmatrix} x_1 \\ x_2 \\ 2x_4 \\ -3\sin(2x_3) \end{bmatrix} \tag{5.19}$$

Then, using the following identity $\cos\left(\sin^{-1} x\right) = \sin\left(\cos^{-1} x\right) = \sqrt{1-x^2}$, the system can be transformed into,

$$\begin{aligned}
\dot{z}_1 &= z_2 \\
\dot{z}_2 &= z_3 + z_3 z_1 + (1+z_1)\left[\frac{z_3^2}{4} + \frac{3}{2}\left(1+\sqrt{1-\frac{z_4^2}{9}}\right)\right] \\
\dot{z}_3 &= z_4 - 4\left(\frac{z_2}{1+z_1}\right)\left(1+\frac{z_3}{2}\right) \\
\dot{z}_4 &= -3z_3\sqrt{1-\frac{z_4^2}{9}}
\end{aligned} \tag{5.20}$$

Let,

$$\mathbf{A} = \begin{bmatrix} 0 & 1 & 0 & 0 \\ 0 & 0 & 1 & 0 \\ 0 & 0 & 0 & 1 \\ 0 & 0 & 0 & 0 \end{bmatrix}, \mathbf{f}(\mathbf{z},u) = \begin{pmatrix} 0 \\ z_3 z_1 + (1+z_1)\left[\frac{z_3^2}{4} + \frac{3}{2}\left(1+\sqrt{1-\frac{z_4^2}{9}}\right)\right] \\ -4\left(\frac{z_2}{1+z_1}\right)\left(1+\frac{z_3}{2}\right) \\ -3z_3\sqrt{1-\frac{z_4^2}{9}} \end{pmatrix} \tag{5.21}$$

$$\mathbf{C} = \begin{bmatrix} 1 & 0 & 0 & 0 \end{bmatrix}$$

Clearly the system is of the from (5.12) with the modification to $\mathbf{f}$ as in (5.14). The candidate observer in (5.15) performs well and is able to estimate the remaining states relatively accurately as compared to the linear observer.

Figure 5.7 depicts the discretized measurements of length and length rate and it is evident that the intervals between measurements are non-uniform. Once again, the dimensions are normalized as described in Section 3.3. Furthermore, there are periods that extend as long as 5-10% of the orbit without a measurement and yet, the observer and controller are still able to achieve successful deployment. This upper limit can in theory be calculated but is quite complex and left for future work. However, when the time between measurements extend beyond this threshold (i.e., when the deployment velocity is slow towards end of deployment), the observer begins to oscillate and potentially diverge. A brute force solution is to decrease the step size between measurements towards the end of deployment. For example, if measurements are collected at every 5m, then towards the end of deployment, measurements should be collected at every 5cm. Again, the exact ratio can be calculated theoretically but is left outside of the scope of this thesis.

Both controllers were simulated with PWPF modulation. Table 5-2 below outlines the simulation parameters. For each case, the system response and the observer error has been plotted. The nonlinear control with the same initial conditions has almost negligible error and the observer is able to estimate the states of the system very effectively. It would be interesting to see the performance of the observer under disturbances such as atmospheric drag but has been left for future work.

In the linear observer case, there was degraded performance due to the presence of the observer, however, in the nonlinear case, these adverse effects are negligible. This can be attributed to the better convergence performance of the nonlinear observer and the use of the full nonlinear model. Furthermore, there is significant performance improvements of the estimation of the length and length rate of the nonlinear observer as compared to its linear counterpart.

Table 5-2 Simulation Parameters for Nonlinear Observer

	Case 1 Linear Control		Case 2 Linear Control		Case 3 Nonlinear Control		Case 4 Nonlinear Control	
	Plant	Observer	Plant	Observer	Plant	Observer	Plant	Observer
x_{10}	-0.99	-0.99	-0.99	-0.99	-0.99	-0.99	-0.99	-0.99
x_{20}	0.5	0.5	0.5	1	2	2	2	2.5
x_{30}	0	0	0	0	0	0	0	0
x_{40}	0	0	0	0	0	0	0	0

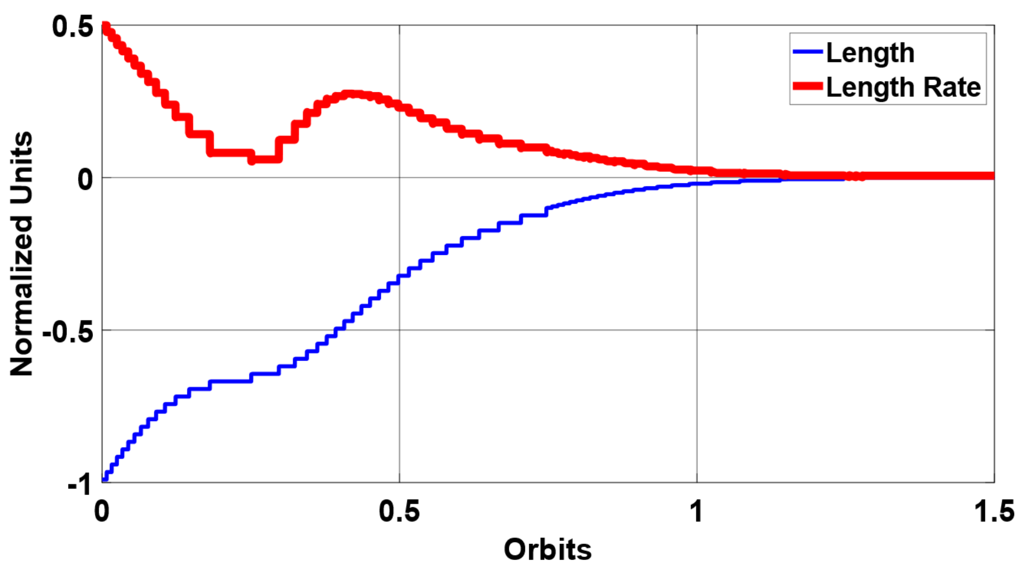

Figure 5.7 Discrete measurements of tether length and length rate.

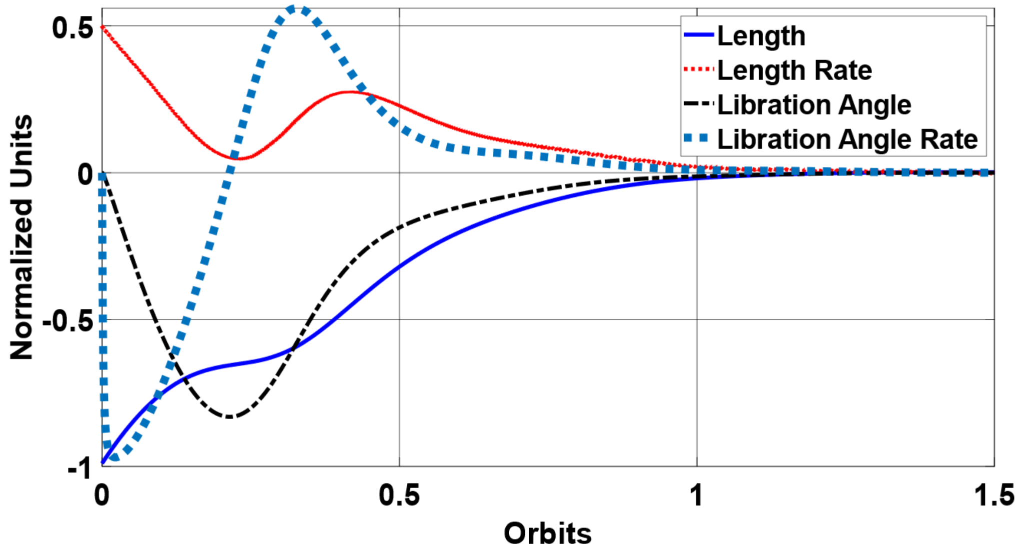

Figure 5.8 Case 1 system response.

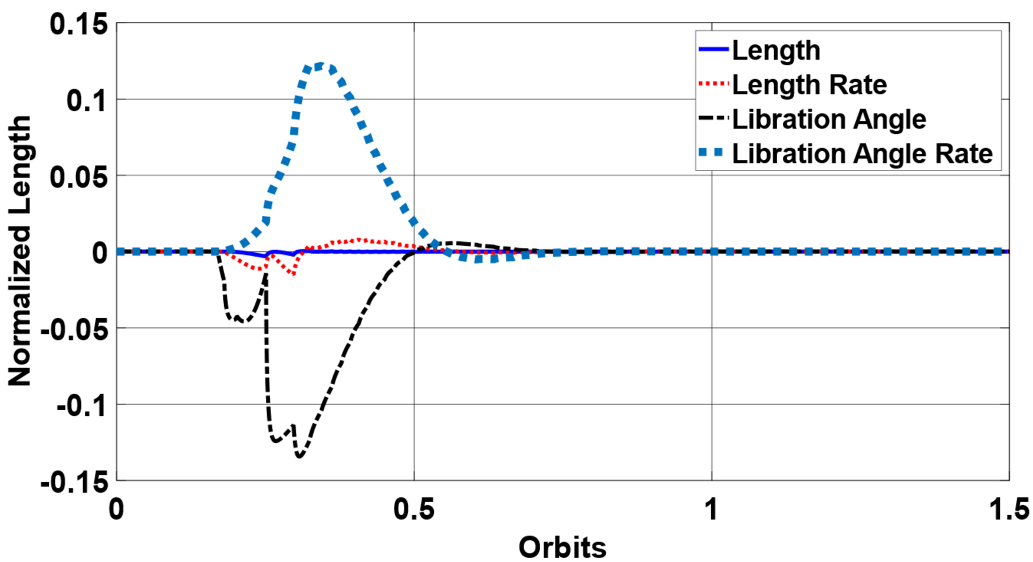

Figure 5.9 Case 1 observer error.

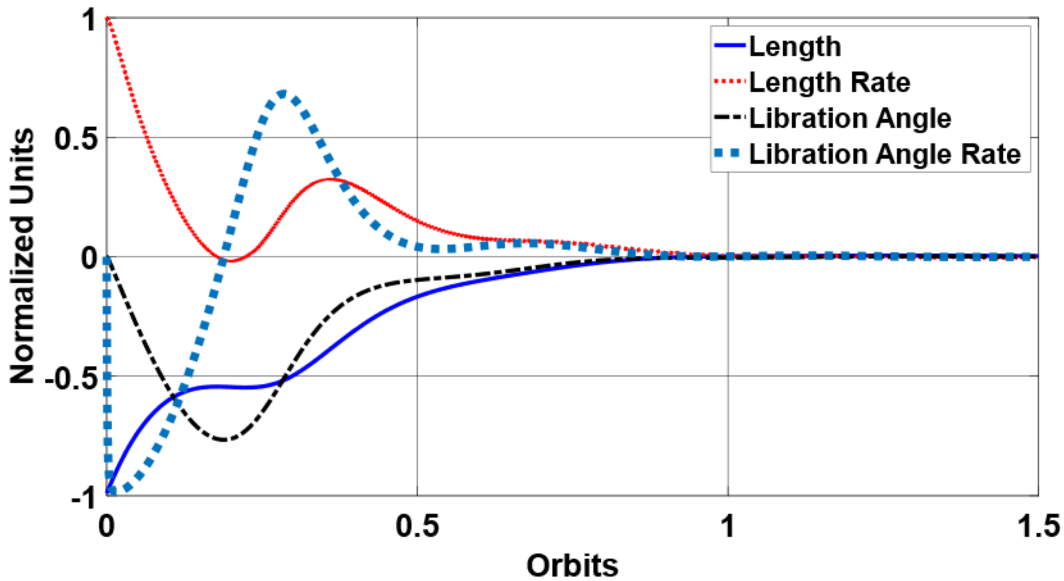

Figure 5.10 Case 2 system response.

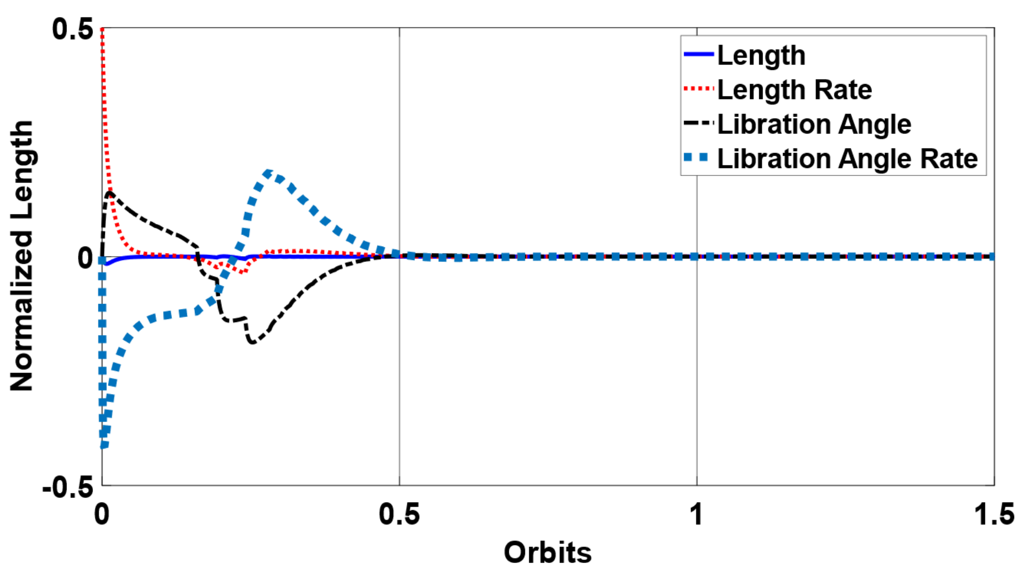

Figure 5.11 Case 2 observer error.

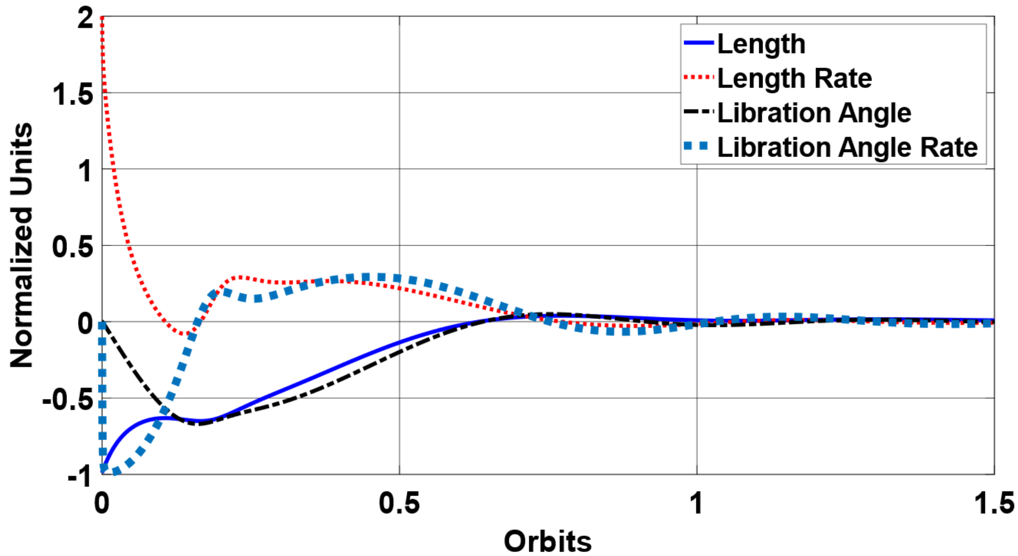

Figure 5.12 Case 3 system response.

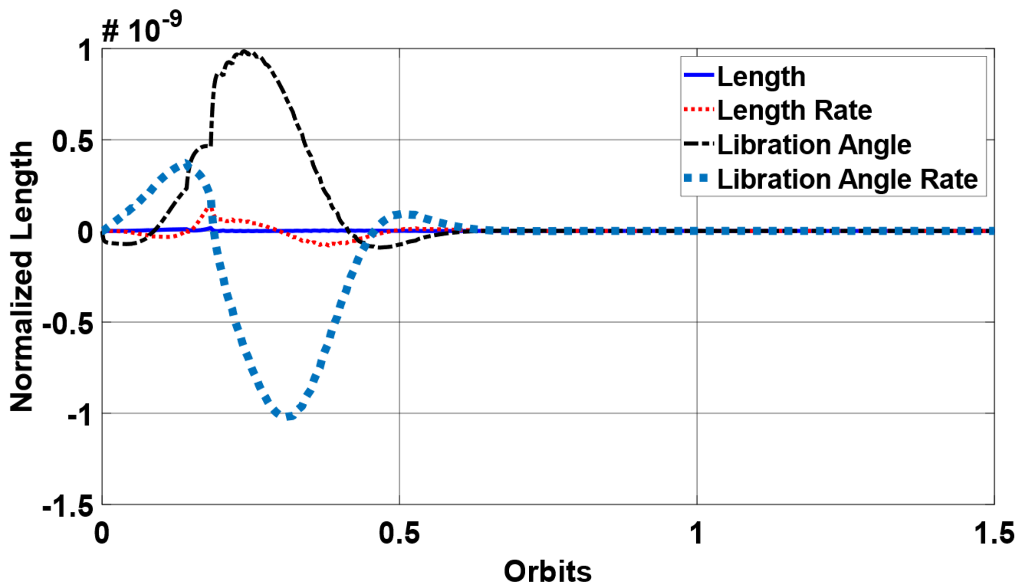

Figure 5.13 Case 3 observer error.

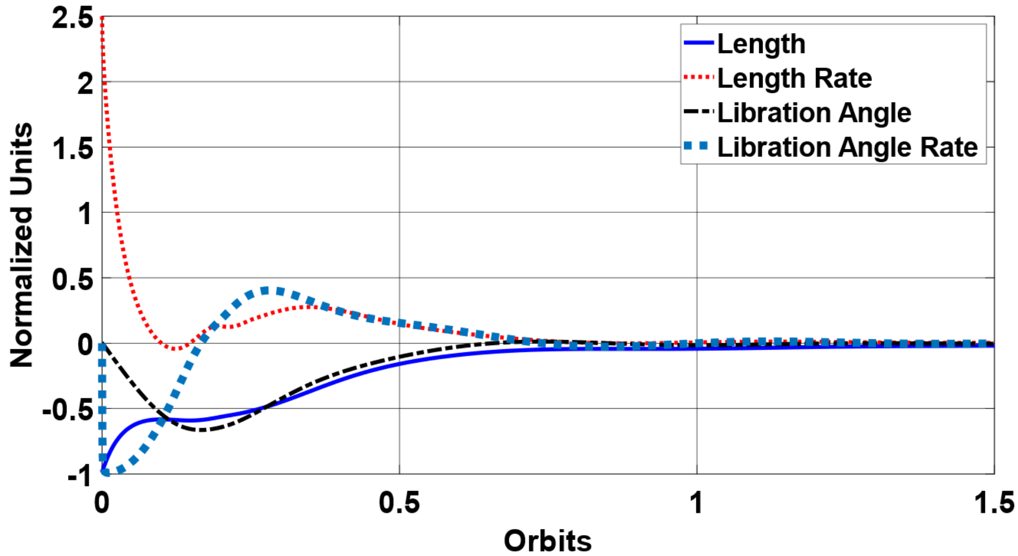

Figure 5.14 Case 4 system response.

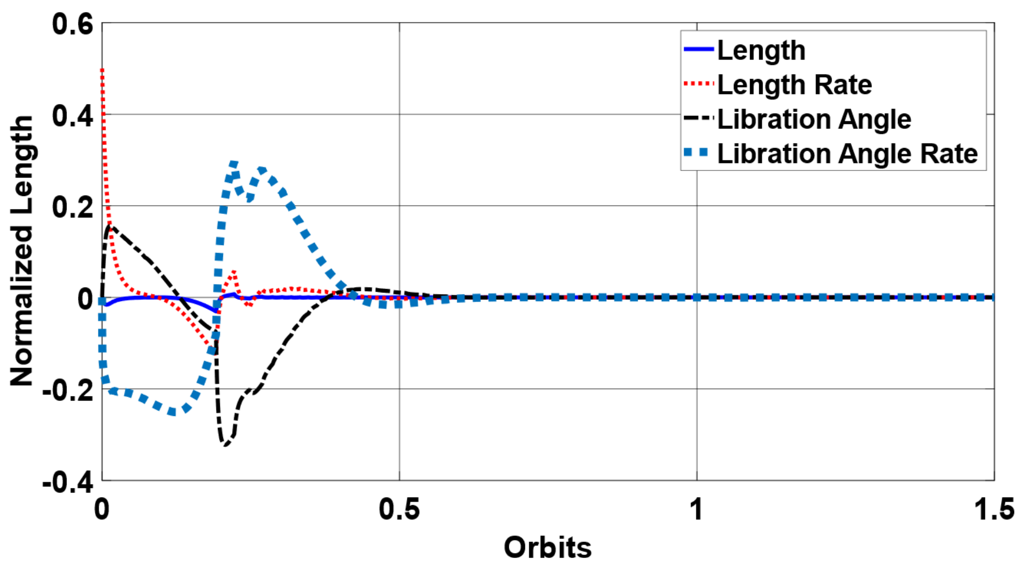

Figure 5.15 Case 4 observer error.

Chapter 6 SOFTWARE-IN-THE-LOOP SIMULATION

Summary: In lieu of ground based experiments, this chapter will focus on the use of commercial software to validate the TSS deployment under higher fidelity dynamics models and a variety of external disturbances. First, rationale and a brief overview of the commercial software and its capabilities will be presented, followed by the integration of the controllers with the commercial software. Finally, a case study is analyzed to show the effectiveness of this approach. In the case study, one simple linear controller is utilized to show a proof-of-concept. The integration of more advanced controllers is left for future work.

6.1 RATIONALE FOR SIL SIMULATION

As mentioned in Section 2.4, ground based experiments for TSS deployment is difficult to procure and conduct. Therefore, in this thesis, advanced simulations are performed and analyzed to supplement this shortcoming and validate the controller development. The controllers are placed in a closed feed-back loop with the commercial software and from this perspective, the plant model is essentially replaced by the commercial software. The advantage of this approach is the ability to include a variety of different plant models and disturbances while iterating rapidly on the controller performance, if necessary.

6.2 COMMERCIAL SOFTWARE

AGI's System Tool Kit (STK) is a powerful tool used to analyze and visualize complex systems such as spacecrafts in low earth orbit. The software contains high fidelity models of the Earth and its atmosphere, as well as common disturbances found in the space environment such as gravitational forces from other bodies (i.e., sun, moon, etc…) and solar radiation to name a couple. The software has many features and tools, but the most relevant features for this thesis are the ability to use these models to propagate the motion of satellites in all six degrees of freedom, as well as the ability to include custom user-define forces during propagation. Since STK does not have any properties or functionality that can be used to simulate the dynamics of the tether, it needs to be artificially included through user-defined functions. STK exposes these functions through a dedicated programming interface with support for various programming languages. An implementation of this approach with VBScript and MATLAB can be found in Appendix A.

6.3 INTEGRATION OF CONTROLLERS WITH COMMERCIAL SOFTWARE

The objective is to simulate the deployment dynamics of the tether in STK. This can be achieved by using a user-defined function to compute the forces the tether exerts on the spacecraft, given the current state and, send it to STK in real-time at every timestep. Then, STK can propagate the motion of the spacecraft as if it were constrained by a tether. This

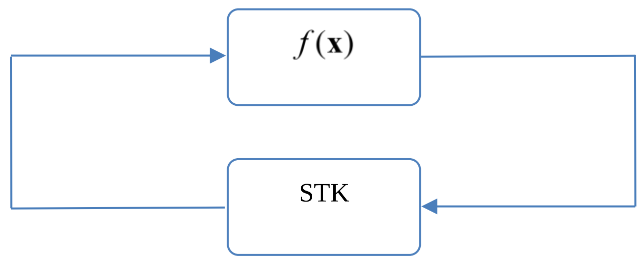

Figure 6.1 Interfacing STK with a user-defined function

is illustrated in Figure 6.1 where $f(\mathbf{x})$ is the user-defined function.

From the discussion in Section 4.1, it is evident that the tether tension is the only force exerted by the tether on each spacecraft, and all other forces are due to orbital dynamics. Therefore, we can leverage STK to compute the complex orbital dynamics which may include a variety of disturbances and utilize the user-defined function to compute the tension in the tether. Interestingly, this result coincides with the objective of the controller. As such, the user-defined function can directly be replaced by the controller. Also, STK can compute attitude dynamics as well, so in theory the effects of the tether on the attitude of the spacecraft can be analyzed but is left out of the scope of this thesis. Assumptions identified in Chapter 3 are still valid where the spacecrafts are considered as point masses connected by a massless rigid tether and the mass of one spacecraft is orders of magnitude larger than the other.

Environmental disturbances are introduced into the system where atmospheric drag is presumed to be the most significant/dominant especially for orbits with altitude less than 500km. Other disturbances such as oblateness of the Earth, solar radiation pressure and third-body gravity perturbations are included but they have negligible effects since the time-scales of the deployment process is much less than that of the effects of the disturbances. Eddy current induced magnetic torque effects on nanosatellites are also ignored since attitude dynamics were neglected. Mechanical disturbances such as those from friction at tether exit and kinks of folded tether are ignored at this stage and is left for future work.

The inputs to the controller will be limited to the length and length rate of the tether to be consistent with the results of this thesis. Since the notion of a tether does not exist in STK and the assumption of a massless and rigid tether still holds, the tether can be replaced by the vector between the two spacecrafts as in Figure 3.1. STK can easily output this vector and its derivative which are used as the length and length rate. Similarly, the controller outputs the tension T in the tether which, STK will view this as an external force on the spacecraft. It is important to note that this force is a vector and in the TSS, the unit force vector coincides with the unit length vector. Therefore, the output of the controller is the unit length vector (which was received as an input) with magnitude T. It is also important to note that these vectors are in the body frame of the main satellite. In STK, the body frame is chosen as the Local-Vertical Local-Horizontal (LVLH) frame.

6.4 CASE STUDY

Consider the TSS system in a low earth orbit with the following properties,

- Mass of the main satellite is 100kg, mass of the sub-satellite is 1kg
- Main satellite is in a circular orbit at an altitude of 400km above the equator
- Air drag acts on both satellites, each with a drag coefficient of 2.2
- Desired tether length 100m

STK's parameters were as follows,

- Epoch Jan. 22nd, 2019 (arbitrarily chosen)
- Earth geoid – EGM2008 with degree/order of 21
- Third-body gravity from Sun and Moon
- Jacchia-Roberts atmospheric density model
- ICRF Coordinate System
- HPOP Propagator
- RKF 7(8) Integrator – Runge-Kutta-Fehlberg integration method of 7th order with 8th order error control for the integration step size

There are many more parameters that can be enabled if greater fidelity is required. Discussion of these options and appropriate trade-offs are left outside the scope of this thesis.

The simple linear controller found in 4.4.2 was chosen for this simulation to provide a proof-of-concept. The gains were recomputed ($k_1 = 4.6, k_2 = 3.6, k_3 = 0, k_4 = 0, k_5 = 3$) since the libration rate is not available for feedback. Also, since the control law is in non-dimensional form, the output was scaled appropriately as in Section 3.3. The results of the simulation are shown in the figures below.

It is evident that controller is still able to achieve its objectives in a much more complex scenario. The error between the results of the MATLAB simulation and STK are reasonable. There exists quite a bit of discrepancy in the length rate (Figure 6.3), libration angle (Figure 6.4) and the beginning of the libration angle rate (Figure 6.5). This could be attributed to the disturbances acting on the system which is not considered in the MATLAB simulation. Furthermore, the errors at the end of Figure 6.3 is a result of numerical error. It is important to note that in these simulations, the tether is considered massless and the atmospheric drag effects of the tether have been neglected. Future work needs to be conducted to address this topic as careful consideration of the tether model in STK is required.

Since STK propagates the motion in all six degrees of freedom, the out-of-plane motion of the tether deployment process can be analyzed. From Figure 6.6, the assumption of weak-coupling between this state and the rest of the system is clearly validated. The slight divergence towards the end of the deployment process is again attributed to numerical error. Therefore, in controller design and analysis, this state can be neglected.

This approach could be extended to much more complex controllers and observers as well. There are two similar approaches that could be utilized. This first is the approach shown in this thesis with the code provided in Appendix A. The second is to connect STK with Simulink (tool part of MATLAB package). This approach may be more desirable when the controllers or observers rely on numerical integrators or first, second, or higher-order dynamics to compute their outputs. A few samples on this approach can be found on the internet for reference.

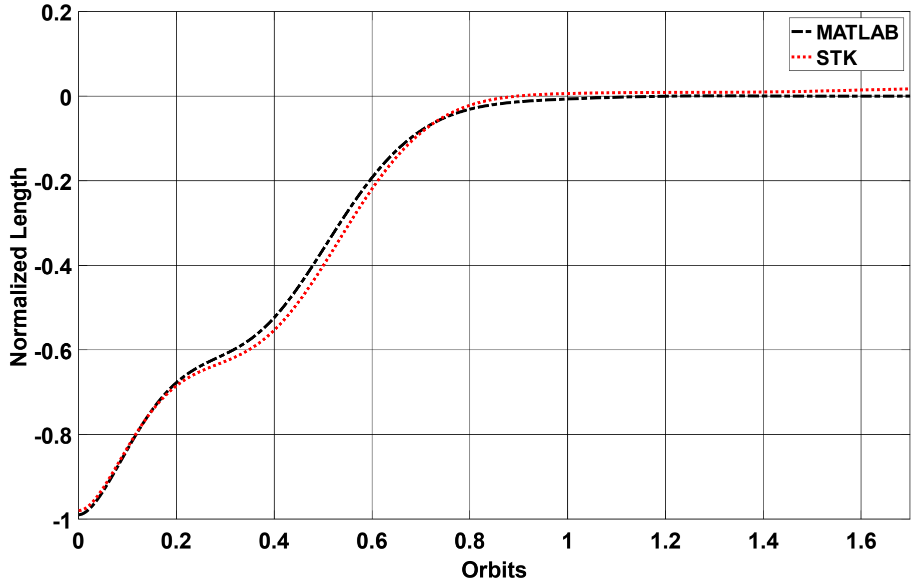

Figure 6.2 Comparison of Deployed Tether Length

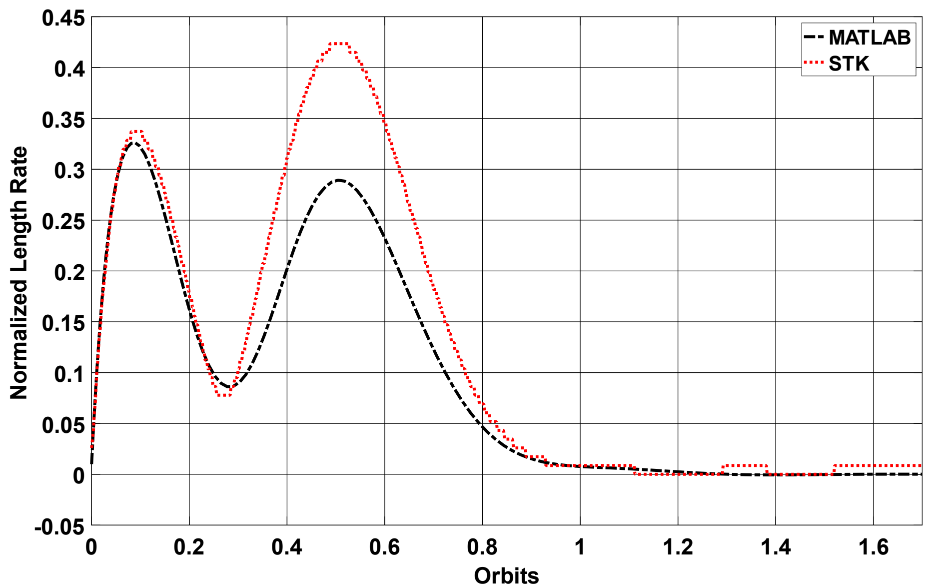

Figure 6.3 Comparison of Tether Velocity

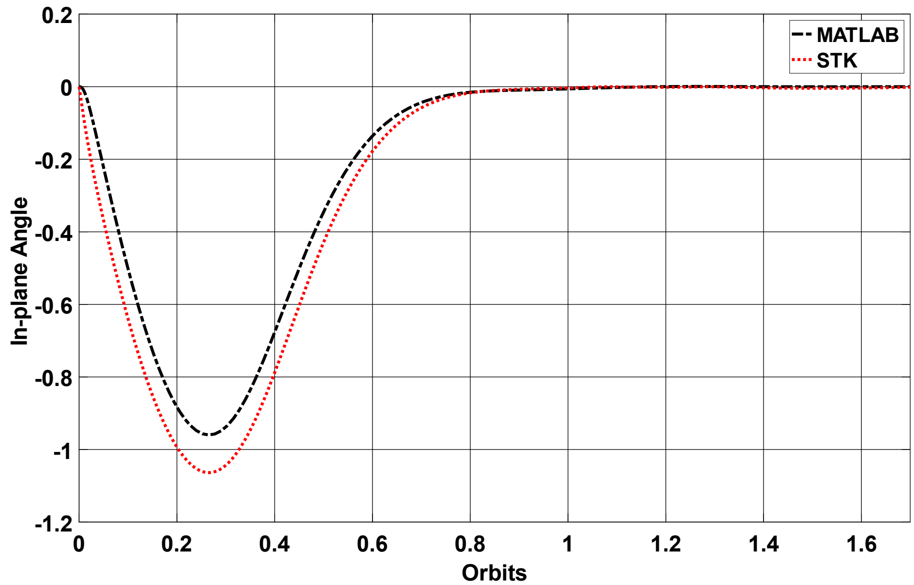

Figure 6.4 Comparison of Libration Angle

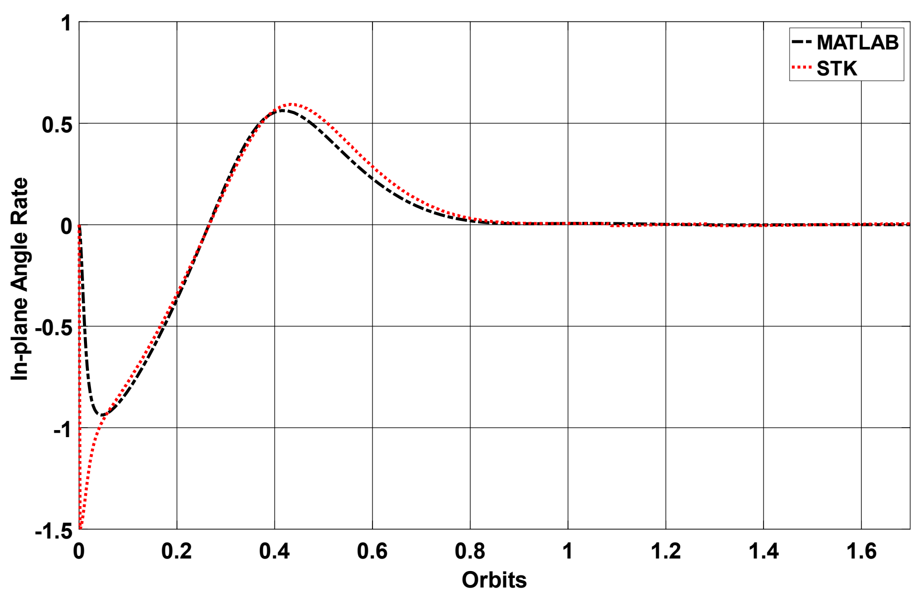

Figure 6.5 Comparison of Libration Angle Rate

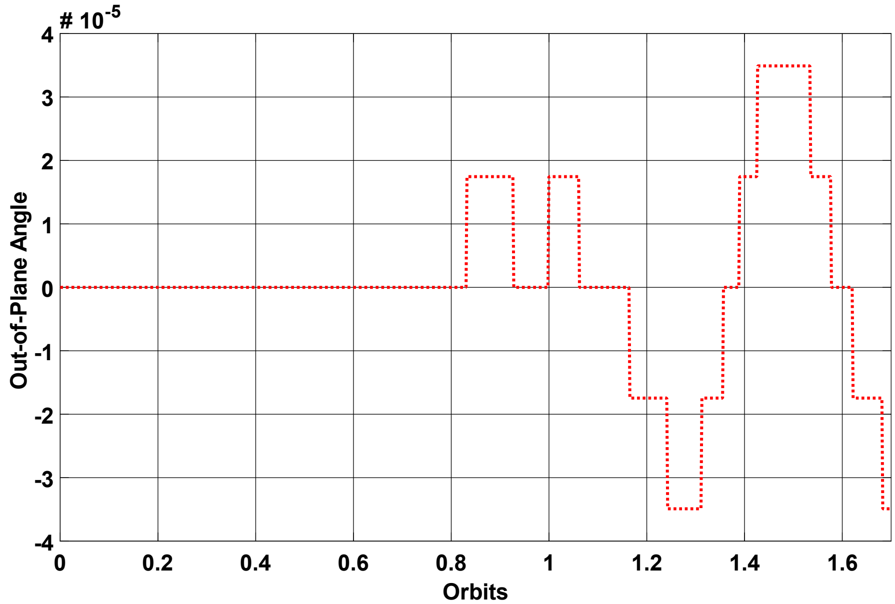

Figure 6.6 Out-of-Plane Tether Libration Angle

Chapter 7 CONCLUSIONS

7.1 SUMMARY OF CONTRIBUTIONS

The main contributions of this thesis are in the development of control laws for the space tether deployment problem, the development of advanced nonlinear observers for state estimation and validation of controllers under advanced plant models and disturbances. The control laws are developed for a deployment mechanism that is compatible with nanosatellites. The contributions are summarized as follows

7.1.1 Deployment Control of Space Tethers with Explicit Velocity Constraint

Most deployment mechanisms utilize a spring to generate an initial impulse and then a braking mechanism to control the deployment process. However, majority of the literature has neglected this property and assume the tether velocity is unconstrained. The limited research that has been conducted on this topic has either leveraged optimal control to achieve this objective or tackled this problem from a trajectory tracking point of view. In this thesis, a framework was developed in which the constraint is guaranteed to be satisfied mathematically. In fact, under the proposed framework, the controller development is decoupled from the constraint itself. Instead, it is shown that the constraint can be achieved through proper selection of control gains.

7.1.2 Observers for Space Tether Deployment Control

Linear controllers can be realized through feedback of the tether length and tether velocity alone. However, the nonlinear controllers rely on all states of the system to be available/measured for feedback. In this thesis, it was shown that the tether system is observable under only the measurement of the tether length. As such, a cost-effective approach is to develop observers to estimate the remaining states. A simple length measurement system used on the DESCENT mission was discussed which introduced a new and challenging problem. The measurements arrived at discrete time-varying intervals. Therefore, the observer would need to predict the states of the system in-between measurements and update its prediction at the measurement itself. Therefore, continuous-discrete observers were developed in this thesis to address this issue.

7.1.3 Software-In-The-Loop (SIL) Simulations

Ground based experiments for the tether deployment problem are difficult/expensive to procure and access. Instead, commercial software with advanced models of the space environment can be used to supplement this shortcoming. The advantage of this approach is the ability to quickly iterate on solutions and analyze the behavior/performance of the system under a variety of disturbances which is not feasible in ground-based experiments. In this thesis, controllers developed in MATLAB generated outputs which were fed into the commercial software. Then, the commercial software would propagate the motion of the system and feed the data back into the controller. The effectiveness of the proposed controllers is shown in these closed-loop simulations.

7.2 SUMMARY OF FINDINGS

This thesis has presented a framework that allows controller development under state constraints. This approach was then leveraged to tackle the TSS deployment problem with a spring-brake actuator. In this deployment mechanism, the tether must be deployed monotonically and cannot be reeled back in. Mathematically, this constraint can be stated as a non-negative tether length velocity throughout the deployment process. Closed-loop controllers that are proved to satisfy these constraints were developed. Furthermore, a new type of observer was applied to the TSS system that allows the measurement systems to be relatively inexpensive. Specifically, the length measurement system which produces measurements at discrete, time-varying intervals at time-scales much larger than controller actuation, were transformed into continuous estimates for closed-loop feedback through the use of a novel continuous-discrete nonlinear observer. Finally, advanced simulations beyond any found in the literature, were utilized to validate the performance of the TSS deployment controller. These simulations introduced advanced plant models and disturbances under which a simple linear controller was validated. The results showed that the simplified dumbbell model is a reasonable description of the physical system and closed-loop control laws derived from this model have relatively good performance.

7.3 FUTURE WORK

There are a few avenues to explore to continue and expand the current work. Potential future directions are discussed below.

1. Experimental validation of the measurement, observer estimation and closed loop

control.

2. Analyze the controller performance with model uncertainties and disturbances. In particular, if the mass of the tether is introduced, the aerodynamic drag would increase significantly.
3. Develop controllers for space tether deployment with two nanosatellites connected by a tether.
4. Consider the effects of attitude dynamics on the deployment process.

Bibliography

[1] Y. Yamagiwa, T. Fujii, K. Nakashima, H. Oshimori, T. Okino, S. Komua, S. Arita, M. Nohmi and Y. Ishikawa, "Space experimental results of STARS-C CubeSat to verify tether deployment in orbit," *Acta astronautica,* vol. In Press, 2020.

[2] J. A. Carroll, "Guidebook for Analysis of Tether Applications," NASA, 1985.

[3] H. Klinkrad, Space Debris: Models and Risk Analysis, Berlin, Germany: Springer, 2006.

[4] T. Furniss, D. Shayler and M. D. Shayler, Praxis Manned Spaceflight Log 1961-2006, Berlin, Germany: Springer, 2007.

[5] M. P. Cartmell and D. J. McKenzie, "A review of space tether research," *Progress in Aerospace Sciences,* vol. 44, no. 1, pp. 1-21, 2008.

[6] P. Williams, A. Hyslop, M. Stelzer and M. Kruijff, "YES2 Optimal Trajectories in presence of eccentricity and aerodynamic drag," *Acta Astronautica,* vol. 64, pp. 745-769, 2009.

[7] M. van Pelt, Space Tethers and Space Elevators, New York, USA: Copernicus, 2009.

[8] J. A. Carroll and J. C. Oldson, "Tethers for Small Satellite Applications," in *AIAA/USU Small Satellite*, Logan, USA, 1995.

[9] L. Johnson, H. A. Fujii and J. R. Sanmartin, "Electrodynamic propulsion system

tether experiment (T-REX)," in *57th JANNAF Joint Propulsion Meetings*, Colorado Springs, USA, 2010.

[10] L. Johnson, H. A. Fujii and J. R. Sanmartin, "Overview of future NASA tether applications," *Advances in Space Research,* vol. 24, no. 8, pp. 1055-1063, 1999.

[11] S. Koss, "Tether deployment mechanism for the advanced tether experiment (ATEx)," in *7th European Space Mechansims & Tribology Symposium*, Netherlands, 1997.

[12] H. Wen, D. P. Jin and H. Hu, "Advances in dynamics and control of tethered satellite systems," *Acta Mechanica Sinica,* vol. 24, no. 3, pp. 229-241, 2008.

[13] E. C. Lorenzini and S. B. Bortolami, "Control and Flight Performance of Tethered Satellite Small Expendable Deployment System-II," *Journal of Guidance, Control and Dynamics,* vol. 19, no. 5, pp. 1148-1156, 1996.

[14] M. Kruijff and E. J. van der Heide, "Qualification and in-flight demonstration of a European tether deployment system on YES2," *Acta Astronautica,* vol. 64, no. 9, pp. 882-905, 2009.

[15] M. Liu, X. Zhan, Z. H. Zhu and B. Liu, "Space tether deployment with explicit non-overshooting length and positive velocity constraints," *Journal of Guidance, Control, and Dynamics,* vol. 40, no. 12, pp. 3310-3315, 2017.

[16] H. Wen, D. P. Jin and H. Y. Hu, "Three-dimensional optimal deployment of a tethered sub satellite with an elastic tether," *International Journal of Computer Mathematics,* vol. 85, no. 6, pp. 915-923, 2008.

[17] P. Williams, "Deployment/retrieval optimization for flexible tethered satellite systems," *Nonlinear Dynamics,* vol. 52, no. 1-2, pp. 159-179, 2008.

[18] P. Williams, "Dynamics and Control of Spinning Tethers for Rendezvous in Elliptic Orbits," *Journal of Vibration and Control,* vol. 12, no. 7, pp. 737-771, 2006.

[19] K. K. Mankala and S. K. Agrawal, "Dynamic Modeling and Simulation of Satellite Tethered Systems," *Journal of Vibration and Acoustics,* vol. 127, no. 2, pp. 144-156, 2005.

[20] M. J. Leamy, A. K. Noor and T. M. Wasfy, "Dynamic simulation of a tethered satellite system using finite elements and fuzzy sets," *Computer Methods in Applied Mechanics and Engineering,* vol. 190, no. 37-38, pp. 4847-4870, 2001.

[21] E. S. Kim and S. R. Vadali, "Modeling issues related to retrieval of flexible tethered satellite systems," *Journal of Guidance, Control, and Dynamics,* vol. 18, no. 5, pp. 1169-1176, 1995.

[22] R. Z. Zhu, D. Lei and H. B. Lin, "Sophisticated dynamical model of tethered satellite systems," *J. Astronaut.,* vol. 20, no. 3, pp. 7-12, 1999.

[23] S. Kawamoto, T. Makida, F. Sasaki, Y. Okawa and S. I. Nishida, "Precise numerical simulations of electrodynamic tethers for an active debris removal system," *Acta Astronautica,* vol. 59, no. 1-5, pp. 139-148, 2006.

[24] J. T. Carter and M. Greene, "Simulation of single tether systems," *Simulation,* vol. 58, no. 1, pp. 42-48, 1992.

[25] K. D. Kumar, "Review on Dynamics and Control of Nonelectrodynamic Tethered

Satellite Systems," *Journal of Spacecraft and Rockets*, vol. 43, no. 4, pp. 705-720, 2006.

[26] B. S. Yu and D. P. Jin, "Deployment and retrieval of tethered satellite system under J2 perturbation and heating effect," *Acta Astronautica*, vol. 67, pp. 845-853, 2010.

[27] A. Darabi and N. Assadian, "Coupled rotational and translational modeling of two satellites connected by a tether and their robust attitude control using optimal offset approach," *Advances in space research*, vol. 63, no. 8, pp. 2455-2468, 2019.

[28] S. Chen, "Attitude dynamic analysis of the end-bodies of space tether system in deployment," *Journal of National University of Defense Technology*, vol. 42, no. 2, pp. 98-106, 2020.

[29] B. S. Yu, H. Wen and D. P. Jin, "Review of Deployment Technology for Tethered Satellite Systems," *Acta Mechanica Sinica*, vol. 34, no. 4, pp. 754-768, 2018.

[30] Y. Chen, R. Huang, L. He, X. Ren and B. Zheng, "Dynamical modelling and control of space tethers: A review of space tether research," *Nonlinear Dynamics*, vol. 77, no. 4, pp. 1077-1099, 2014.

[31] B. Barkow, A. Steindl, H. Troger and G. Wiedermann, "Various Methods of Controlling the Deployment of a Tethered Satellite," *Journal of Vibration and Control*, vol. 9, no. 1-2, pp. 187-208, 2003.

[32] D. J. Pines and A. H. von Flotow, "Two Nonlinear Control Approaches for Retrieval of a Thrusting Tethered Sub-Satellite," *Journal Guidance, Control and Dynamics*, vol. 13, no. 4, pp. 651-658, 1990.

[33] E. S. Kim and S. R. Vadali, "Nonlinear Feedback Deployment and Retrieval of Tethered Satellite Systems," *Journal of Guidance, Control and Dynamics,* vol. 15, no. 1, pp. 28-34, 1991.

[34] S. Pradeep, "A new tension control law for deployment of tethered satellites," *Mechanics Research Communications,* vol. 24, no. 3, pp. 247-254, 1997.

[35] H. Wen, Z. H. Zhu, D. Jin and H. Hu, "Space tether deployment control with explicit tension constraint and saturation function," *Journal of Guidance, Control, and Dynamics,* vol. 39, no. 4, pp. 915-920, 2016.

[36] E. Netzer and T. R. Kane, "Deployment and retrieval optimization of a tethered satellite system," *Journal Guidance, Control and Dynamics,* vol. 16, no. 6, pp. 1085-1091, 1993.

[37] P. Williams and P. Trivailo, "On the optimal deployment and retrieval of tethered satellites," in *The 41st AIAA/ASME/SAE/ASEE Joint Propulsion Conference and Exhibit*, Tucson, 2005.

[38] P. Williams, "Libration Control of Tethered Satellites in Elliptical Orbits," *Journal of Spacecraft and Rockets,* vol. 43, no. 2, pp. 476-479, 2006.

[39] P. Williams, "Optimal Deployment/Retrieval of Tethered Satellites," *Journal of Spacecraft and Rockets,* vol. 45, no. 2, pp. 324-343, 2008.

[40] A. Steindl and H. Troger, "Optimal Control of Deployment of a Tethered Subsatellite," *Nonlinear Dynamics,* vol. 31, no. 3, pp. 257-274, 2003.

[41] A. Steindl, "Optimal deployment of a tethered satellite," in *8th Vienna International*

Conference on Mathematical Modelling, MATHMOD 2015, Vienna, Austria, 2015.

[42] A. Steindl, "Time optimal control for the deployment of a tethered satellite allowing for a massive tether," *Meccanica,* vol. 51, no. 11, pp. 2741-2751, 2016.

[43] F. Hironori and I. Shintaro, "Mission Function Control for Deployment and Retrieval of a Subsatellite," *Journal of Guidance, Control and Dynamics,* vol. 12, pp. 243-247, 1989.

[44] K. Kokubun and H. A. Fujii, "Deployment/Retrieval Control of a Tethered SubSatellite Under Effect of Tether Elasticity," *Journal Guidance, Control and Dynamics,* vol. 19, no. 1, pp. 84-90, 1996.

[45] S. R. Vadali, "Feedback Tether Deployment and Retrieval," *Journal of Guidance, Control and Dynamics,* vol. 14, no. 2, pp. 469-470, 1991.

[46] S. R. Vadali and E. S. Kim, "Feedback Control of Tethered Satellites Using Lyapunov Stability Theory," *Journal of Guidance, Control and Dynamics,* vol. 14, no. 4, pp. 729-735, 1991.

[47] C. Luo, H. Wen and D. Jin, "Deployment of flexible space tether system with satellite attitude stabilization," *Acta astronautica,* vol. 160, pp. 240-250, 2019.

[48] G. Sun and Z. H. Zhu, "Fractional order tension control for stable and fast tethered satellite retrieval," *Acta Astronautica,* vol. 104, no. 1, pp. 304-312, 2014.

[49] G. Sun and Z. H. Zhu, "Fractional-order tension control law for deployment of space tether system," *Journal of Guidance, Control, and Dynamics,* vol. 37, no. 6, pp. 2057-2061, 2014.

[50] R. Mohsenipour, "Robust Performance Control of Space Tether Deployment Using Fractional Order Tension Law," *Journal of Guidance, Control, and Dynamics,* vol. 43, no. 2, pp. 347-353, 2020.

[51] S. Xu, G. Sun, Z. Ma and X. Li, "Fractional-Order Fuzzy Sliding Mode Control for the Deployment of Tethered Satellite System under Input Saturation," *IEEE transactions on aerospace and electronic systems,* vol. 55, no. 2, pp. 747-756, 2019.

[52] J. Kang, Z. H. Zhu, W. Wang, A. Li and C. Wang, "Fractional order sliding mode control for tethered satellite deployment with disturbances," *Advances in Space Research,* vol. 59, no. 1, pp. 263-273, 2017.

[53] X. Zhong, X. Shao, X. Li, Z. Ma and G. Sun, "Fractional Order Adaptive Sliding Mode Control for the Deployment of Space Tethered System with Input Limitation," *IEEE Access,* vol. 6, pp. 48958-48969, 2018.

[54] C. Wang and F. Zhang, "Finite-time stability of an underactuated tethered satellite system," *Acta astronautica,* vol. 159, pp. 199-212, 2019.

[55] Z. Ma and G. Sun, "Full-order sliding mode control for deployment/retrieval of space tether system," in *IEEE International Conference on Systems, Man, and Cybernetics, SMC 2016*, Budapest, Hungary, 2016.

[56] Z. Ma and G. Sun, "Adaptive sliding mode control of tethered satellite deployment with input limitation," *Acta Astronautica,* vol. 127, pp. 67-75, 2016.

[57] Z. Ma, G. Sun and Z. Li, "Dynamic adaptive saturated sliding mode control for deployment of tethered satellite system," *Aerospace Science and Technology,* vol.

66, pp. 355-365, 2017.

[58] S. Chen, A. Li, C. Wang and C. Liu, "Adaptive sliding mode control for deployment of electro-dynamic tether via limited tension and current," *Acta Astronautica,* vol. In Press, 2019.

[59] A. K. Misra and V. J. Modi, "Deployment and Retrieval of Shuttle Supported Tethered Satellites," *Journal of Guidance, Control and Dynamics,* vol. 5, no. 3, pp. 278-285, 1982.

[60] H. Glabel, F. Zimmermann, S. Bruckner and U. M. Schottle, "Adaptive neural control of the deployment procedure for the tether assisted re-entry," *Aerospace Science and Technology,* vol. 8, no. 1, pp. 73-81, 2004.

[61] P. M. Bainum and V. K. Kumar, "Optimal Control of the Shuttle-Tethered-Subsatellite System," *Acta Astronautica,* vol. 7, no. 12, pp. 1333-1348, 1980.

[62] N. Takeichi, M. C. Natori and N. Okuizumi, "Fundamental Strategies for Control of a Tethered System in Elliptical Orbits," *Journal of Spacecraft and Rockets,* vol. 40, no. 1, pp. 119-125, 2002.

[63] B. Barkow, A. Steindl and H. Troger, "A targeting strategy for the deployment of a tethered satellite system," *IMA Journal of Applied Mathematics,* vol. 70, no. 5, pp. 626-644, 2005.

[64] B. S. Yu, D. P. Jin and H. Wen, "A Method for Stable Deployment of an Electrodynamic Tethered Satellite in Three-Dimensional Space," in *13th International Conference on Motion and Vibration Control, MOVIC 2016 and the*

12th International Conference on Recent Advances in Structural Dynamics, RASD 2016, Southampton, United Kingdom, 2016.

[65] H. Wen, D. Jin and H. Hu, "Three-dimensional deployment of electro-dynamic tether via tension and current control with constraints," *Acta Astronautica,* vol. 129, pp. 253-259, 2016.

[66] F. Zhang and P. Huang, "A novel underactuated control scheme for deployment/retrieval of space tethered system," *Nonlinear dynamics,* vol. 95, no. 4, pp. 3465-3476, 2019.

[67] J. Kang and Z. H. Zhu, "A unified energy-based control framework for tethered spacecraft deployment," *Nonlinear dynamics,* vol. 95, no. 2, pp. 1117-1131, 2019.

[68] H. Wen, Z. H. Zhu, D. Jin and H. Hu, "Tension control of space tether via online quasi-linearization iterations," *Advances in Space Research,* vol. 57, no. 3, pp. 754-763, 2016.

[69] B. S. Yu, D. P. Jin and H. Wen, "Analytical deployment control law for a flexible tethered satellite system," *Aerospace Science and Technology,* vol. 66, pp. 294-303, 2017.

[70] G. Shi, Z. Zhu and Z. H. Zhu, "Dynamics and control of tethered multi-satellites in elliptic orbits," *Aerospace Science and Technology,* vol. 91, pp. 41-48, 2019.

[71] A. E. Zakrzhevskii, "Method of Deployment of a Tethered Space System Along the Local Vertical," *International Applied Mechanics,* vol. 51, no. 6, pp. 670-681, 2015.

[72] A. E. Zakrzhevskii, "Method of Deployment of a Space Tethered System Aligned

to the Local Vertical," *Journal of the Astronautical Sciences,* vol. 63, no. 3, pp. 221-236, 2016.

[73] M. Liu, Z. H. Zhu and X. Zhan, "Space tether deployment with explicit maximum libration angle constraint and tension disturbance," *Advances in Space Research,* vol. 62, no. 7, pp. 1853-1862, 2018.

[74] L. Olivieri, F. Sansone, M. Duzzi and A. Francesconi, "TED project: Conjugating technology development and educational activities," *Aerospace,* vol. 6, no. 6, 2019.

[75] U. Bindra and Z. H. Zhu, "Development of an air-bearing inclinable turntable for testing tether deployment," in *AIAA Guidance, Navigation, and Control Conference*, San Diego, United States, 2016.

[76] G. P. Moia, D. P. dos Santos and J. K. Formiga, "Tension force in nanosatellite tethers systems," *Journal of Physics,* vol. 1365, no. 1, 2019.

[77] W. Jung, A. P. Mazzoleni and J. Chung, "Nonlinear dynamic analysis of a three-body tethered satellite system with deployment/retrieval," *Nonlinear Dynamics,* vol. 82, no. 3, pp. 1127-1144, 2015.

[78] Z. Dong, Y. M. Zabolotnov and C. Q. Wang, "Mathematical modeling and analysis of motion of a low-orbital space tether system," *Journal of physics,* vol. 1096, no. 1, 2018.

[79] D. Zhe, Z. Y. Mikhailovich, W. Haiquan and W. Shengjun, "Modeling and Analysis of Deployment Dynamics of a Low-orbital Tethered System," in *2019 International Conference on Advanced Mechatronic Systems*, Kusatsu, Shiga, Japan, 2019.

[80] L. Yi, B. Wang, H. Huang, C. L. Tan and J. F. Guo, "An adaptive mechanism for space tether reel," *Journal of Astronautics,* vol. 35, no. 12, pp. 1379-1387, 2014.

[81] G. Grassi, M. Pezzato, A. Gloder, R. Mantellato, A. Francesconi, E. Lorenzini, A. Rossi and L. Pellegrina, "Design and test in microgravity of a space tether length and length rate measurement device," in *4th IEEE International Workshop on Metrology for AeroSpace, MetroAeroSpace 2017*, Padua, Italy, 2017.

[82] R. Kondo, S. Hara and K. Furuta, "Design of type-1 servo systems possessing prescribed stability margins using a generalized Riccati-type equation," *International Journal of Control,* vol. 46, no. 5, pp. 1525-1545, 1987.

[83] L. C. Hsu and F. R. Chang, "The generalized Ackermann's formula for singular systems," *Systems & Control Letters,* vol. 27, no. 2, pp. 117-123, 1996.

[84] M. Costandin, P. Dobra and B. Gavrea, "A new proof of Ackermann's formula from control theory," *Studia Universitatis Babes-Bolyai Mathematica,* vol. 62, no. 3, pp. 325-329, 2017.

[85] E. E. Zajac, "The Kelvin-Tait_Chetaev Theorem and Extensions," *Journal Aeronautical Science,* vol. 11, no. 2, pp. 46-49, 1964.

[86] C. Wang, P. Wang, A. Li and Y. Guo, "Deployment of Tethered Satellites in Low-Eccentricity Orbits Using Adaptive Sliding Mode Control," *Journal of Aerospace Engineering,* vol. 30, no. 6, p. 04017077, 2017.

[87] T. Levasseur and J. T. Stafford, "Semi-simplicity of invariant holonomic systems on a reduced Lie algebra," *American Journal of Mathematics,* vol. 119, no. 5, pp.

1095-1117, 1997.

[88] F. Mei, "A Method of integrating the equations of motion of non-holonomic systems with higher-order constraints," *Journal of Applied Mathematics and Mechanics,* vol. 55, no. 4, pp. 555-559, 1991.

[89] Y. Lian and G. Tang, "Libration point orbit rendevous using pwpf modulated terminal sliding mode control," *Advances in Space Research,* vol. 52, no. 12, pp. 2156-2167, 2013.

[90] G. Song, N. V. Buck and B. N. Agrawal, "Spacecraft vibration reduction using pulse width pulse frequency modulated input shaper," *Journal of Guidance, Control, and Dynamics,* vol. 22, no. 3, pp. 433-440, 1999.

[91] Q. Hu, "Robust integral variable structure controller and pulse widht pulse frequency modulated input shaper design for flexible spacecraft with mismatched uncertainty/disturbances," *ISA Transactions,* vol. 28, no. 2, pp. 505-518, 2007.

[92] Q. Hu and G. Ma, "Vibration suppression of flexible spacecraft during attitude maneuvers," *Journal of Guidance, Control and Dynamics,* vol. 28, no. 2, pp. 377-380, 2005.

[93] G. Song and B. N. Agrawal, "Vibration suppression of flexible spacecraft during attitude control," *Acta Astronautica,* vol. 49, no. 2, pp. 71-83, 2001.

[94] M. Farza, M. M'Saad, M. Triki and T. Maatoug, "High gain observer for a class of non-triangular systems," *Systems & Control Letters,* vol. 60, no. 1, pp. 27-35, 2011.

[95] A. J. Krener and A. Isidori, "Linearization by output injection and nonlinear

observers," *Systems & Control Letters,* vol. 3, no. 1, pp. 47-52, 1983.

[96] V. Andrieu and L. Praly, "On the Existence of a Kazantzis--Kravaris/Luenberger Observer," *SIAM Journal on Control and Optimization,* vol. 45, no. 2, pp. 432-456, 2006.

[97] R. Rajamani, "Observers for Lipschitz nonlinear systems," *IEEE Transactions on Automatic Control,* vol. 43, no. 3, pp. 397-401, 1998.

[98] N. Kazantzis and C. Kravaris, "Nonlinear observer design using Lyapunov's auxiliary theorem," *Systems & Control Letters*, vol. 34, no. 5, pp. 241-247, 1998.

[99] M. Nadri, H. Hammouri and R. M. Grajales, "Observer Design for Uniformly Observable Systems With Sampled Measurements," *IEEE Transactions on Automatic Control* , vol. 58, no. 3, pp. 757-762, 2013.

[100] M. Nadri, H. Hammouri and C. Astorga, "Observer Design for Continuous-Discrete Time State Affine Systems up to Output Injection," *European Journal of Control,* vol. 10, no. 3, pp. 252-263, 2004.

[101] V. Andrieu and M. Nadri, "Observer design for Lipschitz systems with discrete-time measurements," in *49th IEEE Conference on Decision and Control (CDC)*, Atlanta, USA, 2010.

[102] M. Farza, M. M'Saad, M. L. Fall, E. Pigeon, O. Gehan and K. Busawon, "Continuous-discrete time observers for a class of MIMO nonlinear systems," *IEEE Transactions on Automatic Control,* vol. 59, no. 4, pp. 1060-1065, 2014.

[103] D. A. Padgett and A. P. Mazzoleni, "Analysis and design for nospin tethered satellite

retrieval," *Journal of Guidance, Control and Dynamics*, vol. 30, no. 5, pp. 1516-1519, 2007.

[104] H. Wen, D. P. Jin and H. Y. Hu, "Infinite-horizon control for retrieving a tethered sub satellite via an elastic tether," *Journal of Guidance Control and Dynamics,* vol. 31, no. 4, pp. 899-906, 2008.

[105] B. Wong and C. Damaren, "Control of the Electrodynamic Boom Propulsion System Accounting for Atmospheric Drag," *Journal of Guidance, Control and Dynamics,* vol. 33, no. 5, pp. 1327-1333, 2010.

[106] M. B. Larsen and M. Blanke, "Passivity-Based Control of a Rigid Electrodynamic Tether," *Journal of Guidance, Control and Dynamics,* vol. 34, no. 1, pp. 118-127, 2011.

[107] C. Liu, "Neural Network-Based Adaptive Terminal Sliding Mode Control for the Deployment Process of the Dual-Body Tethered Satellite System," *Proceedings of the Institution of Mechanical Engineers,* vol. 234, no. 6, pp. 1157-1171, 2020.

[108] H. Zhou, "Dynamics and Stable Deployment Control of Space Tethered Formation," *Journal of Astronautics,* vol. 41, no. 4, pp. 410-418, 2020.

[109] X. Zhong, "Backstepping-like nonlinear control for the deployment of tethered satellite system in elliptical orbits," *Journal of Harbin Institute of Technology,* vol. 52, no. 4, pp. 25-30, 2020.

[110] G. R. Sangeetha and H. Ganesan, "Simulation of the Dynamics and Control of Tethered Small Satellite Deployment," in *Advances in Small Satellite Technologies*,

Singapore, 2020.

[111] Y. Ohkawa, S. Kawamoto, T. Okumura, K. Iki, H. Okamoto, K. Inoue, T. Uchiyama and D. Tsujita, "Review of KITE – Electrodynamic tether experiment on the H-II Transfer Vehicle," *Acta Astronautica,* vol. In Press, 2020.

[112] C. Wang, L. Fu, Y. Zabolotnov and A. Li, "Matrix decomposition based control for space tether system with incomplete state feedback," *Journal of Beijing University of Aeronautics and Astronautics,* vol. 45, no. 5, pp. 902-911, 2019.

[113] B. Wang, Z. Meng, C. Jia and P. Huang, "Reel-based Tension Control of Tethered Space Robots," *IEEE transactions on aerospace and electronic systems,* vol. In Press, 2019.

[114] B. S. Yu, L. L. Geng, H. Wen, T. Chen and D. P. Jin, "Ground-based experiments of tether deployment subject to an analytical control law," *Acta Astronautica,* vol. 151, pp. 253-259, 2018.

Appendix A STK SAMPLE CODE

The following sample code was used in the STK Chapter. The VBScript was based off a sample template provided by STK.

Appendix A.1 VBScipt

```
'=====================================================
'  Copyright 2005, Analytical Graphics, Inc.
' =====================================================

'================================
' Matlab specific variables
'================================

Dim m_mFileName
Dim m_MatlabApp

Set m_MatlabApp = nothing
m_mFilename = "example1Hpop"

' NOTE: to attach to an existing matlab session,
' you must execute: enableservice('AutomationServer',true)
' in that matlab session. If you do not, then a new Matlab
' session will be opened

' NOTE: our current experience is that even when you open
' the session yourself and attach to it, it will be closed
' once the plugin component is freed and releases its
' Matlab attachment.

'================================
' Reference Frames Enumeration
'================================
Dim eUtFrameInertial, eUtFrameFixed, eUtFrameLVLH, eUtFrameNTC

eUtFrameInertial        = 0
eUtFrameFixed           = 1
eUtFrameLVLH            = 2
eUtFrameNTC             = 3


'=================================
' Time Scale Enumeration
'=================================
Dim eUTC, eTAI, eTDT, eUT1, eSTKEpochSec, eTDB, eGPS

eUTC            = 0
eTAI            = 1
eTDT            = 2
eUT1            = 3
eSTKEpochSec    = 4
eTDB            = 5
eGPS            = 6


'=================================
' Log Msg Type Enumeration
```

```
'==================================
Dim eLogMsgDebug, eLogMsgInfo, eLogMsgForceInfo, eLogMsgWarning, eLogMsgAlarm

eLogMsgDebug            = 0
eLogMsgInfo             = 1
eLogMsgForceInfo        = 2
eLogMsgWarning          = 3
eLogMsgAlarm            = 4

'=================================
' Sun Position Enumeration
'=================================
Dim eApparentToTrueCB, eApparent, eTrue, eSRP

eApparentToTrueCB  = 0
eApparent          = 1
eTrue              = 2
eSRP               = 3

'=================================
' Accel Type Enumeration
'=================================
Dim eTotalAccel, eTwoBodyAccel, eGravityAccel, ePerturbedGravityAccel, eSolidTidesAccel
Dim eOceanTidesAccel, eDragAccel, eSRPAccel, eThirdBodyAccel, eGenRelativityAccel, eAddedAccel

eTotalAccel             = 0
eTwoBodyAccel           = 1
eGravityAccel           = 2
ePerturbedGravityAccel  = 3
eSolidTidesAccel        = 4
eOceanTidesAccel        = 5
eDragAccel              = 6
eSRPAccel               = 7
eThirdBodyAccel         = 8
eGenRelativityAccel     = 9
eAddedAccel             = 10

' =================================
'  ForceModel Type Enumeration
' =================================

eGravityModel           = 0
eSolidTidesModel        = 1
eOceanTidesModel        = 2
eDragModel              = 3
eSRPModel               = 4
eThirdBodyModel         = 5
eGenRelativityModel     = 6

'===========================================
' AgEAttrAddFlags Enumeration
'===========================================
Dim eFlagNone, eFlagTransparent, eFlagHidden, eFlagTransient, eFlagReadOnly, eFlagFixed

eFlagNone          = 0
eFlagTransparent   = 2
eFlagHidden        = 4
eFlagTransient     = 8
eFlagReadOnly      = 16
eFlagFixed         = 32


'================================
' Global Variables
'================================
Dim m_AgUtPluginSite
```

```
Dim m_AgStkPluginSite
Dim m_AgAttrScope
Dim m_CrdnPluginProvider
Dim m_CrdnConfiguredVector
Dim m_CrdnConfiguredVector_derivative
Dim m_CrdnConfiguredVector_Ref
Dim m_CalcToolProvider

Set m_AgUtPluginSite                                    = Nothing
Set m_AgStkPluginSite                                   = Nothing
Set m_AgAttrScope                                       = Nothing
Set m_CrdnPluginProvider                        = Nothing
Set m_CrdnConfiguredVector                      = Nothing
Set m_CrdnConfiguredVector_derivative   = Nothing
Set m_CrdnConfiguredVector_Ref                  = Nothing
Set m_CalcToolProvider                          = Nothing

Dim m_Name
Dim m_Enabled
Dim m_VectorName
Dim m_VectorName_derivative
Dim m_VectorName_Ref
Dim m_AccelRefFrame
Dim m_AccelRefFrameChoices(3)
Dim m_AccelX
Dim m_AccelY
Dim m_AccelZ
Dim m_MsgStatus
Dim m_EvalMsgInterval
Dim m_PostEvalMsgInterval
Dim m_PreNextMsgInterval
Dim m_PreNextCntr
Dim m_EvalCntr
Dim m_PostEvalCntr
Dim m_Range
Dim m_Range_vel

m_Name                                  = "Matlab.Example1.Hpop.wsc"
m_Enabled                               = true
m_VectorName                    = "Satellite1"
m_VectorName_derivative         = "Satellite1_derivative"
m_VectorName_Ref                = "Body.-Z"

m_AccelRefFrame                 = 0
m_AccelRefFrameChoices(0)   = "eUtFrameInertial"
m_AccelRefFrameChoices(1)   = "eUtFrameFixed"
m_AccelRefFrameChoices(2)   = "eUtFrameLVLH"
m_AccelRefFrameChoices(3)   = "eUtFrameNTC"

m_AccelX                        = 0.0
m_AccelY                        = 0.00
m_AccelZ                        = 0.0
m_MsgStatus                             = false
m_EvalMsgInterval               = 5000
m_PostEvalMsgInterval           = 5000
m_PreNextMsgInterval            = 1000

m_PreNextCntr                   = 0
m_EvalCntr                              = 0
m_PostEvalCntr                  = 0

m_Range   = null
m_Range_vel = null

'======================
```

```
' GetPluginConfig method
'======================
Function GetPluginConfig( AgAttrBuilder )

		If( m_AgAttrScope is Nothing ) Then

			Set m_AgAttrScope = AgAttrBuilder.NewScope()

			'===========================
			' General Plugin attributes
			'===========================
			Call AgAttrBuilder.AddStringDispatchProperty( m_AgAttrScope, "PluginName", "Human readable plugin name or alias",		"Name",	0 )
			Call AgAttrBuilder.AddBoolDispatchProperty  ( m_AgAttrScope, "PluginEnabled",	"If the plugin is enabled or has experience an error", "Enabled",	0 )
			Call AgAttrBuilder.AddStringDispatchProperty( m_AgAttrScope, "VectorName", "Relative vector", "VectorName", 0 )
			Call AgAttrBuilder.AddStringDispatchProperty( m_AgAttrScope, "VectorName_Derivative", "Relative Vector derivative",		"VectorName_Derivative", 0 )
			Call AgAttrBuilder.AddStringDispatchProperty( m_AgAttrScope, "VectorName_Ref", "Reference Vector", "VectorName_Ref", 0 )


			'===========================
			' Propagation related
			'===========================
			Call AgAttrBuilder.AddChoicesDispatchProperty( m_AgAttrScope, "AccelRefFrame", "Acceleration Reference Frame",	"AccelRefFrame", GetAccelRefFrameChoices() )
			Call AgAttrBuilder.AddDoubleDispatchProperty  ( m_AgAttrScope, "AccelX",		"Acceleration in the X direction", "AccelX",	0 )
			Call AgAttrBuilder.AddDoubleDispatchProperty  ( m_AgAttrScope, "AccelY",		"Acceleration in the Y direction", "AccelY",	0 )
			Call AgAttrBuilder.AddDoubleDispatchProperty  ( m_AgAttrScope, "AccelZ",		"Acceleration in the Z direction", "AccelZ",	0 )

			'===========================
			' Messaging related attributes
			'===========================
			Call AgAttrBuilder.AddBoolDispatchProperty( m_AgAttrScope, "UsePropagationMessages",	"Send messages to the message window during propagation",		"MsgStatus",		0 )
			Call AgAttrBuilder.AddIntDispatchProperty ( m_AgAttrScope, "EvaluateMessageInterval",	"The interval at which to send messages from the Evaluate method during propagation", "EvalMsgInterval",	0 )
			Call AgAttrBuilder.AddIntDispatchProperty ( m_AgAttrScope, "PostEvaluateMessageInterval",  "The interval at which to send messages from the PostEvaluate method during propagation", "PostEvalMsgInterval",	0 )
			Call AgAttrBuilder.AddIntDispatchProperty ( m_AgAttrScope, "PreNextStepMessageInterval", "The interval at which to send messages from the PreNextStep method during propagation", "PreNextMsgInterval", 0 )

		End If

		Set GetPluginConfig = m_AgAttrScope

End Function

'===========================
' VerifyPluginConfig method
'===========================
Function VerifyPluginConfig(AgUtPluginConfigVerifyResult)

   Dim Result
   Dim Message

		Result = true
		Message = "Ok"

   If( Not ( m_AccelX <= 10 And m_AccelX >= -10 ) ) Then
```

```
            Result  = false
            Message = "AccelX was not within the range of -10 to +10 meters per second squared"

   ElseIf( Not ( m_AccelY <= 10 And m_AccelY >= -10 ) ) Then

            Result  = false
            Message = "AccelY was not within the range of -10 to +10 meters per second squared"

   ElseIf( Not ( m_AccelZ <= 10 And m_AccelZ >= -10 ) ) Then

            Result  = false
            Message = "AccelZ was not within the range of -10 to +10 meters per second squared"

            End If

            AgUtPluginConfigVerifyResult.Result  = Result
            AgUtPluginConfigVerifyResult.Message = Message

End Function

'======================
' Init Method
'======================
Function Init( AgUtPluginSite )

            Set m_AgUtPluginSite = AgUtPluginSite

            If( Not m_AgUtPluginSite is Nothing ) Then

                        If( m_Enabled = true ) Then

                                    Dim siteName
                                    siteName = m_AgUtPluginSite.SiteName

                                    If(siteName = "IAgStkPluginSite" Or siteName = "IAgGatorPluginSite") Then
                                                Set m_CrdnPluginProvider          = m_AgUtPluginSite.VectorToolProvider
                                                Set m_CalcToolProvider = m_AgUtPluginSite.CalcToolProvider

                                                If(Not m_CrdnPluginProvider is Nothing) Then
                                                            Set m_CrdnConfiguredVector                          =
m_CrdnPluginProvider.ConfigureVector( m_VectorName, "<MySelf>", "LVLH", "<MySelf>")
                                                            Set m_CrdnConfiguredVector_derivative     =
m_CrdnPluginProvider.ConfigureVector( m_VectorName_derivative, "<MySelf>", "LVLH", "<MySelf>")
                                                            Set m_CrdnConfiguredVector_Ref                      =
m_CrdnPluginProvider.ConfigureVector( m_VectorName_Ref, "<MySelf>", "Body", "<MySelf>")
                                                End If

                                                If(Not m_CalcToolProvider is Nothing) Then
                                                            Set m_Range            =
m_CalcToolProvider.GetCalcScalarWithRate("length", "<MyObject>")
                                                            Set      m_Range_vel      =      m_CalcToolProvider.GetCalcScalar("length",
"<MyObject>")
                                                End If

                                                If ( m_MsgStatus = true ) Then

                                                            Call m_AgUtPluginSite.Message( eLogMsgDebug, "Init():" )
                                                            Call m_AgUtPluginSite.Message( eLogMsgDebug, "Init(): AccelRefFrame( "
& GetAccelRefFrame() & " )" )
                                                            Call  m_AgUtPluginSite.Message(  eLogMsgDebug,  "Init():  AccelX(  "  &
m_AccelX & " )" )
                                                            Call  m_AgUtPluginSite.Message(  eLogMsgDebug,  "Init():  AccelY(  "  &
m_AccelY & " )" )
                                                            Call  m_AgUtPluginSite.Message(  eLogMsgDebug,  "Init():  AccelZ(  "  &
m_AccelZ & " )" )
```

```
                    End If

                    If(m_CrdnConfiguredVector is Nothing) Then
                              Call m_AgUtPluginSite.Message( eLogMsgDebug, "Init(): Could not obtain "
& m_VectorName )
                              Call m_AgUtPluginSite.Message( eLogMsgDebug, "Init(): Turning off the
computation of SRP Area" )
                    End If
          Else
                    Call m_AgUtPluginSite.Message( eLogMsgDebug, "Init(): " & siteName & " does not
provide VectorToolProvider" )
                    Call m_AgUtPluginSite.Message( eLogMsgDebug, "Init(): Turning off the computation of
SRP Area" )
          End If
     Else

          Call m_AgUtPluginSite.Message( eLogMsgDebug, "Init(): Disabled" )

     End If

     ' Get handle to Matlab

     If(m_Enabled = true) Then
       Dim filepath
       filepath = ""

       Set m_MatlabApp = GetObject(filepath,"Matlab.Application")

       If(m_MatlabApp is Nothing) Then
                    MsgBox "Cannot get handle to Matlab"
                    m_Enabled = false
     End If

     End If

  End If

  Init = m_Enabled

End Function

'=====================
' PrePropagate Method
'=====================
Function PrePropagate( AgAsHpopPluginResult )

  If( Not m_AgUtPluginSite is Nothing ) Then

     If( m_Enabled = true ) Then

          If( Not AgAsHpopPluginResult is Nothing ) Then

                    'm_SrpIsOn = AgAsHpopPluginResult.IsForceModelOn( eSRPModel )

                    'If(m_SrpIsOn) Then
                    '         m_SRPArea = AgAsHpopPluginResult.SRPArea
                    'End if

          End If

     Else

          If( m_MsgStatus = true ) Then

                    Call m_AgUtPluginSite.Message( eLogMsgDebug, "PrePropagate(): Disabled" )
```

```
                End If
            End If
        End If
        PrePropagate = m_Enabled
End Function
'======================
' PreNextStep Function
'======================
Function PreNextStep( AgAsHpopPluginResult )
        m_PreNextCntr = m_PreNextCntr + 1
        If( Not m_AgUtPluginSite is Nothing ) Then
            If( m_Enabled = true ) Then
                If( m_MsgStatus = true ) Then
                    If( m_PreNextCntr Mod m_PreNextMsgInterval = 0 ) Then
                        Call m_AgUtPluginSite.Message( eLogMsgDebug, "PreNextStep( " &
m_PreNextCntr & " ):" )
                    End If
                End If
            Else
                If( m_MsgStatus = true ) Then
                    Call m_AgUtPluginSite( eLogMsgDebug, "PreNextStep(): Disabled" )
                End If
            End If
        End If
        PreNextStep = m_Enabled
End Function
'=================
' Evaluate Method
'=================
Function Evaluate( AgAsHpopPluginResultEval )
        m_EvalCntr = m_EvalCntr + 1
        If( Not m_AgUtPluginSite is Nothing ) Then
            If( m_Enabled = true ) Then
                Call EvaluateTetherForce( AgAsHpopPluginResultEval)
                Call AgAsHpopPluginResultEval.AddAcceleration( m_AccelRefFrame, m_AccelX, m_AccelY,
m_AccelZ )
                If( m_MsgStatus = true ) Then
```

```
			If( m_EvalCntr Mod m_EvalMsgInterval = 0 ) Then
				Call m_AgUtPluginSite.Message( eLogMsgDebug, "Evaluate( " & m_EvalCntr & " ):" )
			End If
		End If
	Else
		If( m_MsgStatus = true ) Then
			Call m_AgUtPluginSite( eLogMsgDebug, "Evaluate(): Disabled" )
		End If
	End If
End If
Evaluate = m_Enabled
End Function
Function EvaluateTetherForce( ResultEval )

' This interface may not be present
If( Not m_CrdnConfiguredVector is Nothing) Then

'==============================
' Position Velocity variables
'==============================
Dim PosVelArray
Dim PosX_Index, PosY_Index, PosZ_Index
Dim VelX_Index, VelY_Index, VelZ_Index

Set PosVelArray = Nothing
PosX_Index = 0
PosY_Index = 1
PosZ_Index = 2
VelX_Index = 3
VelY_Index = 4
VelZ_Index = 5

'==============================
' Vector variables
'==============================
Dim VecArray
Dim VecX_Index, VecY_Index, VecZ_Index

Set VecArray = Nothing
VecX_Index = 0
VecY_Index = 1
VecZ_Index = 2

'==============================
' Vector derivative variables
'==============================
Dim VecArray_derivative
Dim VecXd_Index, VecYd_Index, VecZd_Index

Set VecArray_derivative = Nothing
VecXd_Index = 0
VecYd_Index = 1
```

```
VecZd_Index = 2

'============================
' Vector Reference variables
'============================
Dim VecArray_Ref
Dim VecXRef_Index, VecYRef_Index, VecZRef_Index
Set VecArray_Ref = Nothing
VecXRef_Index = 0
VecYRef_Index = 1
VecZRef_Index = 2

'============================
' Calculation variables
'============================
Dim VecPosDotProd, VecMag, PosMag, Theta

VecPosDotProd = 0.0
VecMag = 0.0
PosMag = 0.0
Theta  = 0.0
Dim rangeArray, rangeVelArray
Dim length_Index, vel_Index
Set rangeArray = Nothing
length_Index        = 0
vel_Index           = 1

If (Not m_Range Is Nothing) Then
        rangeArray = m_Range.CurrentValue_Array(ResultEval)
        rangeVelArray = m_Range_vel.CurrentValue_Array(ResultEval)
End If


If( Not ResultEval is Nothing ) Then

        PosVelArray = ResultEval.PosVel_Array( eInterial )

        VecArray              =     m_CrdnConfiguredVector.CurrentValue_Array( ResultEval )

        VecArray_derivative   =   m_CrdnConfiguredVector_derivative.CurrentValue_Array( ResultEval )

        VecArray_Ref          =  m_CrdnConfiguredVector_Ref.CurrentValue_Array( ResultEval )


        ' Set variables into the base workspace of Matlab
        Call m_MatlabApp.PutWorkspaceData("posX", "base", CDbl(PosVelArray( PosX_Index )))

        Call m_MatlabApp.PutWorkspaceData("posY", "base", CDbl(PosVelArray( PosY_Index )))

        Call m_MatlabApp.PutWorkspaceData("posZ", "base", CDbl(PosVelArray( PosZ_Index )))

        Call m_MatlabApp.PutWorkspaceData("vectorX", "base", CDbl(VecArray( VecX_Index )))

        Call m_MatlabApp.PutWorkspaceData("vectorY", "base", CDbl(VecArray( VecY_Index )))

        Call m_MatlabApp.PutWorkspaceData("vectorZ", "base", CDbl(VecArray( VecZ_Index )))

        Call m_MatlabApp.PutWorkspaceData("length", "base", CDbl(rangeArray( length_Index )))

        Call m_MatlabApp.PutWorkspaceData("vel", "base", CDbl(rangeArray( vel_Index )))

        ' Execute the mfile on those variables

        Dim outResult

        Call m_MatlabApp.Feval(m_mFilename, 3, outResult, _
```

```
                        "vectorX=", "vectorY=", "vectorZ=", _
                        "length=", "vel=", "posX=", "posY=", "posZ=")

                ' Get the computed variable
                m_AccelX = CDbl(outResult(0))
                m_AccelY = CDbl(outResult(1))
                m_AccelZ = CDbl(outResult(2))

            Else

                If( Not m_AgUtPluginSite is Nothing And m_MsgStatus = true ) Then

                    Call m_AgUtPluginSite.Message( eLogMsgWarning, "Crdn Configured
Vector or Result Eval was null" )

                End If

            End If

        End If

    EvaluateTetherForce = True

End Function

'=================
' PostEvaluate Method
'=================
Function PostEvaluate( AgAsHpopPluginResultPostEval )

    m_PostEvalCntr = m_PostEvalCntr + 1

    If( Not m_AgUtPluginSite is Nothing ) Then

        If( m_Enabled = true ) Then

            If( m_MsgStatus = true ) Then

                Call m_AgUtPluginSite.Message( eLogMsgDebug, "PostEvaluate():" )

            End If

        Else

            If( m_MsgStatus = true ) Then

                Call m_AgUtPluginSite( eLogMsgDebug, "PostEvaluate(): Disabled" )

            End If

        End If

    End If

    PostEvaluate = m_Enabled

End Function

'========================================================
' PostPropagate Method
'========================================================
Function PostPropagate( AgAsHpopPluginResult)

    If( Not m_AgUtPluginSite is Nothing ) Then

        If( m_Enabled = true ) Then
```

```
			If( m_MsgStatus = true ) Then

				Call m_AgUtPluginSite.Message( eLogMsgDebug, "PostPropagate():" )

			End If

		Else

			If( m_MsgStatus = true ) Then

				Call m_AgUtPluginSite.Message( eLogMsgDebug, "PostPropagate(): Disabled" )

			End If

		End If

	End If

	PostPropagate = m_Enabled

End Function

'==========================================================
' Free Method
'==========================================================
Sub Free()

	If( Not m_AgUtPluginSite is Nothing ) Then

		If( m_MsgStatus = true ) Then

			Call m_AgUtPluginSite.Message( eLogMsgDebug, "Free():" )
			Call m_AgUtPluginSite.Message( eLogMsgDebug, "Free(): PreNextCntr( " & m_PreNextCntr & " )"
)
			Call m_AgUtPluginSite.Message( eLogMsgDebug, "Free(): EvalCntr( " & m_EvalCntr & " )" )
			Call m_AgUtPluginSite.Message( eLogMsgDebug, "Free(): PostEvalCntr( " & m_PostEvalCntr & "
)" )

		End If

		Set m_AgUtPluginSite					= Nothing
		Set m_CrdnPluginProvider				= Nothing
		Set m_CrdnConfiguredVector				= Nothing
		Set m_CrdnConfiguredVector_derivative	= Nothing
		Set m_CrdnConfiguredVector_Ref			= Nothing

	End If

End Sub

'============================================================
' Name Method
'============================================================
Function GetName()

	GetName = m_Name

End function

Function SetName( name )

	m_Name = name

End function
```

```
'==============================================================
' Enabled property
'==============================================================
Function GetEnabled()

    GetEnabled = m_Enabled

End Function

Function SetEnabled( enabled )

    m_Enabled = enabled

End Function

'==============================================================
' VectorName property
'==============================================================
Function GetVectorName()

    GetVectorName = m_VectorName

End Function

Function SetVectorName(vectorname)

    m_VectorName = vectorname

End Function

Function GetVectorName_derivative()

    GetVectorName_derivative = m_VectorName_derivative

End Function

Function SetVectorName_derivative(vectorname)

    m_VectorName_derivative = vectorname

End Function

Function GetVectorName_Ref()

    GetVectorName_Ref = m_VectorName_Ref

End Function

Function SetVectorName_Ref(vectorname)

    m_VectorName_Ref = vectorname

End Function

'============================================================
' AccelRefFrame property
'============================================================
Function GetAccelRefFrame()

        GetAccelRefFrame = m_AccelRefFrameChoices( m_AccelRefFrame )

End Function

Function SetAccelRefFrame(accelrefframe)

        If( m_AccelRefFrameChoices(0) = accelrefframe ) Then
```

```
                m_AccelRefFrame = 0

        ElseIf( m_AccelRefFrameChoices(1) = accelrefframe ) Then

                m_AccelRefFrame = 1

        ElseIf( m_AccelRefFrameChoices(2) = accelrefframe ) Then

                m_AccelRefFrame = 2

        ElseIf( m_AccelRefFrameChoices(3) = accelrefframe ) Then

                m_AccelRefFrame = 3

        End If

End Function

'==========================================================
' AccelRefFrameChoices property
'==========================================================
Function GetAccelRefFrameChoices()

    GetAccelRefFrameChoices = m_AccelRefFrameChoices

End Function

Function SetAccelRefFrameChoices(accelrefframechoices)

    m_AccelRefFrameChoices = accelrefframechoices

End Function

'==========================================================
' AccelX property
'==========================================================
Function GetAccelX()

    GetAccelX = m_AccelX

End Function

Function SetAccelX(accelx)

    m_AccelX = accelx

End Function

'==========================================================
' AccelY property
'==========================================================
Function GetAccelY()

    GetAccelY = m_AccelY

End Function

Function SetAccelY(accely)

    m_AccelY = accely

End Function

'==========================================================
' AccelZ property
```

```
'==========================================================
Function GetAccelZ()

    GetAccelZ = m_AccelZ

End Function

Function SetAccelZ(accelz)

    m_AccelZ = accelz

End Function

'=======================================================
' MsgStatus property
'=======================================================
Function GetMsgStatus()

    GetMsgStatus = m_MsgStatus

End Function

Function SetMsgStatus(msgstatus)

    m_MsgStatus = msgstatus

End Function

'========================================================
' EvalMsgInterval property
'========================================================
Function GetEvalMsgInterval()

    GetEvalMsgInterval = m_EvalMsgInterval

End Function

Function SetEvalMsgInterval(evalmsginterval)

    m_EvalMsgInterval = evalmsginterval

End Function

'========================================================
' PostEvalMsgInterval property
'========================================================
Function GetPostEvalMsgInterval()

    GetPostEvalMsgInterval = m_PostEvalMsgInterval

End Function

Function SetPostEvalMsgInterval(postevalmsginterval)

    m_PostEvalMsgInterval = postevalmsginterval

End Function

'========================================================
' PreNextMsgInterval property
'========================================================
Function GetPreNextMsgInterval()

    GetPreNextMsgInterval = m_PreNextMsgInterval

End Function
```

```
Function SetPreNextMsgInterval(prenextmsginterval)

    m_PreNextMsgInterval = prenextmsginterval

End Function

'======================================================
'  Copyright 2005, Analytical Graphics, Inc.
' ======================================================
```

Appendix A.2 MATLAB Script

```
% NOTE: for this example to work, this m-file must be on your Matlab path
%
% Use SetPath in Matlab to set the path or copy this m-file to your m-file
% working area

function [accelX, accelY, accelZ] = example1Hpop(xVec, yVec, zVec, length, vel, posX, posY, posZ)

% Save the data to a text file
fid = fopen('C:\Users\Latheepan\Documents\STKData_3.txt','a');

% Parameters for simulation
r = 6678.14; % km
m = 1; % kg
l_max = 100; % meters

% Input from STK
vec = [xVec, yVec, zVec]; % Vector between satellite and CM
pos = [posX, posY, posZ]; % Vector between satellite and CM
omega = sqrt(398600/r)/r; % rad/s



% Normalize input
length = length/l_max;
vel = vel/(l_max*omega);


% Control Law
k1 = 4.6;
k2 = 3.6;
T = k1*(length - 1) + k2*vel + 3;
T_s = T*m*(omega^2)*l_max; % Re-introduce dimensions

if (norm(vec) == 0)

        % Prevent error
        accelX = 0;
        accelY = 0;
        accelZ = 0;
else
        % Calculate acceleration. Compute unit vector of "vec" and scale

        % vec is in LVLH frame
        accelX = ((T_s/m)/norm(vec))*xVec;
        accelY = ((T_s/m)/norm(vec))*yVec;
        accelZ = ((T_s/m)/norm(vec))*zVec;
end

% Debugging purposes
fprintf(fid, '%f, %f, %f \n', [length vel T_s]);
```

```
fclose(fid);
```